AD-A056 728 IIT RESEARCH INST CHICAGO ILL F/G 20/14
TIME DOMAIN SOLUTIONS FOR ELECTROMAGNETIC COUPLING.(U)
JUN 78 A TAFLOVE F30602-77-C-0163
UNCLASSIFIED RADC-TR-78-142 NL

1 OF 2
AD
A056728

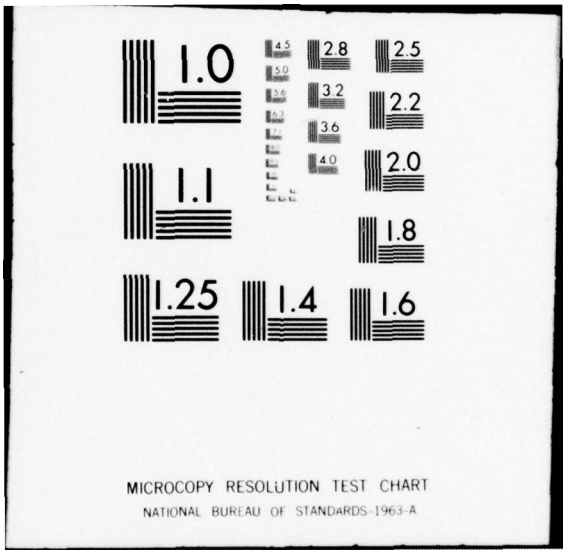
1.0
1.1
1.25
1.4
1.6
1.8
2.0
2.2
2.5
2.8
3.2
3.6
4.0
4.5
5.0
5.6
6.3
MICROCOPY RESOLUTION TEST CHART
NATIONAL BUREAU OF STANDARDS-1963-A

LEVEL II

RADC-TR-78-142
Final Technical Report
June 1978

TIME DOMAIN SOLUTIONS FOR ELECTROMAGNETIC COUPLING

Dr. Allen Taflove

IIT Research Institute

Approved for public release; distribution unlimited.

ROME AIR DEVELOPMENT CENTER
Air Force Systems Command
Griffiss Air Force Base, New York 13441

This report has been reviewed by the RADC Information Office (OI) and is releasable to the National Technical Information Service (NTIS). At NTIS it will be releasable to the general public, including foreign nations.

RADC-TR-78-142 has been reviewed and is approved for publication.

APPROVED: Daniel E. Warren

DANIEL E. WARREN
Project Engineer

APPROVED: Joseph J. Naresky

JOSEPH J. NARESKY
Chief, Reliability & Compatibility Division

FOR THE COMMANDER: John P. Huss

JOHN P. HUSS
Acting Chief, Plans Office

If your address has changed or if you wish to be removed from the RADC mailing list, or if the addressee is no longer employed by your organization, please notify RADC (RBCT) Griffiss AFB NY 13441. This will assist us in maintaining a current mailing list.

Do not return this copy. Retain or destroy.

UNCLASSIFIED

SECURITY CLASSIFICATION OF THIS PAGE (When Data Entered)

REPORT DOCUMENTATION PAGE

READ INSTRUCTIONS BEFORE COMPLETING FORM

1. REPORT NUMBER: RADC-TR-78-142	2. GOVT ACCESSION NO.
3. RECIPIENT'S CATALOG NUMBER	
4. TITLE (and Subtitle): TIME DOMAIN SOLUTIONS FOR ELECTROMAGNETIC COUPLING	5. TYPE OF REPORT & PERIOD COVERED: Final Technical Report 26 Aug 77 - 26 Mar 78
	6. PERFORMING ORG. REPORT NUMBER: N/A
7. AUTHOR(s): Dr. Allen Taflove	8. CONTRACT OR GRANT NUMBER(s): F30602-77-C-0163
9. PERFORMING ORGANIZATION NAME AND ADDRESS: IIT Research Institute, 10 West 35th Street, Chicago IL 60616	10. PROGRAM ELEMENT, PROJECT, TASK AREA & WORK UNIT NUMBERS: 62702F, 23380310
11. CONTROLLING OFFICE NAME AND ADDRESS: Rome Air Development Center (RBCT), Griffiss AFB, NY 13441	12. REPORT DATE: June 1978
	13. NUMBER OF PAGES: 98
14. MONITORING AGENCY NAME & ADDRESS (if different from Controlling Office): Same	15. SECURITY CLASS. (of this report): UNCLASSIFIED
	15a. DECLASSIFICATION/DOWNGRADING SCHEDULE: N/A

16. DISTRIBUTION STATEMENT (of this Report)

Approved for public release; distribution unlimited.

17. DISTRIBUTION STATEMENT (of the abstract entered in Block 20, if different from Report)

Same

18. SUPPLEMENTARY NOTES

RADC Project Engineer: Daniel E. Warren (RBCT)

19. KEY WORDS (Continue on reverse side if necessary and identify by block number)

Electromagnetic Compatibility
Electromagnetic Coupling
Aperture Coupling
Time Domain Solutions
Finite Difference Techniques

20. ABSTRACT (Continue on reverse side if necessary and identify by block number)

This research program investigated a new tool for the analysis of electromagnetic coupling and shielding problems: the finite-difference, time-domain (FD-TD) solution of Maxwell's equations. The objective of the program was to evaluate the suitability of the FD-TD solution to determine the amount of electromagnetic coupling through an aperture into an enclosed conducting container. Two specific geometries were used for the evaluation. The first, a conducting cylinder with one open end. The other, the guidance section of a (Cont'd)

DD FORM 1 JAN 73 1473 EDITION OF 1 NOV 65 IS OBSOLETE

UNCLASSIFIED

SECURITY CLASSIFICATION OF THIS PAGE (When Data Entered)

20 (Cont'd)

missile. Each of the two geometries was modeled to calculate the electromagnetic field coupled into the structure and the results were compared to data previously obtained by other techniques.

TABLE OF CONTENTS

TABLE OF CONTENTS (Cont.)

TABLE OF FIGURES

PREFACE

IIT Research Institute is pleased to submit this Final Report on "Time Domain Solutions for Electromagnetic Coupling," Air Force Contract No. F30602-77-C-0163, IITRI Project No. E6405, to Rome Air Development Center (RADC/RBCT). The principal investigator on this program was Dr. Allen Taflove, and the program duration was 26 August 1977 to 26 March 1978.

Respectfully submitted,
IIT RESEARCH INSTITUTE

Allen Taflove

Dr. Allen Taflove
Research Engineer

APPROVED:

Theodore A. Martin

Theodore A. Martin
Manager
EM Technology Section

TIME DOMAIN SOLUTIONS FOR
ELECTROMAGNETIC COUPLING

Air Force Contract No. F30602-77-C-0163
IITRI Project No. E6405
26 August 1977 - 26 March 1978

FINAL REPORT

1.0 INTRODUCTION

Electromagnetic coupling and shielding problems have traditionally been difficult to treat with analytical or numerical methods because of the failure of these methods to adequately resolve the effects of shield apertures, curvatures, corners, and internal contents. Usually, only relatively simple geometries of shields and shield openings are studied in an attempt to gain insight into the key coupling mechanisms, and to allow a rough estimate of the coupling for more complicated and realistic problems. A method for the direct modeling and solution of realistic problems would eliminate the need for intuition in applying simple models, and would greatly increase the accuracy of the ultimate result.

This research program investigated the application of a new approach for the direct modeling of electromagnetic interaction problems: the finite-difference, time-domain (FD-TD) solution of Maxwell's equations. The FD-TD method treats the irradiation of a structure as an initial value problem. At $t = 0$, a plane wave source of frequency, f, is assumed to be turned on. The propagation of waves from this source is simulated by solving a finite-difference analog of the time-dependent Maxwell's equations on a lattice of cells, including the structure. Time-stepping is continued until the sinusoidal steady state is achieved at each cell. The field envelope, or maximum absolute value, during the final half wave-cycle of time-stepping is taken as the magnitude of the phasor of the steady-state field.

This method has two key advantages relative to available modeling approaches. First, it is simple to implement for complicated metal/dielectric structures because arbitrary electrical parameters can be

assigned to each lattice cell using a data card deck. Second, its computer memory and running time requirement is not prohibitive for many complex structures of interest.

This report first reviews available numerical techniques for the solution of electromagnetic coupling/shielding problems. Then, the basic elements of the FD-TD method are introduced, with detailed derivations where appropriate, and with examples of prior computed results for dielectric structures to establish the expected level of accuracy for general structures. The last section of this report will detail the computed results for the metal geometries modeled in this program effort. Full listings of computer programs employed in this research effort are provided in the Appendix.

2.0 REVIEW OF AVAILABLE NUMERICAL TECHNIQUES

The coupling of electromagnetic fields to the interior of an arbitrary conducting or dielectric structure has been approached using both frequency domain and time domain numerical techniques. This section reviews published work in this area and discusses the problems inherent in present approaches.

2.1 Frequency Domain Techniques

Frequency domain methods are based upon the assumption of an $\exp(j2\pi ft)$ time dependence in the fundamental Maxwell's equations. In general, methods of this type derive a set of linear equations for either field variables or field expansion coefficients, and then solve the linear system with a suitable matrix inversion scheme.

Almost all frequency domain techniques can be placed in the following three classes.

1. Electromagnetic field expansions, in terms of either
   a. Normal modes of the structure,[1]
   b. Analytic continuation of free space modes,[2]
   c. Normal modes of the structure matched to aperture fields determined using a quasi-static approximation,[3]
   d. Normal modes of the structure matched to aperture fields resulting from an exterior region expansion of free space modes.[4]

Using these techniques, the solution is achieved by enforcing the boundary conditions for the fields at a sufficient number of points to specify the surfaces of the structure, and to obtain a set of simultaneous equations for the modal coefficients.

2. Integral equation solutions, set up at either
   a. Surfaces of the structure,[5]
   b. Internal volumes of the structure,[6]
   c. Surfaces of a structure with aperture.[7]

Here, the solution is achieved by enforcing the integral equation at a sufficient number of points to specify the surfaces or volume of the structure, using the method of moments[8] to obtain a set of simultaneous equations for the electromagnetic fields at each enforcement point.

3. Variational solutions, employing specifically the finite element solution of the Helmholtz equation within an unbounded region.[9] Here, the solution is obtained by enforcing the variational principal to obtain a set of simultaneous equations for either field variables or expansion coefficients.

In principle, the accuracy of frequency domain methods is excellent if a sufficiently large set of simultaneous equations is solved. However, each method may have one of two problems when complicated structures are considered. First, excessive computer storage may be required. Second, an excessively complex derivation of the matrix elements may be required. We now consider these possibilities in the context of modeling the interior fields of an arbitrary structure having dimensions on the order of one wavelength.

To illustrate the problem of excessive computer storage requirements, consider the integral equation technique of Ref. 6. Using the authors' maximum allowed solution point spacing of 1/4 wavelength, a total of about $3 \times 4^3 = 192$ equations must be solved to determine the 3 rectangular components of the electric field (or magnetic field) at each of the approximately 4^3 points of the structure. For this case, a maximum of $192^2 \simeq 37{,}000$ interaction coefficients must be stored in the computer to allow inversion of the system matrix, assuming no matrix bandlimiting. Yet, a 1/4 wavelength resolution might be much too coarse to resolve needed details of the structure. If a solution point spacing of 1/8 wavelength is selected, the number, N, of simultaneous equations increases to $3 \times 8^3 = 1536$, and a total of $N^2 \simeq 2.3 \times 10^6$ coefficients must be stored, a 64-fold increase over the previous case. It is seen that, for a fixed structure geometry, the required computer storage varies approximately as the inverse of the sixth power of the resolution. Conversely, for a fixed resolution, the required storage varies as the sixth power of the structure's characteristic dimension. This extremely rapid rate of increase limits the application of

many frequency domain techniques to either two-dimensional irradiation problems (infinitely long cylinders of constant cross section), or simple three-dimensional problems (bodies of revolution, wire grid models of conducting surfaces), which can be solved with relatively few simultaneous equations.

To illustrate the problem of an excessively complex derivation of the matrix elements, we consider the technique of Ref. 2. For each dielectric medium of the arbitrary structure, we would have to assume two field expansions: one inside the medium, and one outside the medium. Field matching would be performed at enough points along the surface of each medium so that its shape would be outlined. At each field matching point, an analytic continuation of the interior and exterior fields would be formulated. Continuation of the interior fields for some media would require multiple individual continuations, to account for elongated geometries, implying multiple summations of spherical Bessel functions. Any change of the structure geometry would require a recalculation of virtually every matrix element involving new analytic continuations. Although the size of the matrix obtained with this method is not excessive, the derivation of the matrix elements is complicated, with the complexity of the derivation a function of the inhomogeneities and geometry of the structure. This implies that a long program development time is required for each new problem.

2.2 Previous Time Domain Techniques

Most previous time domain techniques can be placed in the following four classes:

1. Inverse Fourier transforms of frequency domain solutions, either
   a. Obtained from previously calculated frequency domain solutions[1] possibly via the fast Fourier transform,[10]
   b. Derived in the form of a time convolution.[11]
2. Transformed s-plane methods, for example using
   a. Field expansions, matching at apertures, and the method of moments,[12]
   b. Singularity expansion methods.[13]

3. Integral equation solutions, for example, of the magnetic field, yielding the surface current density induced on bodies of revolution.[14]

4. Transmission line models[15] and antenna models[16] of induced currents and coupling at apertures.

The first class of time domain techniques is seen to suffer the computer storage problems inherent in frequency domain methods, with the added complexity of requiring Fourier transform computational processing. For the second class, field expansion and solution via the method of moments leads again to computer storage problems, while the singularity expansion method is useful for determining the exterior surface current and scattered field, rather than the internal field distribution. The third class of techniques requires computer storage of the surface current and its time derivative at all surface points, for all times between the start of irradiation and the observation time. This again leads to computer storage problems, as did method of moments techniques discussed before. The last group of techniques is suitable principally for thin diameter, cylinder-like structures, and cannot account for details of the interiors of the structures.

In summary, these four classes of time domain techniques are probably unsuited for application to shielding and coupling problems requiring a good amount of detail of the interior of the structure of interest. Computer storage is again a significant problem, as it was for the available frequency domain techniques. The FD-TD method, discussed next, still has the important advantage of allowing excellent resolution of the details of the interior of a structure without exhausting the storage available in large, modern-day computers.

3.0 THE FD-TD METHOD

This section will discuss the following topics relevant to the use of the FD-TD method: 1) a brief history of the development of the method; 2) the basic ideas behind the method; 3) its advantages over the present commonly used approaches; 4) computational details; and 5) past usages and results.

3.1 Development of the Method

The basic finite-difference lattice structure and time stepping algorithm for the FD-TD method was presented by Yee in a 1966 paper.[17] Yee, however, was unable to solve the problems of reflection of outgoing waves at the lattice truncations and the generation of a long pulse or continuous wave without elongating the lattice. Therefore, his results were only of limited use for practical coupling and shielding problems.

The principal investigator of the present contract performed the basic research needed to fully develop the FD-TD method as part of his doctoral dissertation[18] at Northwestern University (1975). The developments included satisfactory approximations to the free space condition at the lattice truncations, and the simulation of a long duration pulse or continuous wave incident on the structure of interest. The basic concepts of the FD-TD method and the initial description of the practical, wave scattering algorithm were presented in a paper in August 1975.[19] This paper applied the method to solve for the standing wave pattern within circular dielectric cylinders subjected to microwave irradiation. Additional problems of this type, dealing with a square dielectric cylinder and a dielectric sphere were solved using the FD-TD method as part of the dissertation. In each of these cases, the availability of exact analytic solutions permitted comparison with the results of the FD-TD method, and the determination of an error bound.

Recognizing that the FD-TD method is ideal for modeling dielectric structures of considerable complexity and inhomogeneity, the principal investigator applied the method to an important and previously incalculable problem, the solution of the electromagnetic fields and induced heating potential within the human eye subjected to microwave irradiation. The

FD-TD method permitted the modeling of the human eye and the various tissues of the bony orbit surrounding the eye in great detail. The results of this study were published in a paper in November 1975.[20] Experimental work performed by others using rabbits has tended to confirm the predictions of the FD-TD eye model.

3.2 Basic Ideas

3.2.1 Wave Tracking

The FD-TD method achieves its flexibility by programming the two fundamental equations of classical electromagnetic theory; Maxwell's time dependent curl equations. Using this method, we can model the propagation of an arbitrary pulsed or continuous wave EM field into a volume of space containing either a dielectric or conducting structure. By time-stepping, i.e., repeatedly solving the finite-difference analog of the curl equations at each point of a space lattice containing the structure of interest, we actually track the incident wave as it first propagates to the structure, and then interacts with it in some way (surface current excitation, diffusion, penetration, etc.). Wave tracking is completed for pulsed irradiation when the desired early or late time behavior is observed; for sinusoidal irradiation, the end point is the attainment of the sinusoidal steady state.

Time-stepping for the FD-TD method is accomplished by what is termed an explicit finite-difference procedure. Here, the value of an electromagnetic field component at the latest time step is computed using only field quantities found during the previous time step, and stored in the computer memory. For example, a particular electric field component, E_x, to be evaluated at point, P, of the finite-difference lattice, is computed using the stored value of E_x at P and the stored values of the magnetic field components, H_y and H_z, at the lattice points immediately adjacent to P. In this way, the unknown field quantity is an explicit function of known field quantities. Thus, no simultaneous equations are needed to compute the fields at the latest time step. Further, computation can proceed one lattice point at a time, and the new field value at each point can be placed immediately in memory.

3.2.2 Modeling the Structure of Interest

The finite-difference formulation of the FD-TD method allows the simple and straightforward modeling of arbitrary dielectric/conducting structures. This is because the space containing the model of the structure is divided up into discrete volumes, or unit cells. The simplest case is that of a cubic unit cell, which results in a cubic lattice approximation of the geometry. For this case, the structure of interest is mapped into the space lattice by first choosing the dimensions of the unit cell, and then assigning appropriate values of electrical permittivity and conductivity to each unit cell of the lattice. Thus, inhomogeneities or fine details of the structure can be modeled with a maximum resolution of one unit cell; thin surfaces can be modeled as infinitely thin, stepped-edge sheets. The computer program is written so that only a set of data cards is required to specify the complete geometry and dielectric characteristics of an arbitrary structure. No special handling of electromagnetic boundary conditions at media interfaces is required because the Maxwell curl equations generate these conditions in a natural way by themselves. Therefore, the basic computer program need not be modified to change from structure to structure, assuming that the lattice volume used is sufficient to fully contain each structure.

3.2.3 The Lattice Truncation Conditions

A basic problem with any finite-difference solution of Maxwell's equations in an unbounded region is the treatment of the field vector components at the lattice truncation. Because of computer storage limitations, the lattice must terminate close to the model structure in a region where the nature of the scattered wave is not clearly known. Proper truncation of the lattice requires that any outgoing wave disappears at the lattice boundary without reflection during the continuous time stepping of the algorithm. Improper truncation would cause error for all time steps after the spurious wave reflections return to the vicinity of the model structure.

The FD-TD method achieves an excellent approximation of reflection-free lattice truncations. This is accomplished by the introduction of a small, anisotropic loss into the region external to the model structure and

a wave-field propagation condition at each truncation point. It can be shown that the resulting error due to spurious wave reflections at the lattice truncations is reduced to less than about five percent by using this technique.

3.2.4 The Plane Wave Source Condition

Another basic problem with any finite-difference solution of Maxwell's equations in an unbounded region is the generation of a long duration pulse or a continuous sinusoidal wave. Although such a wave could be programmed as an initial condition, this would result in a waste of computer storage because the lattice would have to be elongated to initially contain the full pulse or wave train. Another possibility would be to vary the electric field at all points along one end face of the lattice in a pulsed or sinusoidal manner. This lattice plane would then radiate the desired plane wave toward the model structure. However, such a specification of field values at a lattice truncation plane, without consideration of the values of any possible outgoing scattered waves, would cause undesired reflection of such waves and significant error, as discussed in the previous topic.

The FD-TD method achieves an excellent simulation of a long duration pulse or a continuous sinusoidal wave without requiring any additional computer storage or causing any additional wave reflections. This is accomplished by using a program instruction which simulates the linear superposition of an arbitrary incoming plane wave with the ambient scattered fields at all points on a single, transverse lattice plane located between the model structure and one of the lattice truncation planes. The desired incident wave is generated at the superposition plane. But, most importantly, any outgoing scattered wave can propagate right through the wave source plane without reflection and reach the lattice truncation plane beyond to be absorbed. This condition simulates an arbitrary plane wave originating at infinity, and a scattered wave returning to infinity, without permitting any interaction between the two waves except at the model structure. It can be shown that the error resulting from this simulation is negligible (less than one percent).

3.3 Advantages

The FD-TD method has the following advantages relative to available frequency domain and time domain techniques for electromagnetic coupling and shielding problems.

1. The required computer storage of the FD-TD method increases only as the third-power of the ratio of overall structure size to spatial resolution, regardless of the internal complexity of the structure. Other computer techniques which require the solution of simultaneous equations usually have a sixth-power dependence on the size-to-resolution ratio for complex, inhomogeneous structures. This is a fundamental dimensional advantage for the FD-TD method which allows it to model geometries not solvable by any other procedure.

2. The FD-TD method can model the surfaces, apertures, and interiors of complex structures in a straightforward manner on a finite-difference lattice. Only a data card deck need be punched to specify the geometry of an arbitrary scatterer or shield. The maximum resolution is limited only by the size of the basic lattice unit cell.

3. The FD-TD method can model structures with square corners in a natural way if a cubic finite-difference lattice is used. This avoids the problem of dealing with the current and field singularities often found at corners, which lead to slow convergence or erroneous results with other approaches.

4. The FD-TD method allows a natural and simple treatment of the following cases which are difficult or impossible to handle in any other way:

   a. Dielectrics, conductors, and permeable media which are anisotropic and/or nonlinear;

   b. Charged particles or other ionized media within the structure, due possibly to system generated EMP;

c. Irradiation sources which are either continuous wave, pulsed, amplitude modulated, or frequency modulated;

d. Irradiation source or material boundaries which are moving at relativistic speeds.

5. The FD-TD method allows a unified treatment of free space irradiation problems, waveguide obstacle problems, or combinations of the above, i.e., waveguide applicators for diathermy or hyperthermia, waveguide antennas, etc.

3.4 Computational Details for a Uniform, Cubic Lattice

3.4.1 System of Finite-Difference Equations

Using the MKS system of units, and assuming that the dielectric parameters, μ, ε, and σ, are independent of time, the following system of scalar equations is equivalent to Maxwell's equations in the rectangular coordinate system (x, y, z):

$$\frac{\partial H_x}{\partial t} = \frac{1}{\mu}\left(\frac{\partial E_y}{\partial z} - \frac{\partial E_z}{\partial y}\right) \tag{1a}$$

$$\frac{\partial H_y}{\partial t} = \frac{1}{\mu}\left(\frac{\partial E_z}{\partial x} - \frac{\partial E_x}{\partial z}\right) \tag{1b}$$

$$\frac{\partial H_z}{\partial t} = \frac{1}{\mu}\left(\frac{\partial E_x}{\partial y} - \frac{\partial E_y}{\partial x}\right) \tag{1c}$$

$$\frac{\partial E_x}{\partial t} = \frac{1}{\varepsilon}\left(\frac{\partial H_z}{\partial y} - \frac{\partial H_y}{\partial z} - \sigma E_x\right) \tag{1d}$$

$$\frac{\partial E_y}{\partial t} = \frac{1}{\varepsilon}\left(\frac{\partial H_x}{\partial z} - \frac{\partial H_z}{\partial x} - \sigma E_y\right) \tag{1e}$$

$$\frac{\partial E_z}{\partial t} = \frac{1}{\varepsilon}\left(\frac{\partial H_y}{\partial x} - \frac{\partial H_x}{\partial y} - \sigma E_z\right) \tag{1f}$$

Yee[17] originally introduced a set of finite-difference equations for the

system of Equations (1a) - (1f). Following Yee's notation, we denote a space point in a cubic lattice as

$$(i,j,k) = (i\delta, j\delta, k\delta) \tag{2}$$

and any function of space and time as

$$F^n(i,j,k) = F(i\delta, j\delta, k\delta, n\delta t), \tag{3}$$

where $\delta = \delta x = \delta y = \delta z$ is the space increment, δt is the time increment, and i, j, k, and n are integers. Yee used centered finite-difference expressions for the space and time derivatives that are both simply programmed and second-order accurate in δ and in δt, respectively:

$$\frac{\partial F^n(i,j,k)}{\partial x} = \frac{F^n(i+\frac{1}{2},j,k) - F^n(i-\frac{1}{2},j,k)}{\delta} + O(\delta^2) \tag{4}$$

$$\frac{\partial F^n(i,j,k)}{\partial t} = \frac{F^{n+\frac{1}{2}}(i,j,k) - F^{n-\frac{1}{2}}(i,j,k)}{\delta t} + O(\delta t^2) \tag{5}$$

To achieve the accuracy of Equation (4), and to realize all of the space derivatives of Equations (1a) - (1f), Yee positioned the components of $\bar{E}$ and $\bar{H}$ about a unit cell of the lattice as shown in Figure 1. To achieve the accuracy of Equation (5), he evaluated $\bar{E}$ and $\bar{H}$ at alternate half time steps. The result of these assumptions is the following general system of finite-difference equations for the system of Equations (1a) - (1f):

$$H_x^{n+\frac{1}{2}}(i,j+\tfrac{1}{2},k+\tfrac{1}{2}) = H_x^{n-\frac{1}{2}}(i,j+\tfrac{1}{2},k+\tfrac{1}{2}) + \frac{\delta t}{\mu(i,j+\frac{1}{2},k+\frac{1}{2})\delta}\left[E_y^n(i,j+\tfrac{1}{2},k+1) - E_y^n(i,j+\tfrac{1}{2},k) + E_z^n(i,j,k+\tfrac{1}{2}) - E_z^n(i,j+1,k+\tfrac{1}{2})\right] \tag{6a}$$

$$H_y^{n+\frac{1}{2}}(i+\tfrac{1}{2},j,k+\tfrac{1}{2}) = H_y^{n-\frac{1}{2}}(i+\tfrac{1}{2},j,k+\tfrac{1}{2}) + \frac{\delta t}{\mu(i+\frac{1}{2},j,k+\frac{1}{2})\delta}\left[E_z^n(i+1,j,k+\tfrac{1}{2}) - E_z^n(i,j,k+\tfrac{1}{2}) + E_x^n(i+\tfrac{1}{2},j,k) - E_x^n(i+\tfrac{1}{2},j,k+1)\right] \tag{6b}$$

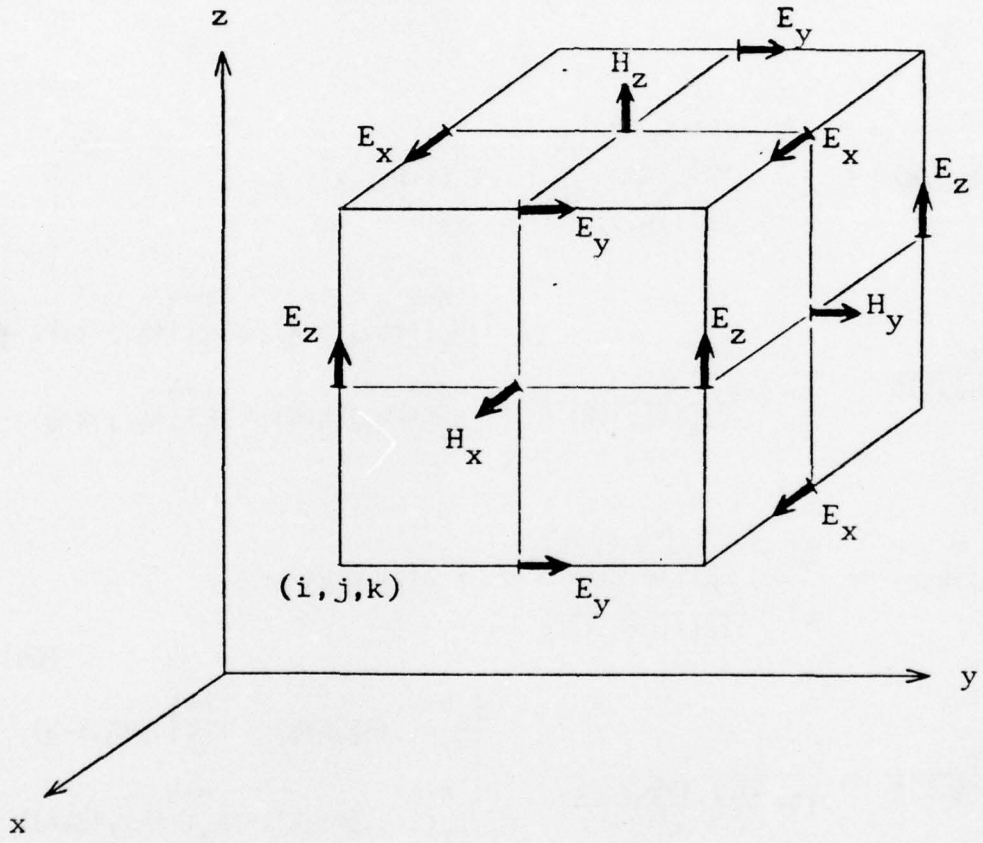

Fig. 1 POSITIONS OF THE FIELD COMPONENTS ABOUT A UNIT CELL OF THE YEE LATTICE

$$H_z^{n+\frac{1}{2}}(i+\tfrac{1}{2},j+\tfrac{1}{2},k) = H_z^{n-\frac{1}{2}}(i+\tfrac{1}{2},j+\tfrac{1}{2},k) +$$

$$\frac{\delta t}{\mu(i+\frac{1}{2},j+\frac{1}{2},k)\delta}\left[\begin{matrix} E_x^{n}(i+\frac{1}{2},j+1,k) - E_x^{n}(i+\frac{1}{2},j,k) + \\ E_y^{n}(i,j+\frac{1}{2},k) - E_y^{n}(i+1,j+\frac{1}{2},k)\end{matrix}\right] \qquad (6c)$$

$$E_x^{n+1}(i+\tfrac{1}{2},j,k) = \frac{\left[1 - \frac{\sigma(i+\frac{1}{2},j,k)\delta t}{2\varepsilon(i+\frac{1}{2},j,k)}\right]}{\left[1 + \frac{\sigma(i+\frac{1}{2},j,k)\delta t}{2\varepsilon(i+\frac{1}{2},j,k)}\right]} \cdot E_x^{n}(i+\tfrac{1}{2},j,k) +$$

(6d)

$$\frac{\delta t}{\varepsilon(i+\frac{1}{2},j,k)\delta} \cdot \frac{1}{\left[1 + \frac{\sigma(i+\frac{1}{2},j,k)\delta t}{2\varepsilon(i+\frac{1}{2},j,k)}\right]} \cdot \left[\begin{matrix} H_z^{n+\frac{1}{2}}(i+\frac{1}{2},j+\frac{1}{2},k) - H_z^{n+\frac{1}{2}}(i+\frac{1}{2},j-\frac{1}{2},k) + \\ H_y^{n+\frac{1}{2}}(i+\frac{1}{2},j,k-\frac{1}{2}) - H_y^{n+\frac{1}{2}}(i+\frac{1}{2},j,k+\frac{1}{2})\end{matrix}\right]$$

$$E_y^{n+1}(i,j+\tfrac{1}{2},k) = \frac{\left[1 - \frac{\sigma(i,j+\frac{1}{2},k)\delta t}{2\varepsilon(i,j+\frac{1}{2},k)}\right]}{\left[1 + \frac{\sigma(i,j+\frac{1}{2},k)\delta t}{2\varepsilon(i,j+\frac{1}{2},k)}\right]} \cdot E_y^{n}(i,j+\tfrac{1}{2},k) +$$

(6e)

$$\frac{\delta t}{\varepsilon(i,j+\frac{1}{2},k)\delta} \cdot \frac{1}{\left[1 + \frac{\sigma(i,j+\frac{1}{2},k)\delta t}{2\varepsilon(i,j+\frac{1}{2},k)}\right]} \cdot \left[\begin{matrix} H_x^{n+\frac{1}{2}}(i,j+\frac{1}{2},k+\frac{1}{2}) - H_x^{n+\frac{1}{2}}(i,j+\frac{1}{2},k-\frac{1}{2}) + \\ H_z^{n+\frac{1}{2}}(i-\frac{1}{2},j+\frac{1}{2},k) - H_z^{n+\frac{1}{2}}(i+\frac{1}{2},j+\frac{1}{2},k)\end{matrix}\right]$$

$$E_z^{n+1}(i,j,k+\tfrac{1}{2}) = \frac{\left[1 - \frac{\sigma(i,j,k+\frac{1}{2})\delta t}{2\varepsilon(i,j,k+\frac{1}{2})}\right]}{\left[1 + \frac{\sigma(i,j,k+\frac{1}{2})\delta t}{2\varepsilon(i,j,k+\frac{1}{2})}\right]} \cdot E_z^{n}(i,j,k+\tfrac{1}{2}) +$$

(6f)

$$\frac{\delta t}{\varepsilon(i,j,k+\frac{1}{2})\delta} \cdot \frac{1}{\left[1 + \frac{\sigma(i,j,k+\frac{1}{2})\delta t}{2\varepsilon(i,j,k+\frac{1}{2})}\right]} \cdot \left[\begin{matrix} H_y^{n+\frac{1}{2}}(i+\frac{1}{2},j,k+\frac{1}{2}) - H_y^{n+\frac{1}{2}}(i-\frac{1}{2},j,k+\frac{1}{2}) + \\ H_x^{n+\frac{1}{2}}(i,j-\frac{1}{2},k+\frac{1}{2}) - H_x^{n+\frac{1}{2}}(i,j+\frac{1}{2},k+\frac{1}{2})\end{matrix}\right]$$

With the system of Equations (6a) - (6f), the new value of a field vector component at any lattice point depends only on its previous value and on the previous values of the components of the other field vector at adjacent points. Therefore, at any given time step, the computation of a field vector may proceed one point at a time.

Many electromagnetic interaction problems involve nonpermeable media and can be approached using a fixed time step and space increment. For such problems (including the cylinder and nose cone geometries specified for this research effort), the quantity $\delta t/\mu(i,j,k)\delta$ is constant for all (i,j,k) of the lattice, and the Yee system of Equations (6a) - (6f) can be simplified to reduce computer running time in the following manner. We define the constants:

$$R = \delta t/2\varepsilon_o \tag{7a}$$

$$R_a = \delta t^2/(\delta^2 \mu_o \varepsilon_o) \tag{7b}$$

$$R_b = \delta t/\mu_o \delta \tag{7c}$$

$$C_a(m) = \frac{1 - R\sigma(m)/\varepsilon_r(m)}{1 + R\sigma(m)/\varepsilon_r(m)} \tag{7d}$$

$$C_b(m) = \frac{R_a}{\varepsilon_r(m) + R\sigma(m)} \tag{7e}$$

where m is an integer denoting a particular dielectric or conducting medium in the space to be modeled. We also define the proportional electric-field vector

$$\tilde{E} = R_b \bar{E} \tag{8}$$

Using the definitions of Equations (7a) - (7e) and (8), we rewrite Equations (6a) - (6c) as:

$$H_x^{n+\frac{1}{2}}(i,j+\tfrac{1}{2},k+\tfrac{1}{2}) = H_x^{n-\frac{1}{2}}(i,j+\tfrac{1}{2},k+\tfrac{1}{2}) + \tilde{E}_y^n(i,j+\tfrac{1}{2},k+1) - \tilde{E}_y^n(i,j+\tfrac{1}{2},k) + \tilde{E}_z^n(i,j,k+\tfrac{1}{2}) - \tilde{E}_z^n(i,j+1,k+\tfrac{1}{2}) \tag{9a}$$

$$H_y^{n+\frac{1}{2}}(i+\tfrac{1}{2},j,k+\tfrac{1}{2}) = H_y^{n-\frac{1}{2}}(i+\tfrac{1}{2},j,k+\tfrac{1}{2}) + \tilde{E}_z^{n}(i+1,j,k+\tfrac{1}{2}) - \tilde{E}_z^{n}(i,j,k+\tfrac{1}{2}) + \tilde{E}_x^{n}(i+\tfrac{1}{2},j,k) - \tilde{E}_x^{n}(i+\tfrac{1}{2},j,k+1) \quad (9b)$$

$$H_z^{n+\frac{1}{2}}(i+\tfrac{1}{2},j+\tfrac{1}{2},k) = H_z^{n-\frac{1}{2}}(i+\tfrac{1}{2},j+\tfrac{1}{2},k) + \tilde{E}_x^{n}(i+\tfrac{1}{2},j+1,k) - \tilde{E}_x^{n}(i+\tfrac{1}{2},j,k) + \tilde{E}_y^{n}(i,j+\tfrac{1}{2},k) - \tilde{E}_y^{n}(i+1,j+\tfrac{1}{2},k) \quad (9c)$$

This modification eliminates the three multiplications needed by Yee in the $\overline{H}$ part of the algorithm. Further, we rewrite Equations (6d) - (6f) as:

$m = MEDIA(i+\tfrac{1}{2},j,k)$

$$\tilde{E}_x^{n+1}(i+\tfrac{1}{2},j,k) = C_a(m)\tilde{E}_x^{n}(i+\tfrac{1}{2},j,k) + C_b(m)[H_z^{n+\frac{1}{2}}(i+\tfrac{1}{2},j+\tfrac{1}{2},k) - H_z^{n+\frac{1}{2}}(i+\tfrac{1}{2},j-\tfrac{1}{2},k) + H_y^{n+\frac{1}{2}}(i+\tfrac{1}{2},j,k-\tfrac{1}{2}) - H_y^{n+\frac{1}{2}}(i+\tfrac{1}{2},j,k+\tfrac{1}{2})] \quad (9d)$$

$m = MEDIA(i,j+\tfrac{1}{2},k)$

$$\tilde{E}_y^{n+1}(i,j+\tfrac{1}{2},k) = C_a(m)\tilde{E}_y^{n}(i,j+\tfrac{1}{2},k) + C_b(m)[H_x^{n+\frac{1}{2}}(i,j+\tfrac{1}{2},k+\tfrac{1}{2}) - H_x^{n+\frac{1}{2}}(i,j+\tfrac{1}{2},k-\tfrac{1}{2}) + H_z^{n+\frac{1}{2}}(i-\tfrac{1}{2},j+\tfrac{1}{2},k) - H_z^{n+\frac{1}{2}}(i+\tfrac{1}{2},j+\tfrac{1}{2},k)] \quad (9e)$$

$m = MEDIA(i,j,k+\tfrac{1}{2})$

$$\tilde{E}_z^{n+1}(i,j,k+\tfrac{1}{2}) = C_a(m)\tilde{E}_z^{n}(i,j,k+\tfrac{1}{2}) + C_b(m)[H_y^{n+\frac{1}{2}}(i+\tfrac{1}{2},j,k+\tfrac{1}{2}) - H_y^{n+\frac{1}{2}}(i-\tfrac{1}{2},j,k+\tfrac{1}{2}) + H_x^{n+\frac{1}{2}}(i,j-\tfrac{1}{2},k+\tfrac{1}{2}) - H_x^{n+\frac{1}{2}}(i,j+\tfrac{1}{2},k+\tfrac{1}{2})] \quad (9f)$$

This modification eliminates the need for computer storage of separate ε and σ arrays. Now, only a MEDIA array which specifies the type-integer of the dielectric or conducting medium at the location of each electric field

component in the lattice need be stored. In addition, the ε_r and σ of each medium can now be changed without having to re-punch a large data card deck, if the basic structure geometry is unchanged. Such a change involves only the recalculation of the few values of $C_a(m)$ and $C_b(m)$.

3.4.2 Choice of Space and Time Increments

The choice of δ and δt is motivated by the reasons of accuracy and algorithm stability, respectively. To insure the accuracy of the computed spatial derivatives of the electromagnetic fields, δ must be small compared to a wavelength (usually $\leq \lambda/10$). Further, to insure that the cubic lattice approximation to the surfaces of the structure modeled is not too coarse, δ must be small compared to the overall dimensions of the structure.

To insure the stability of the time-stepping algorithm of Equations (9a) - (9f), δt is chosen to satisfy the inequality

$$\delta t \leq \left(\frac{1}{\delta x^2} + \frac{1}{\delta y^2} + \frac{1}{\delta z^2}\right)^{-\frac{1}{2}} c_{max}^{-1} \tag{10}$$

$$\leq \frac{\delta}{c_{max}\sqrt{3}} \quad \text{(for a cubic lattice)}$$

where c_{max} is the maximum wave phase velocity within the model. The corresponding stability criterion set forth by Yee in Equations (7) and (8) of his paper is incorrect. The derivation of Equation (10) is outlined as follows.

Derivation of the Stability Criterion

For convenience, we consider a normalized region of space with $\mu = 1$, $\varepsilon = 1$, $\sigma = 0$, and $c = 1$. Letting $j = \sqrt{-1}$, we rewrite Maxwell's equations as

$$j \nabla \times (\bar{H} + j\bar{E}) = \partial(\bar{H} + j\bar{E})/\partial t, \tag{11a}$$

or more simply as

$$j \nabla \times \bar{V} = \partial\bar{V}/\partial t, \quad \text{where } \bar{V} = \bar{H} + j\bar{E}. \tag{11b}$$

The stability of a particular numerical representation of Equation (11b) can be examined simply by considering the following pair of eigenvalue problems:

$$\partial/\partial t\Big|_{\text{numerical}} \overline{V} = \lambda \overline{V} \tag{12a}$$

$$j\,\nabla\Big|_{\text{numerical}} \times \overline{V} = \lambda \overline{V}. \tag{12b}$$

Using the numerical time derivative given by Equation (5), Equation (12a) gives

$$(\overline{V}^{\,n+\frac{1}{2}} - \overline{V}^{\,n-\frac{1}{2}})/\delta t = \lambda \overline{V}^{\,n}. \tag{13}$$

Defining a solution growth factor $q = \overline{V}^{\,n+\frac{1}{2}}/\overline{V}^{\,n-\frac{1}{2}}$, and substituting into Equation (13), we solve for q:

$$q = \lambda\delta t/2 \pm \sqrt{1 + (\lambda\delta t/2)^2}. \tag{14}$$

Algorithm stability requires that $|q| \leq 1$ for all possible spatial modes in the lattice. For this to occur,

$$\text{Re}\,\lambda = 0; \quad |\text{Im}\,\lambda| \leq 2/\delta t. \tag{15}$$

We now let

$$\overline{V}(\ell,m,n) = \overline{V}_o \exp[j(k_x \ell\delta x + k_y m\delta y + k_z n\delta z)] \tag{16}$$

represent an arbitrary lattice spatial mode. Using the numerical space derivation formulation of Equation (4), Equation (12b) yields

$$-2\left[\frac{\sin(\frac{1}{2}k_x\delta x)}{\delta x}, \frac{\sin(\frac{1}{2}k_y\delta y)}{\delta y}, \frac{\sin(\frac{1}{2}k_z\delta z)}{\delta z}\right] \times \overline{V}(\ell,m,n) = \lambda\overline{V}(\ell,m,n). \tag{17}$$

After performing the cross product and writing the x, y, and z component equations, the resulting system is solved for λ^2:

$$\lambda^2 = -4\left[\frac{\sin^2(\frac{1}{2}k_x\delta x)}{\delta x^2} + \frac{\sin^2(\frac{1}{2}k_y\delta y)}{\delta y^2} + \frac{\sin^2(\frac{1}{2}k_z\delta z)}{\delta z^2}\right] \tag{18}$$

For all possible k_x, k_y, k_z,

$$\text{Re}\,\lambda = 0; \quad |\text{Im}\,\lambda| \leq 2\left(\frac{1}{\delta x^2} + \frac{1}{\delta y^2} + \frac{1}{\delta z^2}\right)^{\frac{1}{2}}. \tag{19}$$

To satisfy the stability condition of Equation (15) for the arbitrary lattice spatial mode, we set

$$2\left(\frac{1}{\delta x^2} + \frac{1}{\delta y^2} + \frac{1}{\delta z^2}\right)^{\frac{1}{2}} \leq 2/\delta t. \qquad (20)$$

The algorithm stability condition follows immediately from Equation (20). In an inhomogeneous region of space, it is difficult to determine a spectrum of λ, analogous to Equation (19), for all possible lattice spatial modes. For absolute algorithm stability, Equation (10) suffices because it represents a "worst case" choice of δt.

3.4.3 Lattice Truncation Conditions

A basic consideration with the FD-TD lattice is the treatment of the field vector components at the lattice truncation planes. Inspection of Equations (9a) - (9f) indicates that the values of such components cannot be determined from the system of finite-difference equations because of the centered nature of the spatial derivatives. Therefore, these values must be computed using an auxiliary truncation condition. However, great care must be taken because this condition must not cause the spurious reflection of waves scattered outward from the structure modeled, as observed by Yee. The goal of formulating the truncation condition is to make the lattice truncation planes invisible to all possible waves propagating within the lattice, as shown in Figure 2.

A desirable truncation condition relates in a simple way the values of the field components at the truncation planes to field component values at points one or more δ within the lattice. We now consider examples of such a truncation for cases of FD-TD lattices in one and three dimensions.

One-Dimensional Case

For simplicity, we consider waves having only the $\tilde{E}_z$ and H_x components and propagating in the $\pm y$ directions. The one-dimensional FD-TD lattice is simply a y-directed line of points having the $\tilde{E}_z$ and H_x components interleaved and separated from each other by 0.5 δy. The lattice is assumed to extend from an $\tilde{E}_z$ component at point $y = 0$ to another $\tilde{E}_z$ component at point $y = J\delta y$. A time step of $\delta t = \delta y/c$ is used; a value which is the maximum allowed by the stability condition of Equation (10) for this lattice ($\delta x = \delta z = \infty$).

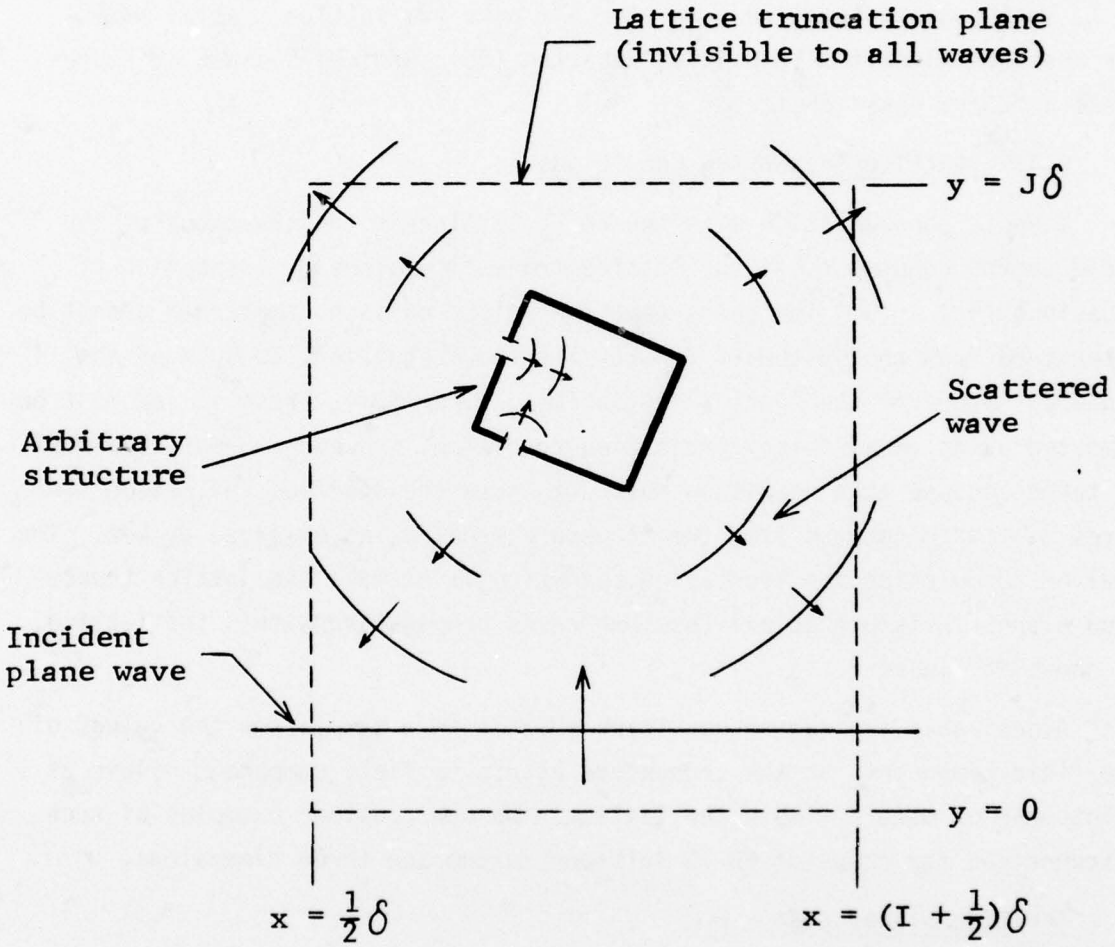

Fig. 2 IDEAL FD-TD LATTICE TRUNCATION CONDITIONS

Subject to these assumptions, the truncation condition at point y = 0,

$$\tilde{E}_z^n(0) = \tilde{E}_z^{n-1}(1) \tag{21a}$$

simulates the free space propagation of the magnitude of $\tilde{E}_z$ from the point "1" to the truncation point "0" in one time step (the free-space propagation delay implied by the time-step relation). This is an exact truncation for this lattice in that all possible -y-directed waves are absorbed at 0 without reflection. If we wish to simulate the truncation of the lattice at point y = Jδ, the truncation condition

$$\tilde{E}_z^n(J) = \tilde{E}_z^{n-1}(J-1) \tag{21b}$$

is exact for all possible +y-directed waves at this point.

Three-Dimensional Case

Here, we consider waves having all six field components and propagating in all possible directions. The lattice is assumed to extend from:

H_y and H_z components at $x = \frac{1}{2}\delta$ to

H_y and H_z components at $x = (I + \frac{1}{2})\delta$;

$\tilde{E}_x$ and $\tilde{E}_z$ components at y = 0 to

$\tilde{E}_x$ and $\tilde{E}_z$ components at $y = J\delta$;

$\tilde{E}_x$ and $\tilde{E}_y$ components at z = 0 to

$\tilde{E}_x$ and $\tilde{E}_y$ components at $z = K\delta$.

A time step of $\delta t = \delta/2c$ is used, a value which is about 13% lower than the maximum allowed ($\delta t = \delta/\sqrt{3}\ c$) by the stability condition of Equation (10) for this lattice ($\delta x = \delta y = \delta z = \delta$).

No simple, exact truncation condition, analogous to Equations (21a) and (21b), is apparent for this three-dimensional space lattice. This is because we cannot assume the outgoing waves to be plane and normally incident on one lattice boundary. At any truncation point, the local angle of incidence of these waves relative to the truncation plane is unknown. Further, several

different waves having different local angles of incidence may arrive at the same time. No simple truncation condition can account for all of these possibilities. Therefore, we can arrive at only an approximate condition that reduces the effective lattice boundary reflection coefficient to an acceptable level.

A set of simple, approximate truncation conditions that can be used with good results is as follows.

<u>At x = ½ δ</u>:

$$H_y^n(\tfrac{1}{2},j,k+\tfrac{1}{2}) = [H_y^{n-2}(3/2,j,k-\tfrac{1}{2}) + H_y^{n-2}(3/2,j,k+\tfrac{1}{2}) + H_y^{n-2}(3/2,j,k+3/2)]/3 \quad (22a)$$

$$H_z^n(\tfrac{1}{2},j+\tfrac{1}{2},k) = [H_z^{n-2}(3/2,j+\tfrac{1}{2},k-1) + H_z^{n-2}(3/2,j+\tfrac{1}{2},k) + H_z^{n-2}(3/2,j+\tfrac{1}{2},k+1)]/3 \quad (22b)$$

<u>At x = (I + ½) δ</u>:

$$H_y^n(I+\tfrac{1}{2},j,k+\tfrac{1}{2}) = [H_y^{n-2}(I-\tfrac{1}{2},j,k-\tfrac{1}{2}) + H_y^{n-2}(I-\tfrac{1}{2},j,k+\tfrac{1}{2}) + H_y^{n-2}(I-\tfrac{1}{2},j,k+3/2)]/3 \quad (22c)$$

$$H_z^n(I+\tfrac{1}{2},j+\tfrac{1}{2},k) = [H_z^{n-2}(I-\tfrac{1}{2},j+\tfrac{1}{2},k-1) + H_z^{n-2}(I-\tfrac{1}{2},j+\tfrac{1}{2},k) + H_z^{n-2}(I-\tfrac{1}{2},j+\tfrac{1}{2},k+1)]/3 \quad (22d)$$

<u>At y = 0</u>:

$$E_x^n(i+\tfrac{1}{2},0,k) = E_x^{n-2}(i+\tfrac{1}{2},1,k) \quad (23a)$$

$$E_z^n(i,0,k+\tfrac{1}{2}) = E_z^{n-2}(i,1,k+\tfrac{1}{2}) \quad (23b)$$

<u>At y = J δ</u>:

$$E_x^n(i+\tfrac{1}{2},J,k) = E_x^{n-2}(i+\tfrac{1}{2},J-1,k) \quad (23c)$$

$$E_z^n(i,J,k+\tfrac{1}{2}) = E_z^{n-2}(i,J-1,k+\tfrac{1}{2}) \quad (23d)$$

At z = 0:

$$\tilde{E}_x^n(i+\tfrac{1}{2},j,0) = [\tilde{E}_x^{n-2}(i-\tfrac{1}{2},j,1) + \tilde{E}_x^{n-2}(i+\tfrac{1}{2},j,1) + \tilde{E}_x^{n-2}(i+3/2,j,1)]/3 \quad (24a)$$

$$\tilde{E}_y^n(i,j+\tfrac{1}{2},0) = [\tilde{E}_y^{n-2}(i-1,j+\tfrac{1}{2},1) + \tilde{E}_y^{n-2}(i,j+\tfrac{1}{2},1) + \tilde{E}_y^{n-2}(i+1,j+\tfrac{1}{2},1)]/3 \quad (24b)$$

At z = K δ:

$$\tilde{E}_x^n(i+\tfrac{1}{2},j,K) = [\tilde{E}_x^{n-2}(i-\tfrac{1}{2},j,K-1) + \tilde{E}_x^{n-2}(i+\tfrac{1}{2},j,K-1) + \tilde{E}_x^{n-2}(i+3/2,j,K-1)]/3 \quad (24c)$$

$$\tilde{E}_y^n(i,j+\tfrac{1}{2},K) = [\tilde{E}_y^{n-2}(i-1,j+\tfrac{1}{2},K-1) + \tilde{E}_y^{n-2}(i,j+\tfrac{1}{2},K-1) + \tilde{E}_y^{n-2}(i+1,j+\tfrac{1}{2},K-1)]/3 \quad (24d)$$

Equations (22) - (24) allow the field value at any truncation point to rise to approach the field value of any outgoing wave, thus lowering the effective truncation plane reflection coefficient. This is done by modeling the propagation of an outgoing wave from the lattice plane adjacent to the truncation, to the lattice plane at the truncation, in two time steps (the free-space propagation delay implied by the time-step relation). The averaging process is used to take into account the possible local angles of incidence of the outgoing wave at the truncation and possible multiple incidences.

Truncation conditions (22) - (24) are useful for an assumed +y-directed incident plane wave with field components E_z and H_x. For such a wave, Equation (23) represents exact truncations similar to Equation (21). In addition, Equations (22) and (24) have no effect on the propagation of such a wave, which lacks H_y, H_z, E_x, and E_y. Thus, this set of truncation conditions effectively makes the lattice boundary planes invisible to a +y-directed incident plane wave.

Use of Exterior-Region Anisotropy

One way of reducing spurious reflections at the lattice truncations is to introduce an anisotropic lossy medium outside of the modeled structure. Properly constituted, the medium would attenuate field components present only in the scattered wave, leaving the incident plane wave unaffected.

For the three-dimensional case, this can be easily done by specifying an anisotropic conductivity, σ_{ext}, in the free-space region exterior to the structure. Equation (9f), the finite-difference equation for $\tilde{E}_z$, requires $\sigma_{ext} = 0$ to insure that the incident wave is not attenuated. However, we may assume a small value of σ_{ext} for Equations (9d) and (9c), the finite-difference equations for $\tilde{E}_x$ and $\tilde{E}_y$, without affecting the propagation of the incident wave or the penetrating wave within the structure. This assumption results in attenuation of the $\tilde{E}_x$ and $\tilde{E}_y$ components of the exterior diffracted wave, and thus, reduces z-directed wave reflections at the lattice truncations.

Effect on Algorithm Stability

The stability condition of Equation (10) is valid for the Yee, or null choice, of lattice truncation conditions. This is because Yee's set of truncation conditions causes total reflection of all lattice wave modes at the surface planes of the lattice, and thus, introduces no new wave modes. However, introduction of Equations (22) - (24) to the three-dimensional algorithm is found to increase the strictness of the stability condition. For the three-dimensional case, some case must be taken to avoid algorithm instability.

The nature of the instability of the three-dimensional algorithm is of importance. First, it is late in appearance, requiring more than five-hundred time steps for a 2×10^4 - cell lattice, and more than one-thousand time steps for a 6×10^4 - cell lattice. Second, its initial visibility is delayed by either increasing the size of the lattice, or by increasing the losses of the dielectric media of the lattice. This suggests the importance of wave propagation effects in the growth of the instability.

There are two likely solutions to the problem of algorithm instability. First, δt can be reduced. This, however, would complicate the programming of the truncation conditions because a wave would no longer propagate across a free-space unit cell of the lattice in an integral number of time steps.

The second solution is much simpler since it does not require programming for interpolating field values at the truncation planes between time steps. This solution is merely to set a lower bound of about 10^5 cells

on the size of the FD-TD lattice used, thus delaying the onset of the instability for several thousand time steps. In most cases, such a delay would be sufficient for the computed solution to reach the sinusoidal steady state. For many problems, the use of a 10^5 - cell lattice is not at all extravagant and allows the problem of algorithm instability to be essentially forgotten. The computer runs in the present research program for the cylinder and the missile nose cone employ this solution. They use, respectively, 94,000 cells--800 time steps and 58,000 cells--900 time steps, without any apparent instability of the computed solution.

3.4.4 Plane Wave Source Condition

Another basic consideration with the FD-TD method is the simulation of the continuous, sinusoidal, incident plane wave. Yee specified the shape and direction of propagation of an incident wave pulse by inserting all of its field values as initial conditions over a portion of the lattice. However, the Yee approach is clearly inadequate for a continuous wave train because a very elongated lattice would be needed to contain the wave as an initial condition, wasting much computer storage.

In this section, we discuss the simulation of an incident, +y-directed plane wave using a source condition localized at only one lattice plane, and invisible to all scattered waves propagating within the lattice. This allows a compact lattice and maximum utilization of the available computer storage.

The most simple approach to this problem is to vary the electric field at all points along lattice plane y = 0 in a sinusoidal manner. This plane would then radiate the desired plane wave. However, such a specification of field values at a lattice truncation plane, without consideration of the values of the fields of any possible outgoing, scattered waves, would cause undesired wave reflections.

A more desirable plane wave source condition would take into account the scattered fields at the source plane. For the three-dimensional case, a useful wave source condition at plane $y = j_s\delta$ (near $y = 0$) is as follows:

$$\tilde{E}_z^n(i,j_s,k+\tfrac{1}{2}) \leftarrow R_b \sin(2\pi f n\delta t) + \tilde{E}_z^n(i,j_s,k+\tfrac{1}{2}) \qquad (25)$$

where f is the irradiation frequency and R_b is defined by Equation (7c). Equation (25) is a modification of the Maxwell's equations algorithm for all points on the lattice plane $y = j_s\delta$. At each point on this source plane, the computer first calculates $\tilde{E}_z^n$ in the normal manner of the algorithm, and stores the value in memory. Then, the value of the sinusoid is calculated and added to the stored value of $\tilde{E}_z^n$. Finally, this modified value of $\tilde{E}_z^n$ is stored in memory. In effect, Equation (25) simulates the linear superposition of a +y-directed plane wave and the ambient field along the source plane. This condition permits any scattered, outgoing wave to propagate right through the wave source plane without reflection, and reach the lattice truncation at y = 0 to be absorbed.

3.4.5 Symmetry Conditions

An important savings of computer memory and program execution time results if even symmetry of the modeled structure about one or two lattice planes can be assumed. In this section, we discuss the programming of this symmetry for the three-dimensional case.

For the three-dimensional case, the modeled structure is assumed to be evenly symmetric about lattice planes $x = (\bar{I} + \frac{1}{2})\delta$ and $z = \bar{K}\delta$:

$$\varepsilon,\sigma(I+\tfrac{1}{2}+h,j,k) = \varepsilon,\sigma(\bar{I}+\tfrac{1}{2}-h,j,k), \quad \mu = \mu_o \tag{26a}$$

$$\varepsilon,\sigma(i,j,\bar{K}+h) = \varepsilon,\sigma(i,j,\bar{K}-h) \tag{26b}$$

The incident radiation is assumed to be a +y-directed plane wave, with the field components $\tilde{E}_z$ and H_x naturally having even symmetry about any lattice plane x = constant or z = constant. Therefore, we conclude that the $\tilde{E}_z$ and H_x components of the total field possess even symmetry about the lattice planes $x = (\bar{I}+\frac{1}{2})\delta$ and $z = \bar{K}\delta$:

$$\tilde{E}_z^n(\bar{I}+\tfrac{1}{2}+h,j,k+\tfrac{1}{2}) = \tilde{E}_z^n(\bar{I}+\tfrac{1}{2}-h,j,k+\tfrac{1}{2}) \tag{27a}$$

$$H_x^{n+\frac{1}{2}}(\bar{I}+\tfrac{1}{2}+h,j+\tfrac{1}{2},k+\tfrac{1}{2}) = H_x^{n+\frac{1}{2}}(\bar{I}+\tfrac{1}{2}-h,j+\tfrac{1}{2},k+\tfrac{1}{2}) \tag{27b}$$

$$\tilde{E}_z^n(i,j,\bar{K}+h) = \tilde{E}_z^n(i,j,\bar{K}-h) \tag{27c}$$

$$H_x^{n+\frac{1}{2}}(i,j+\tfrac{1}{2},\bar{K}+h) = H_x^{n+\frac{1}{2}}(i,j+\tfrac{1}{2},\bar{K}-h) \tag{27d}$$

To develop a convenient set of symmetry conditions, we follow a procedure detailed below. This results in

$$\tilde{E}_x^{n+1}(\bar{I}+\tfrac{1}{2},j,k) = H_y^{n+\frac{1}{2}}(\bar{I}+\tfrac{1}{2},j,k+\tfrac{1}{2}) = H_z^{n+\frac{1}{2}}(\bar{I}+\tfrac{1}{2},j+\tfrac{1}{2},k) = 0 \text{ for all } n; \quad (28a)$$

$$H_z^{n+\frac{1}{2}}(i+\tfrac{1}{2},j+\tfrac{1}{2},\bar{K}) = \tilde{E}_x^{n}(i+\tfrac{1}{2},j,\bar{K}) = \tilde{E}_y^{n}(i,j+\tfrac{1}{2},\bar{K}) = 0 \text{ for all } n. \quad (28b)$$

Equations (28a) and (28b) are sufficient to truncate the FD-TD lattice at planes $x = (\bar{I}+\tfrac{1}{2})\delta$ and $z = \bar{K}\delta$, respectively, by permitting the calculation of the complete set of field components, with full specification of the assumed even symmetry.

Derivation of the Symmetry Conditions

A. Plane $x = (\bar{I}+\tfrac{1}{2})\delta$

The symmetry conditions for the $\tilde{E}_x$, H_y, and H_z field components at lattice plane $x = (\bar{I}+\tfrac{1}{2})\delta$ are derived from time-stepping algorithm Equations (9a) - (9d) and symmetry assumptions (26a), (27a), and (27b). The first step of the derivation involves the determination of the type of symmetry exhibited by $\tilde{E}_y$ about plane $x = (\bar{I}+\tfrac{1}{2})\delta$. To begin, we write Equation (9a) for $i = \bar{I}$ and for $i = \bar{I}+1$:

$$H_x^{n+\frac{1}{2}}(\bar{I},j+\tfrac{1}{2},k+\tfrac{1}{2}) = H_x^{n-\frac{1}{2}}(\bar{I},j+\tfrac{1}{2},k+\tfrac{1}{2}) + \tilde{E}_y^{n}(\bar{I},j+\tfrac{1}{2},k+1) - \tilde{E}_y^{n}(\bar{I},j+\tfrac{1}{2},k) + \tilde{E}_z^{n}(\bar{I},j,k+\tfrac{1}{2}) - \tilde{E}_z^{n}(\bar{I},j+1,k+\tfrac{1}{2}) \quad (29a)$$

$$H_x^{n+\frac{1}{2}}(\bar{I}+1,j+\tfrac{1}{2},k+\tfrac{1}{2}) = H_x^{n-\frac{1}{2}}(\bar{I}+1,j+\tfrac{1}{2},k+\tfrac{1}{2}) + \tilde{E}_y^{n}(\bar{I}+1,j+\tfrac{1}{2},k+1) - \tilde{E}_y^{n}(\bar{I}+1,j+\tfrac{1}{2},k) + \tilde{E}_z^{n}(\bar{I}+1,j,k+\tfrac{1}{2}) - \tilde{E}_z^{n}(\bar{I}+1,j+1,k+\tfrac{1}{2}) \quad (29b)$$

Using the symmetry conditions of (27a) and (27b) for the case $h = \tfrac{1}{2}$, we subtract Equation (29b) from (29a) and simplify:

$$\tilde{E}_y^{n}(\bar{I},j+\tfrac{1}{2},k+1) - \tilde{E}_y^{n}(\bar{I}+1,j+\tfrac{1}{2},k+1) = \tilde{E}_y^{n}(\bar{I},j+\tfrac{1}{2},k) - \tilde{E}_y^{n}(\bar{I}+1,j+\tfrac{1}{2},k) \quad (30)$$

Equation (30) is in the form $f(j+\tfrac{1}{2},k+1) = f(j+\tfrac{1}{2},k)$. This implies a solution

of the type $f(j+\frac{1}{2},k) = C_{j+\frac{1}{2}}$, where $C_{j+\frac{1}{2}}$ is a constant. We thus have

$$\tilde{E}_y^n(\bar{I},j+\tfrac{1}{2},k) - \tilde{E}_y^n(\bar{I}+1,j+\tfrac{1}{2},k) = C_{j+\frac{1}{2}}. \tag{31a}$$

We argue that the symmetry of the problem precludes the possibility of a constant step discontinuity of $\tilde{E}_y$ across the plane of symmetry. Therefore, $C_{j+\frac{1}{2}}$ must equal zero and

$$\tilde{E}_y^n(\bar{I},j+\tfrac{1}{2},k) = \tilde{E}_y^n(\bar{I}+1,j+\tfrac{1}{2},k). \tag{31b}$$

Equation (31b) is a statement of the even symmetry of $\tilde{E}_y$ about plane $x = (\bar{I}+\frac{1}{2})\delta$.

Now, we may derive the symmetry conditions for $\tilde{E}_x$, H_y, and H_z at plane $x = (\bar{I}+\frac{1}{2})\delta$. Using symmetry condition (27a) for the case $h = \frac{1}{2}$, we write Equation (9b) for $i = \bar{I}$:

$$H_y^{n+\frac{1}{2}}(\bar{I}+\tfrac{1}{2},j,k+\tfrac{1}{2}) = H_y^{n-\frac{1}{2}}(\bar{I}+\tfrac{1}{2},j,k+\tfrac{1}{2}) + \tilde{E}_x^n(\bar{I}+\tfrac{1}{2},j,k) - \tilde{E}_x^n(\bar{I}+\tfrac{1}{2},j,k+1) \tag{32a}$$

Using the derived symmetry condition of Equation (31b), we write Equation (9c) for $i = \bar{I}$:

$$H_z^{n+\frac{1}{2}}(\bar{I}+\tfrac{1}{2},j+\tfrac{1}{2},k) = H_z^{n-\frac{1}{2}}(\bar{I}+\tfrac{1}{2},j+\tfrac{1}{2},k) + \tilde{E}_x^n(\bar{I}+\tfrac{1}{2},j+1,k) - \tilde{E}_x^n(\bar{I}+\tfrac{1}{2},j,k) \tag{32b}$$

From Equations (32a) and (32b), we see that H_y and H_z at the symmetry plane can depart from their zero initial conditions only if $\tilde{E}_x(\bar{I}+\frac{1}{2},j,k)$ assumes some non-zero values. Yet, from Equation (9d), $\tilde{E}_x$ at the symmetry plane is seen to remain at zero if $H_y(\bar{I}+\frac{1}{2},j,k+\frac{1}{2})$ and $H_z(\bar{I}+\frac{1}{2},j+\frac{1}{2},k)$ are zero. Therefore, using an inductive argument, we conclude that these three field components must remain at zero for all time steps. Equation (28a) is a statement of this behavior.

B. Plane $z = \bar{K}\delta$

The symmetry conditions for the $\tilde{E}_x$, $\tilde{E}_y$, and H_z field components at lattice plane $z = \bar{K}\delta$ are derived from time-stepping algorithm Equations (9c) - (9f) and symmetry assumptions (26b), (27c), and (27d). The first step of

the derivation involves the determination of the type of symmetry exhibited by H_y about plane $z = \bar{K}\delta$. To begin, we write Equation (9f) for $k = \bar{K}-1$ and for $k = \bar{K}$:

$$m_1 = \text{MEDIA}(i,j,\bar{K}-\tfrac{1}{2})$$

$$\tilde{E}_z^{n+1}(i,j,\bar{K}-\tfrac{1}{2}) = C_a(m_1)\tilde{E}_z^{n}(i,j,\bar{K}-\tfrac{1}{2}) + C_b(m_1)[H_y^{n+\frac{1}{2}}(i+\tfrac{1}{2},j,\bar{K}-\tfrac{1}{2}) - H_y^{n+\frac{1}{2}}(i-\tfrac{1}{2},j,\bar{K}-\tfrac{1}{2}) + H_x^{n+\frac{1}{2}}(i,j-\tfrac{1}{2},\bar{K}-\tfrac{1}{2}) - H_x^{n+\frac{1}{2}}(i,j+\tfrac{1}{2},\bar{K}-\tfrac{1}{2})] \quad (33a)$$

$$m_2 = \text{MEDIA}(i,j,\bar{K}+\tfrac{1}{2})$$

$$\tilde{E}_z^{n+1}(i,j,\bar{K}+\tfrac{1}{2}) = C_a(m_2)\tilde{E}_z^{n}(i,j,\bar{K}+\tfrac{1}{2}) + C_b(m_2)[H_y^{n+\frac{1}{2}}(i+\tfrac{1}{2},j,\bar{K}+\tfrac{1}{2}) - H_y^{n+\frac{1}{2}}(i-\tfrac{1}{2},j,\bar{K}+\tfrac{1}{2}) + H_x^{n+\frac{1}{2}}(i,j-\tfrac{1}{2},\bar{K}+\tfrac{1}{2}) - H_x^{n+\frac{1}{2}}(i,j+\tfrac{1}{2},\bar{K}+\tfrac{1}{2})] \quad (33b)$$

Using the symmetry conditions of Equations (26b), (27c), and (27d) for the case $h = \frac{1}{2}$, we subtract Equation (33b) from (33a) and simplify:

$$H_y^{n+\frac{1}{2}}(i+\tfrac{1}{2},j,\bar{K}-\tfrac{1}{2}) - H_y^{n+\frac{1}{2}}(i+\tfrac{1}{2},j,\bar{K}+\tfrac{1}{2}) = H_y^{n+\frac{1}{2}}(i-\tfrac{1}{2},j,\bar{K}-\tfrac{1}{2}) - H_y^{n+\frac{1}{2}}(i-\tfrac{1}{2},j,\bar{K}+\tfrac{1}{2}) \quad (34)$$

Equation (34) is in the form $f(i+\frac{1}{2},j) = f(i-\frac{1}{2},j)$. This implies a solution of the type $f(i+\frac{1}{2},j) = C_j$, where C_j is a constant. We thus have

$$H_y^{n+\frac{1}{2}}(i+\tfrac{1}{2},j,\bar{K}-\tfrac{1}{2}) - H_y^{n+\frac{1}{2}}(i+\tfrac{1}{2},j,\bar{K}+\tfrac{1}{2}) = C_j. \quad (35a)$$

We argue that the symmetry of the problem precludes the possibility of a constant step discontinuity of H_y across the plane of symmetry. Therefore, C_j must equal zero and

$$H_y^{n+\frac{1}{2}}(i+\tfrac{1}{2},j,\bar{K}-\tfrac{1}{2}) = H_y^{n+\frac{1}{2}}(i+\tfrac{1}{2},j,\bar{K}+\tfrac{1}{2}). \quad (35b)$$

Equation (35b) is a statement of the even symmetry of H_y about plane $z = \bar{K}\delta$.

Now, we may derive the symmetry conditions for $\tilde{E}_x$, $\tilde{E}_y$, and H_z at plane $z = \bar{K}\delta$. Using the derived symmetry condition of Equation (35b), we write Equation (9d) for $k = \bar{K}$:

$$m = MEDIA(i+\tfrac{1}{2},j,\bar{K})$$

$$\tilde{E}_x^{n+1}(i+\tfrac{1}{2},j,\bar{K}) = C_a(m)\tilde{E}_x^{n}(i+\tfrac{1}{2},j,\bar{K}) + C_b(m)[H_z^{n+\frac{1}{2}}(i+\tfrac{1}{2},j+\tfrac{1}{2},\bar{K}) - H_z^{n+\frac{1}{2}}(i+\tfrac{1}{2},j-\tfrac{1}{2},\bar{K})] \quad (36a)$$

Using symmetry condition (27d) for the case $h = \frac{1}{2}$, we write Equation (9e) for $k = \bar{K}$:

$$m = MEDIA(i,j+\tfrac{1}{2},\bar{K})$$

$$\tilde{E}_y^{n+1}(i,j+\tfrac{1}{2},\bar{K}) = C_a(m)\tilde{E}_y^{n}(i,j+\tfrac{1}{2},\bar{K}) + C_b(m)[H_z^{n+\frac{1}{2}}(i-\tfrac{1}{2},j+\tfrac{1}{2},\bar{K}) - H_z^{n+\frac{1}{2}}(i+\tfrac{1}{2},j+\tfrac{1}{2},\bar{K})] \quad (36b)$$

From Equations (36a) and (36b), we see that $\tilde{E}_x$ and $\tilde{E}_y$ at the symmetry plane can depart from their zero initial conditions only if $H_z(i+\frac{1}{2},j+\frac{1}{2},\bar{K})$ assumes some non-zero values. Yet, from Equation (9c), H_z at the symmetry plane is seen to remain at zero if $\tilde{E}_x(i+\frac{1}{2},j,\bar{K})$ and $\tilde{E}_y(i,j+\frac{1}{2},\bar{K})$ are zero. Therefore, using an inductive argument, we conclude that these three field components must remain at zero for all time steps. Equation (28b) is a statement of this behavior.

3.5 Review of Past Usages and Results

In this section, we review past usages and results of the FD-TD method for simple two and three-dimensional dielectric geometries, with an objective of establishing the level of accuracy of the method. Three sources of error have been considered: the approximation of the space and time derivatives of Maxwell's equations by finite-difference expressions; the residual wave reflections at the lattice truncations; and the stepped-surface approximation of the shape of a curved scatterer. The computed results used in this discussion were obtained by the principal investigator during his Ph.D. dissertation work in 1974 and 1975.

3.5.1 Irradiation of a Plane Dielectric Slab

First considered as a source of error was the approximation of the space and time derivatives of Maxwell's equations by finite-difference expressions. To isolate this error source, a scattering problem had to be formulated that eliminated error due to the approximations of the shape of the scatterer or of the lattice truncations. Such a problem was the steady plane-wave irradiation (at normal incidence) of a flat dielectric slab, because the boundaries of the slab could be defined exactly by two parallel lattice planes. Further, for a +y-directed incident wave, all scattered waves had to propagate in either the +y or -y directions; a situation where the lattice truncation conditions were exact. Therefore, any observed error in the results could be attributed to the finite-difference approximations of the derivatives.

For ease in understanding the results, the slab was assumed to be lossless and one-half wavelength thick. These conditions were fulfilled by a 3 cm thick slab, with relative permittivity equal to 4, irradiated at 2.5 GHz. The geometry of this slab relative to the problem lattice is detailed in Figure 3a for two lattice resolutions: $\delta = 0.3$ cm $= \lambda_d/20$; and $\delta = 0.6$ cm $= \lambda_d/10$.

Figure 3b graphs the maximum absolute value, or envelope, of $E_z^n(j)$ computed during the wave half-cycle preceding the termination of the algorithm at n_{max}. n_{max} was chosen large enough to allow all values of E_z within the lattice to reach the sinusoidal steady state. For the coarse-lattice case, $\delta t = 10$ psec and the envelope was observed for $130 \leq n \leq 150$. For the fine-lattice case, $\delta t = 5$ psec and the envelope was observed for $250 \leq n \leq 300$. Each case represented an algorithm time of 1500 psec, or 3.75 wave cycles at 2.5 GHz, required to reach the steady state.

For the fine-lattice case, the envelope was virtually indistinguishable from the exact solution calculated from basic microwave theory. In front of the slab, a standing wave ratio of about 1.04 was observed. Within the slab, the envelope decreased to exactly one-half the incident field magnitude. In back of the slab, the envelope was constant and had the same value as the incident field magnitude. These results were in excellent agreement with the exact solution obtained either by viewing the slab as a 1:1 impedance

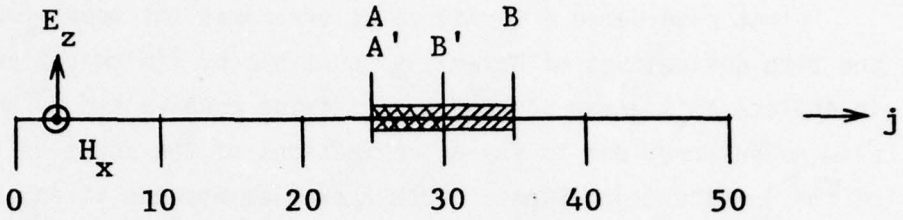

δ = 0.3 cm (slab AB); 0.6 cm (slab A'B')

(a) Geometry

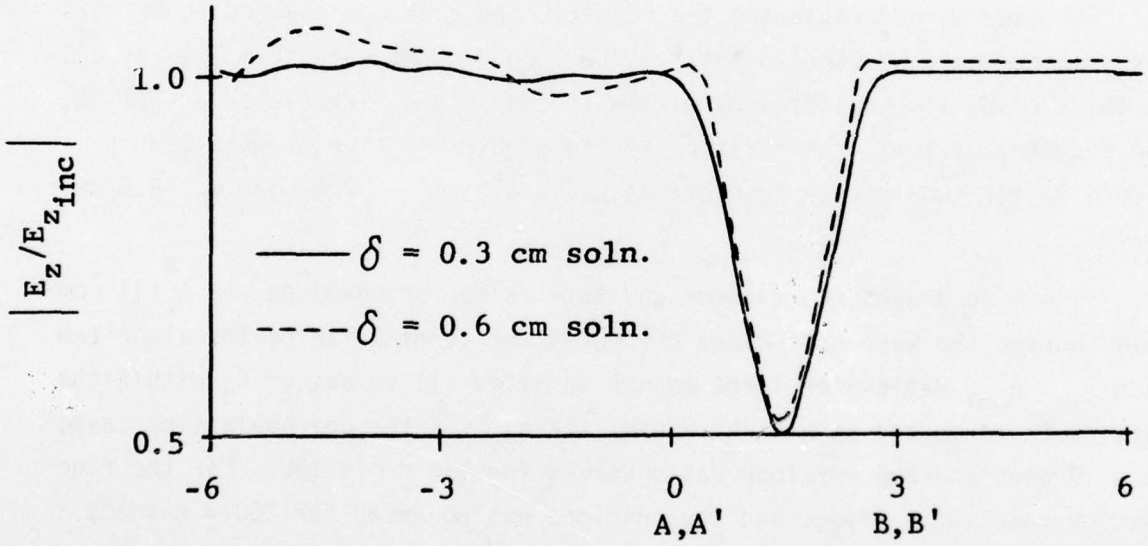

Distance from front face of slab (cm)

(b) Computed Electric Field

Fig. 3 IRRADIATION OF A PLANE DIELECTRIC SLAB

transformer between its two faces, or by using an infinite series approach. The maximum error was about $\pm 2\%$. For the coarse-lattice case, error was evident in the computation of the envelope in front of the slab. Here, a standing wave ratio of about 1.13 was observed. The maximum error was estimated to be about $\pm 7\%$.

To insure that the uncertainty caused by the finite-difference approximations of the field derivatives is significantly less than $\pm 10\%$, it was seen that a lattice resolution of $\delta \leq \lambda/20$ must be maintained. For inhomogeneous scatterers, λ of this criterion should be taken as the minimum value expected within the lattice.

3.5.2 Irradiation of a Square Dielectric Cylinder

Next considered as a source of error was the presence of residual wave reflections due to imperfect lattice truncations. To isolate this error source, a scattering problem had to be formulated that generated a roughly radially-propagating diffracted wave (to test the truncation conditions at non-normal incidence) without having additional error due to any stepped-edge approximation of a curved boundary of the scatterer. Such a problem was the TM irradiation of an infinitely-long, rectangular, dielectric cylinder, with the incident wave propagating normally to one cylinder face. Here, the boundary of the cylinder could be defined exactly by intersecting lattice planes; yet, the desired diffracted wave would be generated. Any error in the results in excess of that observed for the plane dielectric slab problem could thus be directly attributed to spurious wave reflections at the lattice truncation planes.

For ease in understanding the results, the cylinder scattering problem was assumed to have the geometry analyzed by Tong[21] with a surface integral equation approach. Tong's cylinder was composed of lossless dielectric with $\varepsilon_r = 3.84$, and had a square cross section with diameter $d = \lambda_0/\pi$. This condition was fulfilled by a 3.82 cm diameter square cylinder, irradiated at 2.5 GHz. The geometry of this scatterer relative to the problem lattice is detailed in Figure 4a for two lattice resolutions: $\delta = 0.095$ cm $= \lambda_d/64$, for cylinder perimeter ABCD; and $\delta = 0.191$ cm $= \lambda_d/32$, for cylinder perimeter A'B'C'D'.

Figure 4b graphs the computed results for the envelope of the cylinder's surface electric field, $E_z^n(s)$, along perimeters ABCD and A'B'C'D', as well as Tong's solution. (Here, s represents a normalized position along the perimeter.) For the ABCD solution, δt = 1.59 psec and the envelope was observed for $630 \leq n \leq 756$. For the A'B'C'D' solution, δt = 3.18 psec and the envelope was observed for $315 \leq n \leq 378$. Each case represented an algorithm time of 1200 psec, or 3.0 wave cycles at 2.5 GHz, required to reach the steady state.

Since the lattice resolutions for both cases of Figure 4 were finer than that of the slab problem of Figure 3, it was inferred that the error due to the finite-difference approximations of the derivatives was less than $\pm$2% for each case. Any error above this limit was assumed due to residual wave reflections at the lattice truncations. Over most of the surface of the cylinder, the error level of each FD-TD solution was comparable and limited to about $\pm$10%. The principal disagreement between the FD-TD solutions, and the largest error of the ABCD case, occurred at the electric field minimum. Evidently, the interaction of the cylinder and the lattice truncations was so weak that it could influence the computed results only a field minima. It was concluded that the FD-TD lattice truncation conditions lead to an error level of less than $\pm$10% at most points, even for small spacings between the structure modeled and the lattice truncations.

3.5.3 Irradiation of a Circular Dielectric Cylinder

The stepped-surface, or lattice, approximation of the shape of a curved scatterer was next considered as a source of error. To estimate this error source, the TM irradiation of an infinitely-long, circular dielectric cylinder was modeled. Here, in addition to error due to imperfect lattice truncations, modeling error was introduced because the cylinder surface could not be exactly defined by combinations of intersecting lattice planes. In effect, spurious wave diffraction effects were caused at each intersection of two planes. The magnitude of this additional error could be estimated by comparing the accuracy of the circular cylinder model to that of the square cylinder model of Figure 4.

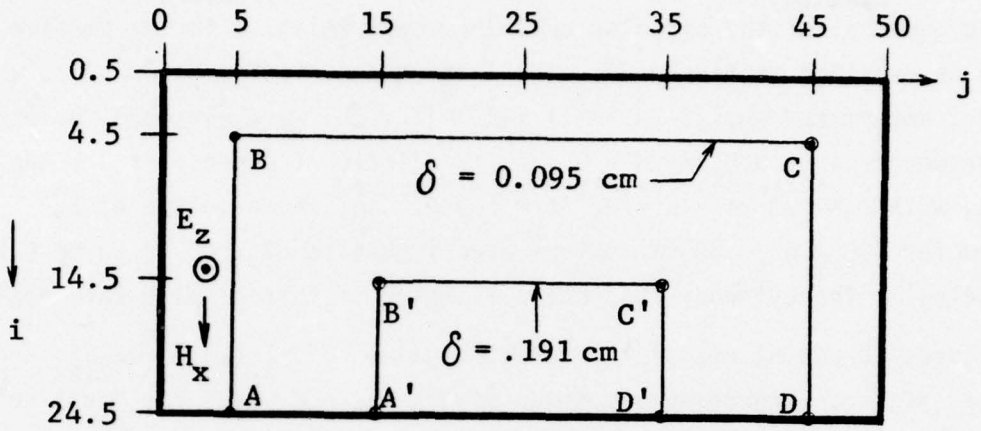

(a) Geometry

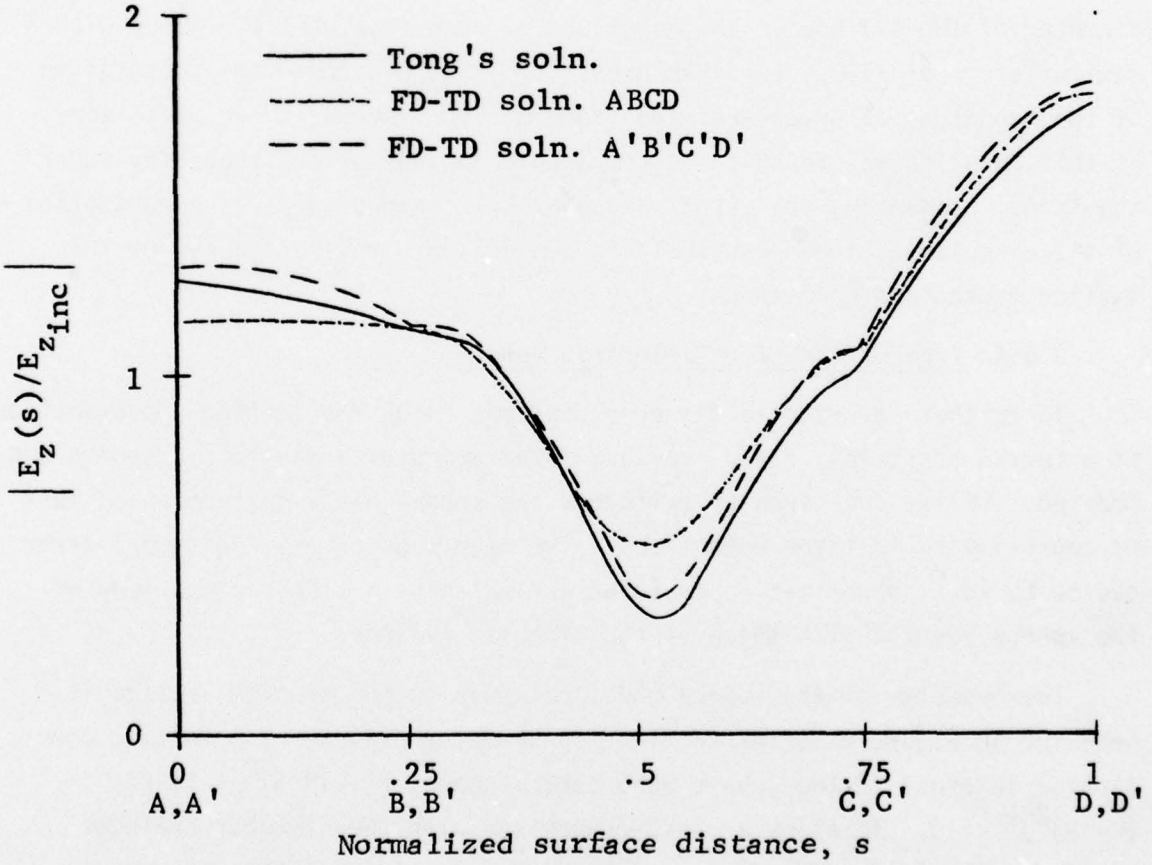

(b) Computed Electric Field

Fig. 4 IRRADIATION OF A SQUARE DIELECTRIC CYLINDER

The geometry of the circular cylinder model relative to the problem lattice is detailed in Figure 5a. The lattice coordinates internal to the cylinder, determined by $[(i-24.5)^2 + j-25)^2]^{\frac{1}{2}} \leq 20$, were assigned the dielectric parameters $\varepsilon_r = 4.0$ and $\sigma = 0$. An irradiation frequency of 2.5 GHz was assumed, with $\delta = 0.3$ cm $= \lambda_d/20$, $\delta t = 5$ psec, and the envelope of E_z^n observed for $460 \leq n \leq 500$ (a maximum algorithm time of 2500 psec, or 6.25 wave cycles). The cylinder thus had a diameter of 1 free-space wavelength.

Figures 5b and 5c detail the computed values of $|E_z(24,j)|/E_{z_{inc}}$ and $|E_z(15,j)|/E_{z_{inc}}$, respectively. These figures also present the exact solution calculated using the summed-mode series technique of Jones.[22] As seen in the figures, the FD-TD solution located the positions of the peaks and nulls of the electric field with a maximum error of $\pm\delta$, or about $\pm 3\%$ of the diameter of the cylinder. The magnitude of each peak was determined with a maximum error of $\pm 10\%$. Error in excess of 10% appeared in the computation of the magnitude of several of the field minima. Overall, the uncertainty of this solution was found to be comparable to that of the square cylinder solution. Evidently, the error caused by the stepped-surface approximation of the circular cylinder was small in comparison with that caused by the lattice truncation conditions.

3.5.4 Irradiation of a Dielectric Sphere

To further investigate the error introduced by the lattice approximation of a curved scatterer, the plane-wave irradiation of a dielectric sphere was modeled. Unlike the circular cylinder, the sphere has a surface which must be approximated in three dimensions. The magnitude of any additional error caused by this approximation could be estimated by a simple comparison of the sphere results with those of the circular cylinder.

The geometry of the sphere model relative to the problem lattice is depicted in Figure 6 at the two lattice symmetry planes. The lattice coordinates internal to the sphere were determined by $[(i-19.5)^2 + (j-20)^2 + (k-19)^2]^{\frac{1}{2}} \leq 15$. To allow a close comparison with the circular cylinder results, all of the dielectric and program parameters of that run were repeated, namely: $\varepsilon_r = 4.0$; $\sigma = 0$; $f = 2.5$ GHz; $\delta = 0.3$ cm $= \lambda_d/20$; $\delta t = 5$ psec; and envelope observation for $460 \leq n \leq 500$. The sphere thus had a

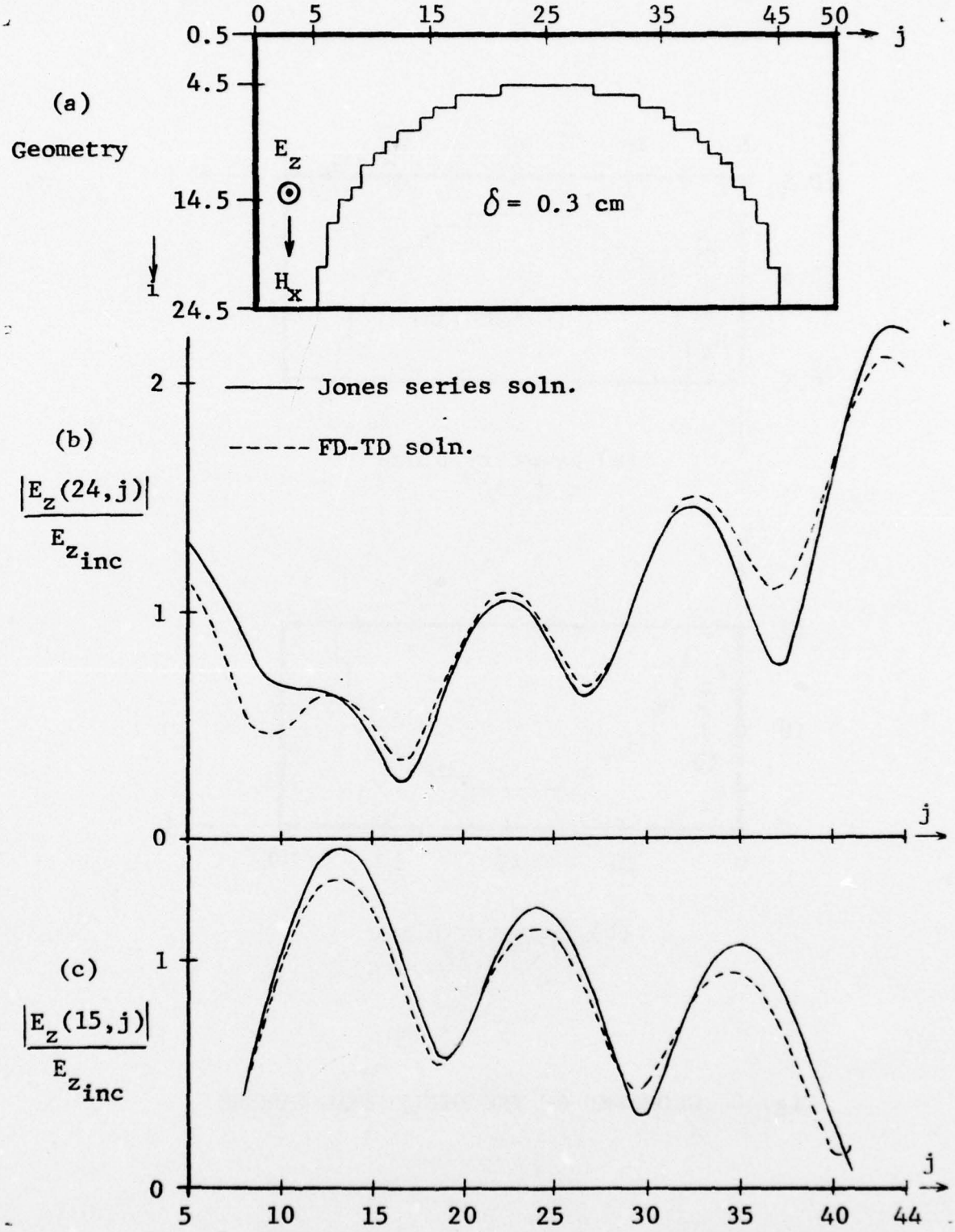

Fig. 5 IRRADIATION OF A CIRCULAR DIELECTRIC CYLINDER

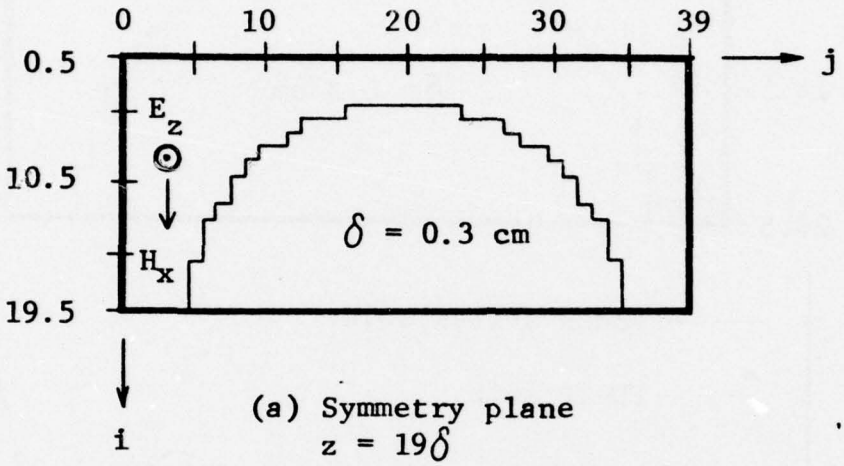

(a) Symmetry plane
$z = 19\delta$

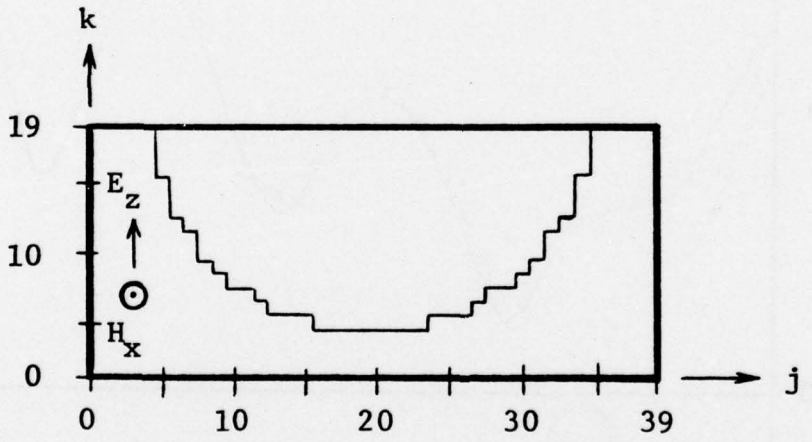

(b) Symmetry plane
$x = 19.5\delta$

Fig. 6 GEOMETRY OF THE DIELECTRIC SPHERE

diameter of 0.75 free-space wavelength. To reduce spurious reflections at the lattice truncations (as discussed in Section 3.4.3), a value of σ_{ext} equal to 0.1 mho/m was assumed.

Figures 7a and 7b detail the computed, normalized values of two electric field components near the sphere irradiation axis: $|E_y(19.5,j,18)|/E_{z_{inc}}$ and $|E_z(19,j,18.5)|/E_{z_{inc}}$. These figures also present the exact solution calculated using the summed-mode series technique of Stratton.[23] As seen in the figures, the FD-TD solution located the positions of the peaks and nulls of the electric field with a maximum error of $\pm\delta$, or about $\pm$3% of the diameter of the sphere. The magnitude of each peak was determined with a maximum error of $\pm$10%. Overall, the uncertainty of this solution was found to be comparable to that of the square and circular cylinder solutions. Evidently, the error caused by the stepped approximation of the surface of the sphere in three dimensions was small in comparison with that caused by the lattice truncation conditions. It was, therefore, concluded that the three dimensional FD-TD program allows solutions with a level of accuracy comparable to that of the two dimensional program.

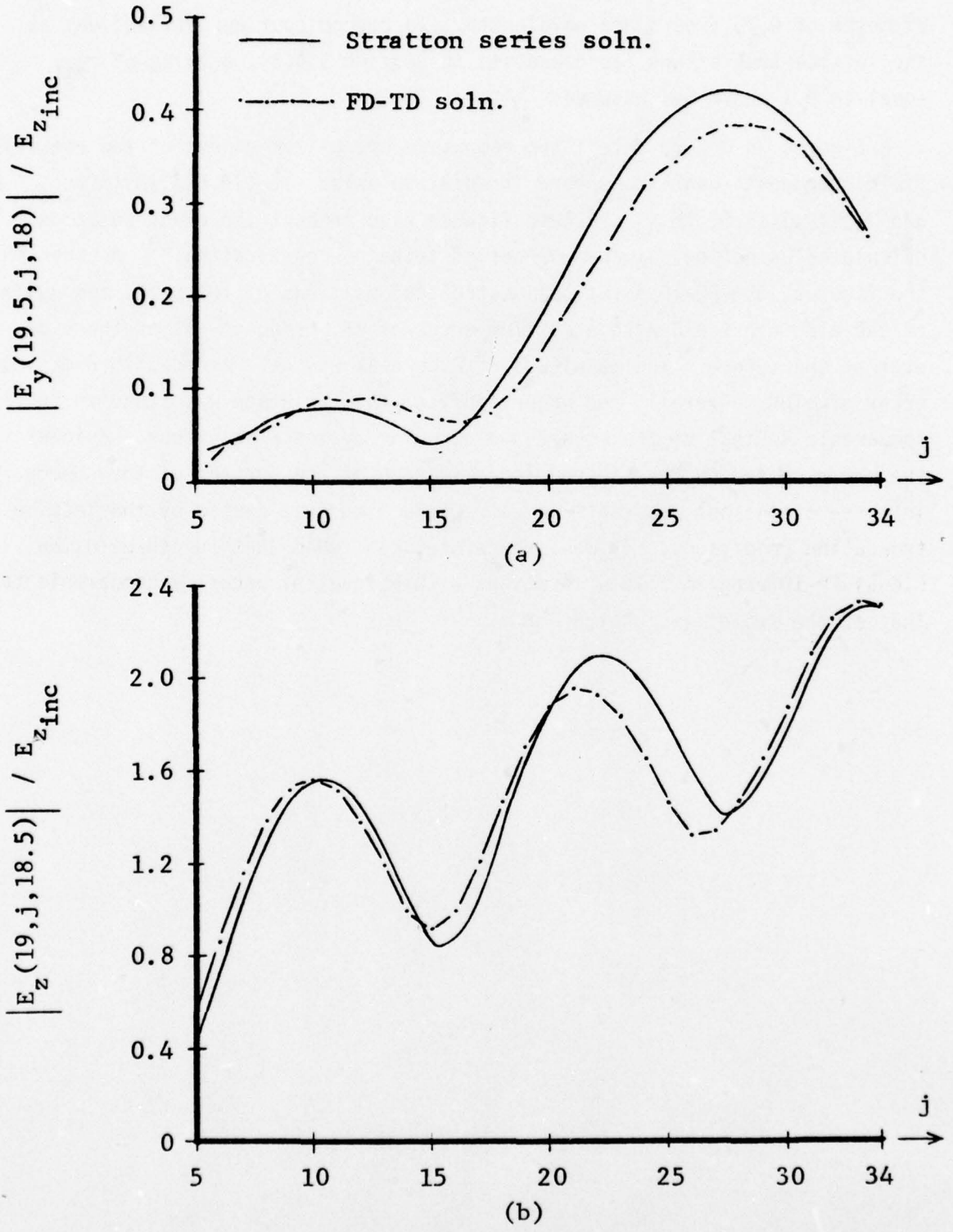

Fig. 7 COMPUTED ELECTRIC FIELDS WITHIN A DIELECTRIC SPHERE

4.0 DESCRIPTION OF THE PRESENT RESEARCH PROGRAM

4.1 Introduction

Electromagnetic coupling and shielding problems have traditionally been difficult to treat with analytical or numerical methods because of the failure of these methods to adequately resolve the effects of the apertures, curvatures, corners, and internal contents of structures. A practical numerical method has been desired to allow the direct modeling and solution of complex realistic coupling problems. The purpose of this research program was to evaluate the suitability of the finite-difference time-domain (FD-TD) solution method for Maxwell's equations to determine the amount of electromagnetic coupling through an aperture into an enclosed conducting container.

The FD-TD method allows, in principle, the computation of the internal fields of complex conducting geometries. However, before the present research program, this method had not been utilized and evaluated for any conducting geometries. To build up confidence in the FD-TD method for future applications, it was desired to evaluate the usage of the method for certain simple, generic metal structures.

During the present research program, two specific metal structures were used in this evaluation: the first, an aluminum cylinder with one open end; the second, the nose cone section of a missile. Each structure was modeled using the FD-TD method to compute the internal EM fields generated by an incident plane wave propagating along the structure axis. The results of the cylinder model were then compared to available theoretical and experimental data. Final evaluation of the nose cone results will be possible when reliable experimental data for this geometry is obtained in a future research program.

The following section describes each coupling-analysis problem considered and summarizes the steps taken to solve each problem. Detailed descriptions of the results follow in succeeding sections.

4.2 Description of Coupling-Analysis Problems Considered

4.2.1 Task 1: Prediction of the Coupling Into an Open-Ended Cylinder

The FD-TD technique was employed to solve the following electromagnetic coupling problem:

Interacting structure - Circular (19.0 cm diameter), 68.5 cm long, open-ended aluminum cylinder, as shown in Figure 8;

Incident wave - 300 MHz plane wave propagating down the cylinder axis toward its open end;

Desired fields - Each component of total $\bar{E}$ and total $\bar{H}$ in the axial cross-section plane of the cylinder down to 40 cm from the open end. First, with the cross-section plane parallel to the incident $\bar{E}$, and again with the plane parallel to the incident $\bar{H}$;

Resolution - 0.5 cm uniformly throughout the mapping planes;

Plotted values - In decibels relative to an incident $\bar{E}$ of 1 volt/meter and an incident $\bar{H}$ of 1/377 ampere/meter.

To solve this coupling problem, an existing FD-TD computer code was suitably modified to model the cylinder of Figure 8. The following steps were taken:

a. The existing FD-TD computer code was modified for the Control Data STAR-100 computer. A 24 x 163 x 24 - cell lattice was programmed, with even symmetry of the incident fields and cylinder assumed about lattice planes $x = 24.5\delta$ and $z = 24\delta$.

b. The cylinder geometry of Figure 8 was mapped into the new finite-difference lattice for a unit cell diameter of $\delta = 0.5$ cm.

c. The FD-TD program was run for this geometry for 800 time steps (equivalent to 2.0 cycles of the incident wave) assuming lossless air within the cylinder. 10^6 words of memory and 3.5 minutes of central processor time were required on the STAR-100.

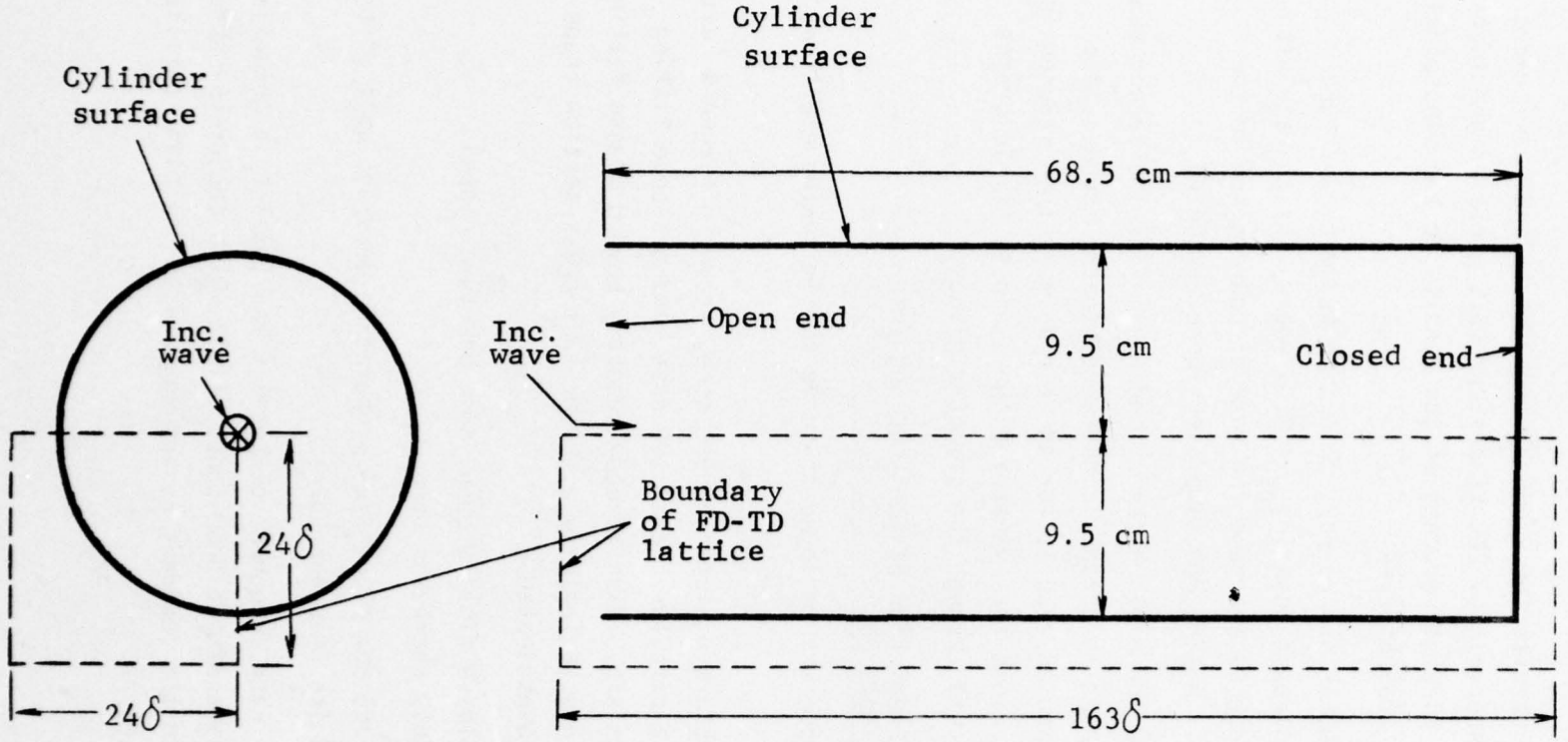

Fig. 8 OPEN-ENDED ALUMINUM CYLINDER GEOMETRY OF TASK 1 (not to scale)

d. The computed results for $\overline{E}$ and $\overline{H}$ along the cylinder axis were plotted at intervals of 200 time steps (0.5 cycle of the incident wave). Slow convergence of the results to the sinusoidal steady state was observed.

e. The FD-TD program was re-run, this time assuming a slight amount of isotropic loss (σ_{int} = 0.01 mho/m) for the air within the cylinder to increase the rate of convergence to the steady state. Again, 800 time steps were completed.

f. Plotting of $\overline{E}$ and $\overline{H}$ along the cylinder axis for the second run indicated a much more rapid convergence to the steady state. The final computed results for the fields were then reduced to contour maps along the symmetry planes, and to simple graphs at selected cuts through the symmetry planes.

4.2.2 Task 2: Prediction of the Coupling Into a Missile Nose Cone

The FD-TD technique was employed to solve the following electromagnetic coupling problem:

Interacting structure - Aluminum nose cone, shown in Figure 9, with two apertures: a circular one in the nose, and a sleeve fitting located 23-1/3 cm aft. Missile body geometry beyond sleeve fitting assumed to continue to infinity with constant cross-section shape. Aperture cases investigated:

Trial 1 - Sleeve fitting open, nose aperture closed,
Trial 2 - Both apertures open;

Incident wave - 300 MHz plane wave propagating down the axis of the structure toward its nose aperture;

Desired fields - Each component of total $\overline{E}$ and total $\overline{H}$ in the axial cross-section plane of the nose cone. First, with the cross-section plane parallel to the incident $\overline{E}$, and again with the plane parallel to the incident $\overline{H}$;

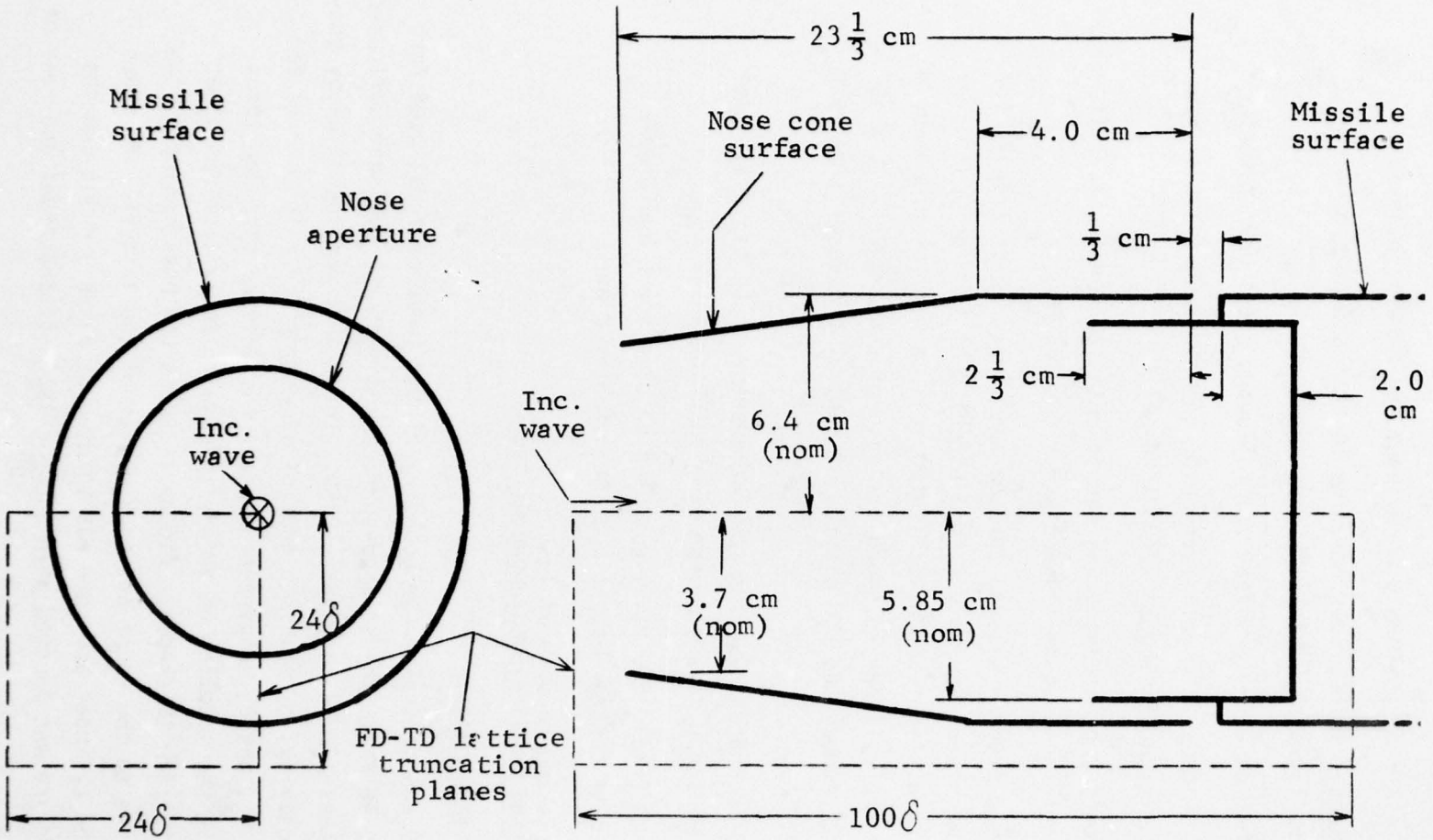

Fig. 9 NOSE CONE GEOMETRY OF TASK 2 (not to scale)

Resolution - 1/3 cm uniformly throughout the mapping planes;

Plotted values - In decibels relative to an incident $\bar{E}$ of 1 volt/meter and an incident $\bar{H}$ of 1/377 ampere/meter.

To solve this coupling problem, the following steps were taken:

a. The 24 x 163 x 24 - cell lattice of the aluminum cylinder program was truncated to 24 x 100 x 24 cells.

b. The geometry of Figure 9 was mapped into the new finite-difference lattice for a unit cell diameter of δ = 1/3 cm.

c. The FD-TD program was run for the aperture case of Trial 1 for 900 time steps (equivalent to 1.5 cycles of the incident wave), assuming a slight amount of isotropic loss (σ_{int} = 0.025 mho/m) within the cylinder to speed the rate of convergence. 6×10^5 words of memory and 2.8 minutes of central processor time were required.

d. The FD-TD program was run for the aperture case of Trial 2 for 900 time steps, assuming the same interior loss, σ_{int}.

e. For each trial, the final computed results for $\bar{E}$ and $\bar{H}$ were reduced to contour maps along the symmetry planes.

4.3 Details and Results of Task 1: Coupling Into an Open-Ended Cylinder

4.3.1 Cylinder Model

Figures 10 and 11 depict the geometry of the cylinder model used for Task 1. Figure 10 shows the stepped-surface model of the cylinder wall used for lattice planes j = 14 through j = 150. This model was specified by setting the conductivity, σ, equal to that of aluminum (3.7×10^7 mho/m) for individual E_x, E_y, and E_z components nearest the desired circular locus. This resulted in the modeling of the cylinder wall as an aluminum sheet having virtually zero thickness. Figure 11 shows the positioning of the cylinder relative to the front and back planes of the lattice. As shown in this figure, the cylinder aperture was located at plane j = 14, and the cylinder back-plane was located at plane j = 151. To the front and rear of

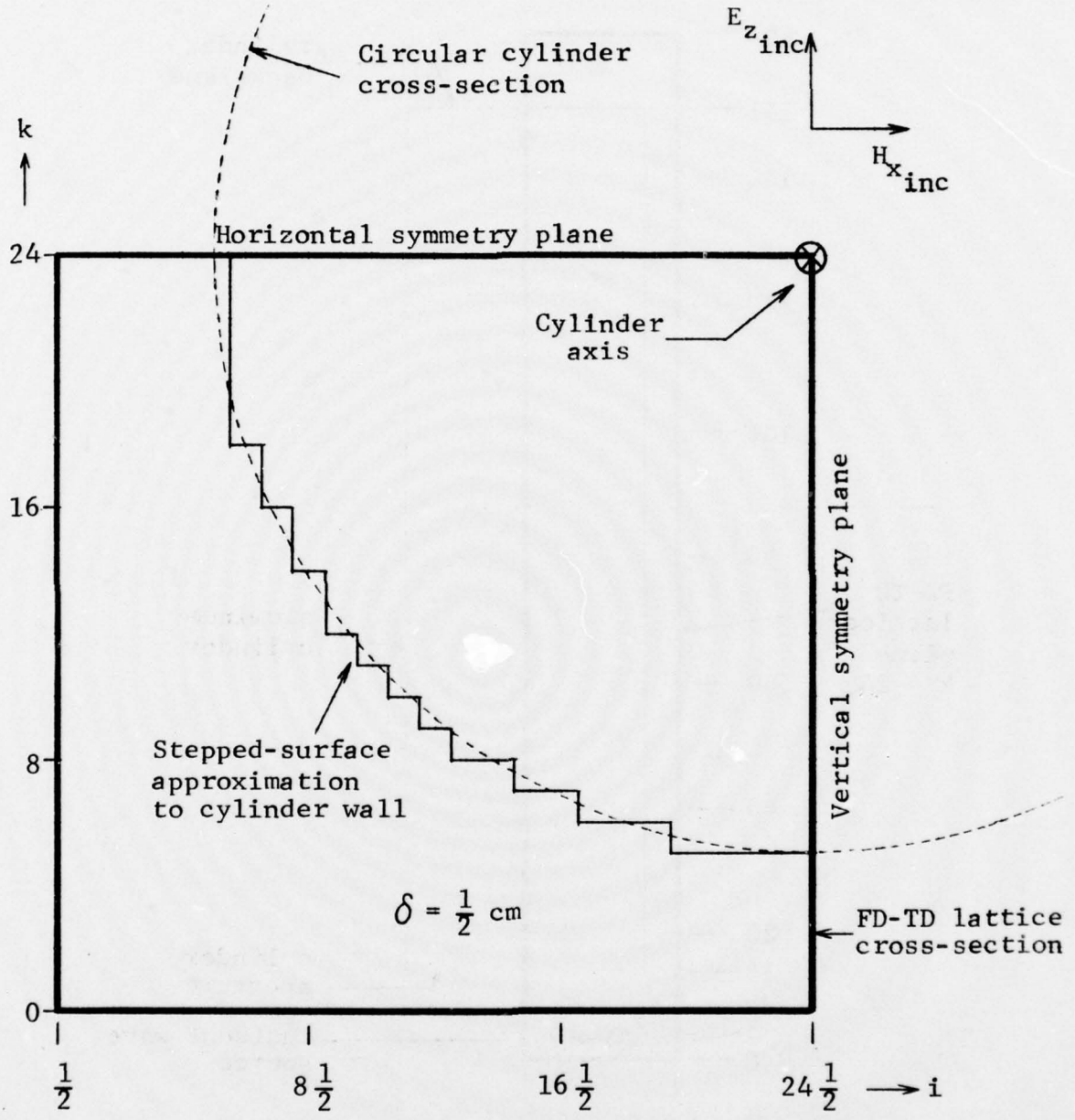

Fig. 10 CROSS-SECTION OF CYLINDER MODEL FOR TASK 1

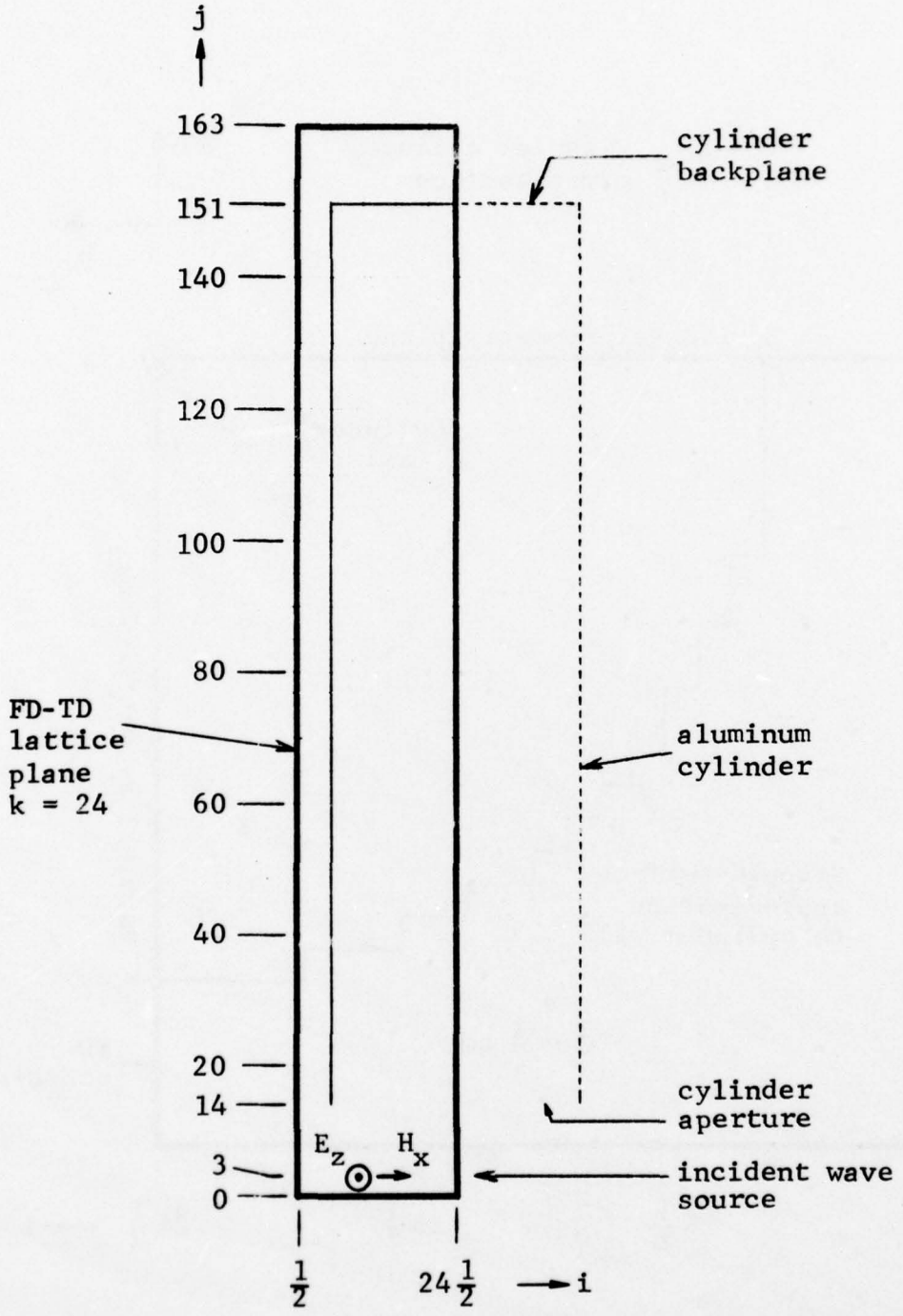

Fig. 11 VIEW OF CYLINDER MODEL FOR TASK 1
AT HORIZONTAL SYMMETRY PLANE

the cylinder lay regions of air. In the front air region, the simulated 300 MHz incident wave was generated at plane j = 3 with the field components E_z and H_x.

For all lattice cells exterior to the model cylinder, the anisotropic conductivity, σ_{ext}, equal to 0.01 mho/m was assumed to help improve the lattice truncation conditions, as discussed in Section 3.4.3. This value of σ_{ext} caused the exponential decay of E_x and E_y fields in the exterior region with an effective skin depth of about 110 lattice cells.

Using the computer program listed in Appendix A, the cylinder model was completely specified by punching 3 groups of 24 cards, giving a total of 72 cards. Card group 1 specified the air medium of the lattice in front and back of the cylinder (planes j = 0 through j = 13 and planes j = 152 through j = 163). Card group 2 specified the stepped-surface model of the cylinder (planes j = 14 through j = 150). Finally, card group 3 specified the cylinder backplane (plane j = 151). The format of the data cards is discussed in Appendix A.

4.3.2 Convergence of the Computer Fields

Two 800 time-step programs (each equivalent to 2.0 cycles of the incident wave) were run during Task 1 in order to investigate the rate of convergence of the computed fields to the sinusoidal steady state. The first program assumed lossless air within the cylinder; the second program assumed a small isotropic conductivity, σ_{int}, equal to 0.01 mho/m within the cylinder. The purpose of modeling the slightly lossy air was to cause the reactive fields within the cylinder to converge more rapidly to the expected beyond-cutoff condition.

Figures 12 and 13 are graphs of the computed total electric field, $|E_z/E_{z_{inc}}|$ (in decibels) along the axis of the cylinder for the cases of σ_{int} = 0 and σ_{int} = 0.01 mho/m, respectively. In Figure 12, curves are plotted for the cases n = 400 and n = 800 time steps; in Figure 13, curves are plotted for n = 200, n = 400, n = 600, and n = 800 time steps. Each curve gives the computed field envelope during the 200 time-steps period (0.5 cycle of the incident wave) before the specified value of n. In Figure 13, it should be noted that, at 200 time steps, the incident wave penetrated

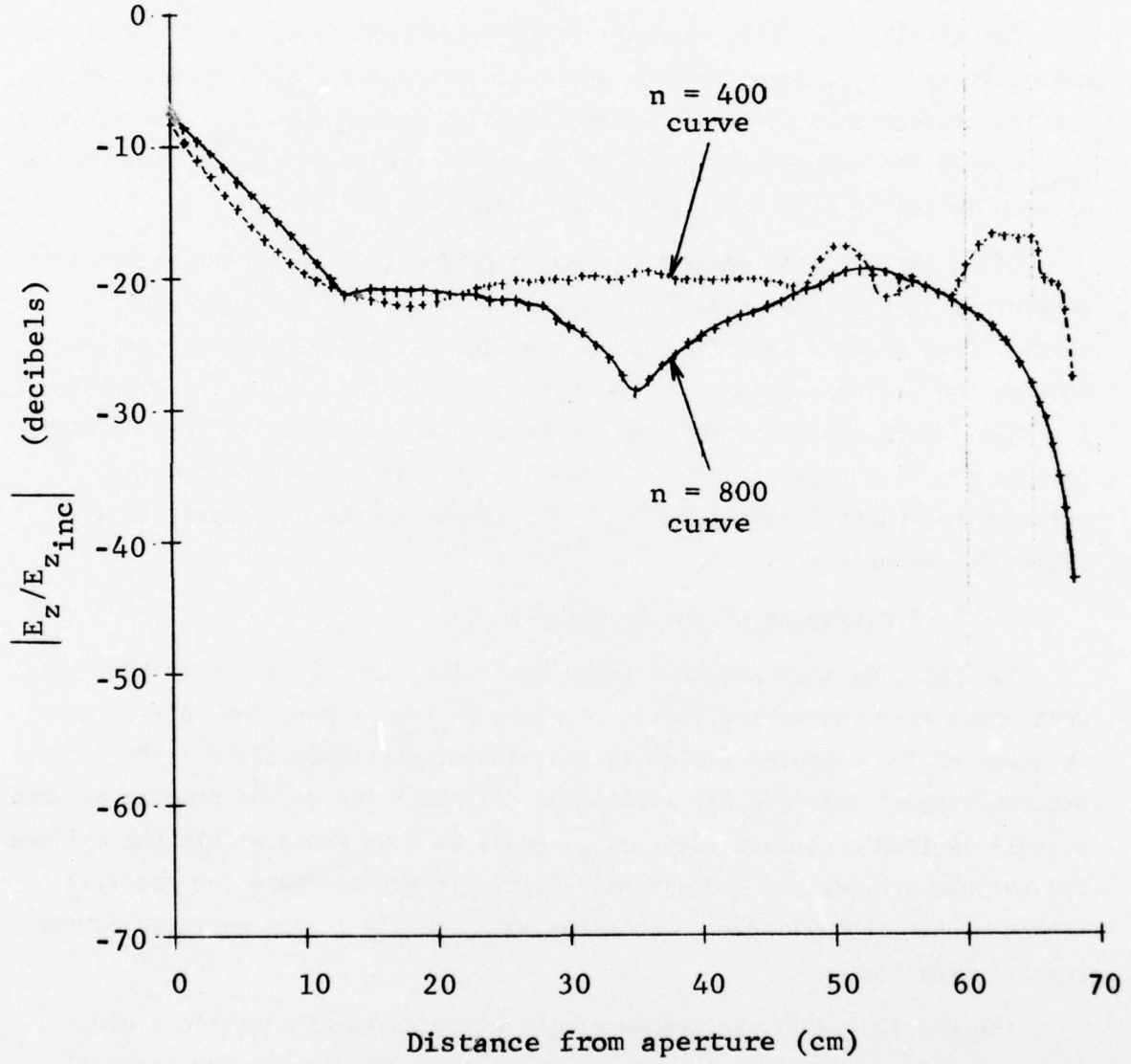

Fig. 12 COMPUTED ELECTRIC FIELD ALONG CYLINDER AXIS (σ_{int} = 0 CASE)

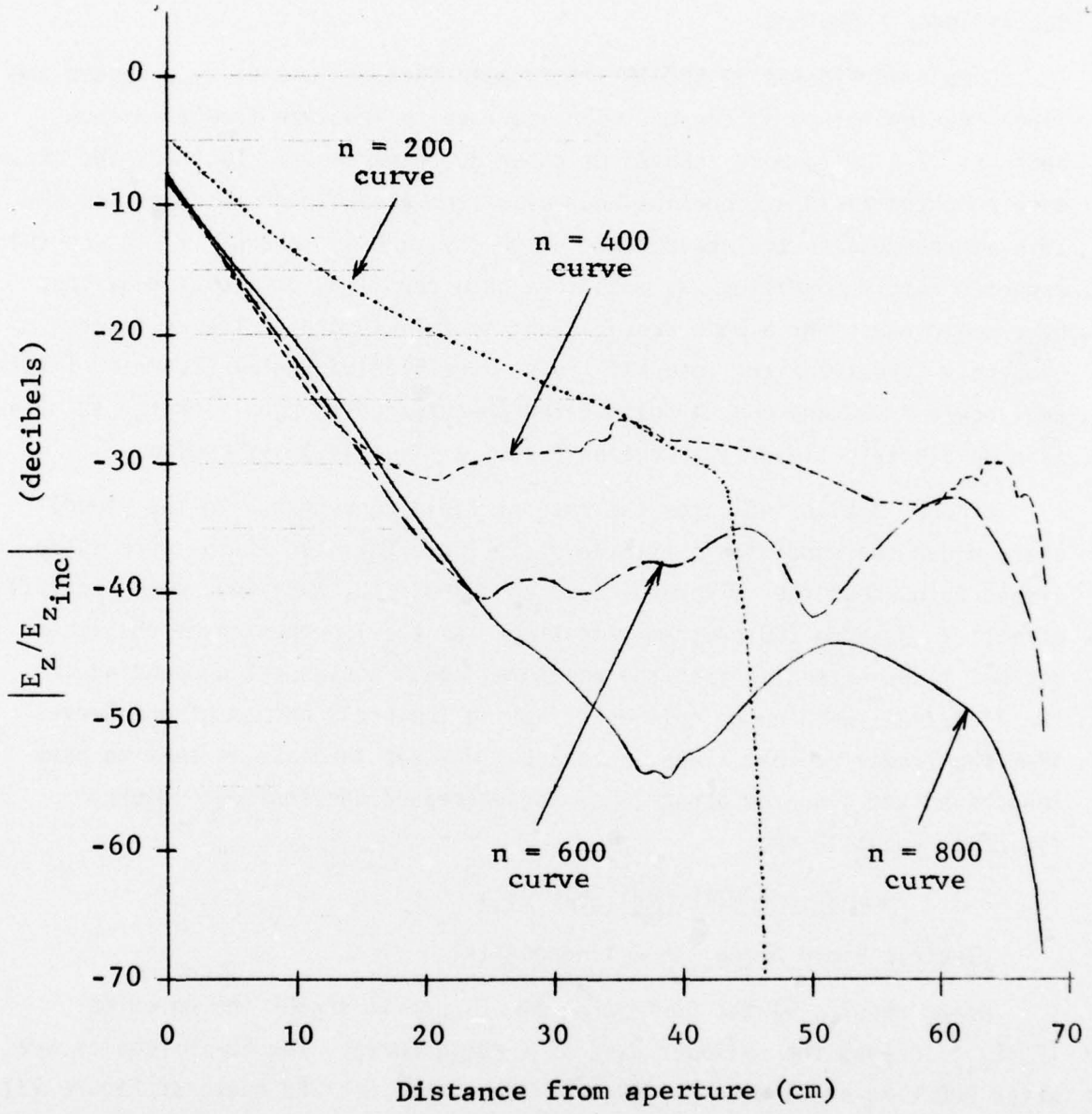

Fig. 13 COMPUTED ELECTRIC FIELD ALONG CYLINDER AXIS (σ_{int} = 0.01 mho/m CASE)

only about 45 cm into the cylinder, causing the sharp downward break of the n = 200 curve. For all other curves, the incident wave penetrated fully to the cylinder backplane.

Comparing Figures 12 and 13, it is seen that the use of σ_{int} caused the linear decibel slope at the cylinder aperture to lengthen from a maximum depth of 12.5 cm to more than 25 cm after 800 time steps. Further, the ultimate computed field attenuation increased from about 30 dB to almost 55 dB. This improvement in the convergence of the cylinder's internal fields to the expected cutoff condition was much more than the 11 dB of field decay that σ_{int} would cause for a wave propagating the full length of the cylinder. Evidently, the transient internal fields were highly reactive (carried little real power flow) and quickly dissipated when forced to supply energy to maintain an electric field distribution across a slightly lossy medium.

Figure 13 also indicates the rate of field convergence to the steady state under the condition of finite σ_{int}. Once the wave fields were established throughout the cylinder (curves n = 400, 600, and 800), the principal effect of an added 200 program time steps was the lengthening of the linear decibel slope extending from the aperture, and a consequent deepending of the field null within the cylinder. Noting the break points of the curves from the linear decibel slope, each 200 time-step increase is seen to have lengthened the slope by about 10 cm and decreased the residual internal fields by about 10 dB.

4.3.3 Comparison With Available Data

Electric Field Along the Cylinder Axis

Using results of the FD-TD program, Figure 14 graphs the computed $|E_z/E_{z_{inc}}|$ along the cylinder axis as a solid curve. The FD-TD results are after 800 time steps with σ_{int} = 0.01 mho/m (the n = 800 curve of Figure 13). For comparison, experimental results[24] are shown as circled points, and computed results using the BOR-3 body of revolution code[24] are graphed as a dashed curve.

From Figure 14, it is seen that the FD-TD curve lies between the BOR-3 theory and the experimental results. The FD-TD and BOR-3 curves have nearly

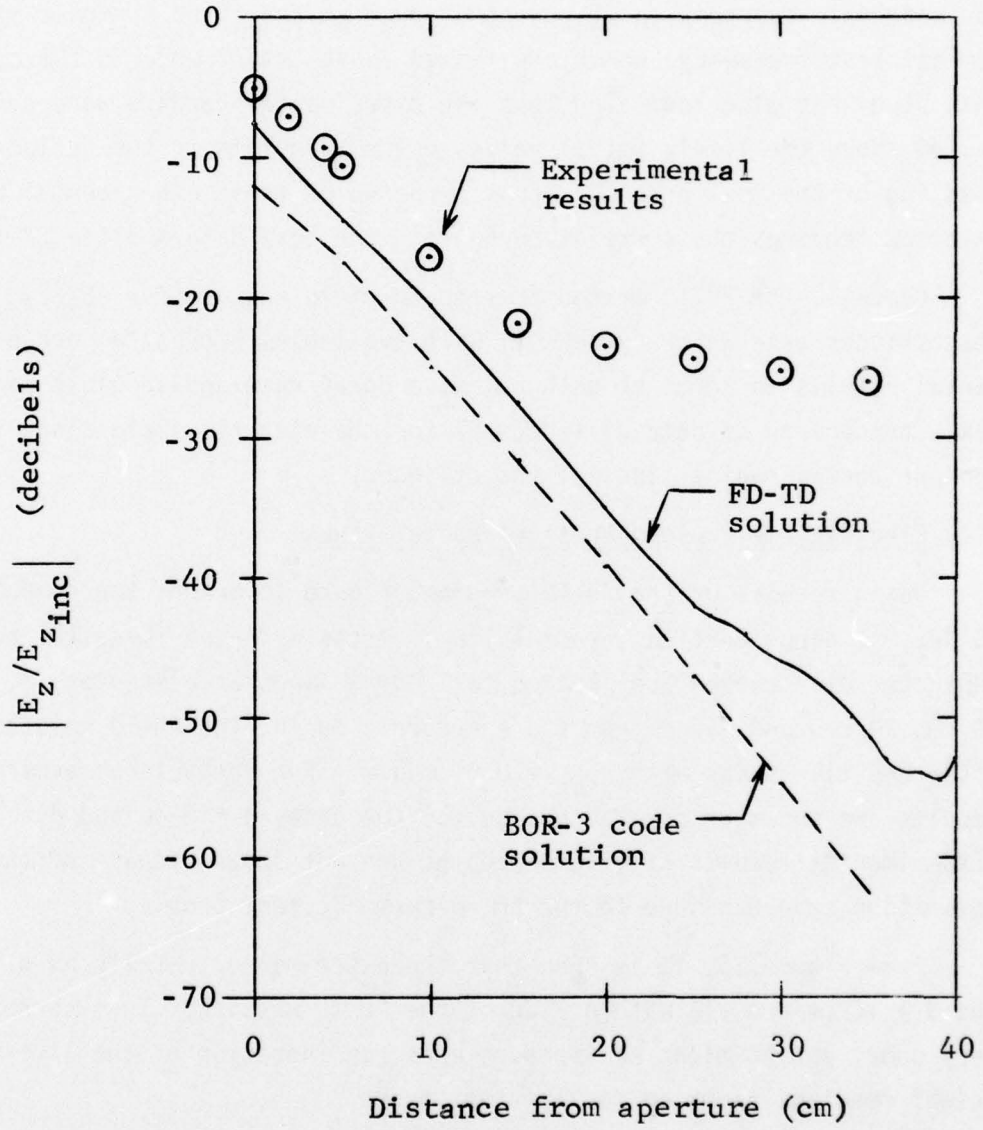

Fig. 14 COMPARISON OF RESULTS FOR THE ELECTRIC FIELD ALONG THE CYLINDER AXIS

the same slope down to about -55 dB, where the FD-TD curve levels off. However, the experimental results level out at only -30 dB. A previous study of the experimental procedure has shown that this saturation was due to inadequate suppression of radiated power at the third harmonic of the nominal test frequency, which excited an above-cutoff mode in the cylinder.[25] This study has also indicated that the experimental results were consistently 1-2 dB above the likely actual values due to problems in the design and mounting of the test probe.[25] Consideration of these experimental uncertainties improves the correlation between the test data and the FD-TD results.

Overall, the FD-TD method is seen to yield results for $|E_z/E_{z_{inc}}|$ along the cylinder axis which agree well with available theoretical and experimental results in terms of both relative decay rate and absolute magnitudes. Next, comparison of data will be made for the electric field along vertical and horizontal radial lines of the cylinder.

Electric Field Along Vertical Radial Lines

Using results of the FD-TD program, Figure 15 graphs the computed $|E_z/E_{z_{inc}}|$ along vertical, radial lines of the cylinder (parallel to $E_{z_{inc}}$). Separate solid curves are plotted for radial lines at distances, d, of 0 cm, 10 cm, 20 cm, and 35 cm from the aperture. Again, the FD-TD results are after 800 time steps with σ_{int} = 0.01 mho/m. For comparison, experimental results are shown as circled points for the cases d = 0 cm and d = 10 cm. (Experimental results at greater depths are not shown because of their rapid saturation at -30 dB due to the third-harmonic test problem.)

From Figure 15, it is seen that the experimental results at d = 0 cm and d = 10 cm are all within 2 dB of the FD-TD results. This correlation is very good; yet it might be improved upon consideration of the likely 1-2 dB "high" readings reported for the test probe.

Electric Field Along Horizontal Radial Lines

Figure 16 is similar to Figure 15 except that $|E_z/E_{z_{inc}}|$ is graphed along several horizontal radial lines of the cylinder (parallel to $H_{x_{inc}}$). The experimental results are seen to be within 3 dB of the FD-TD results over most of the range of the results.

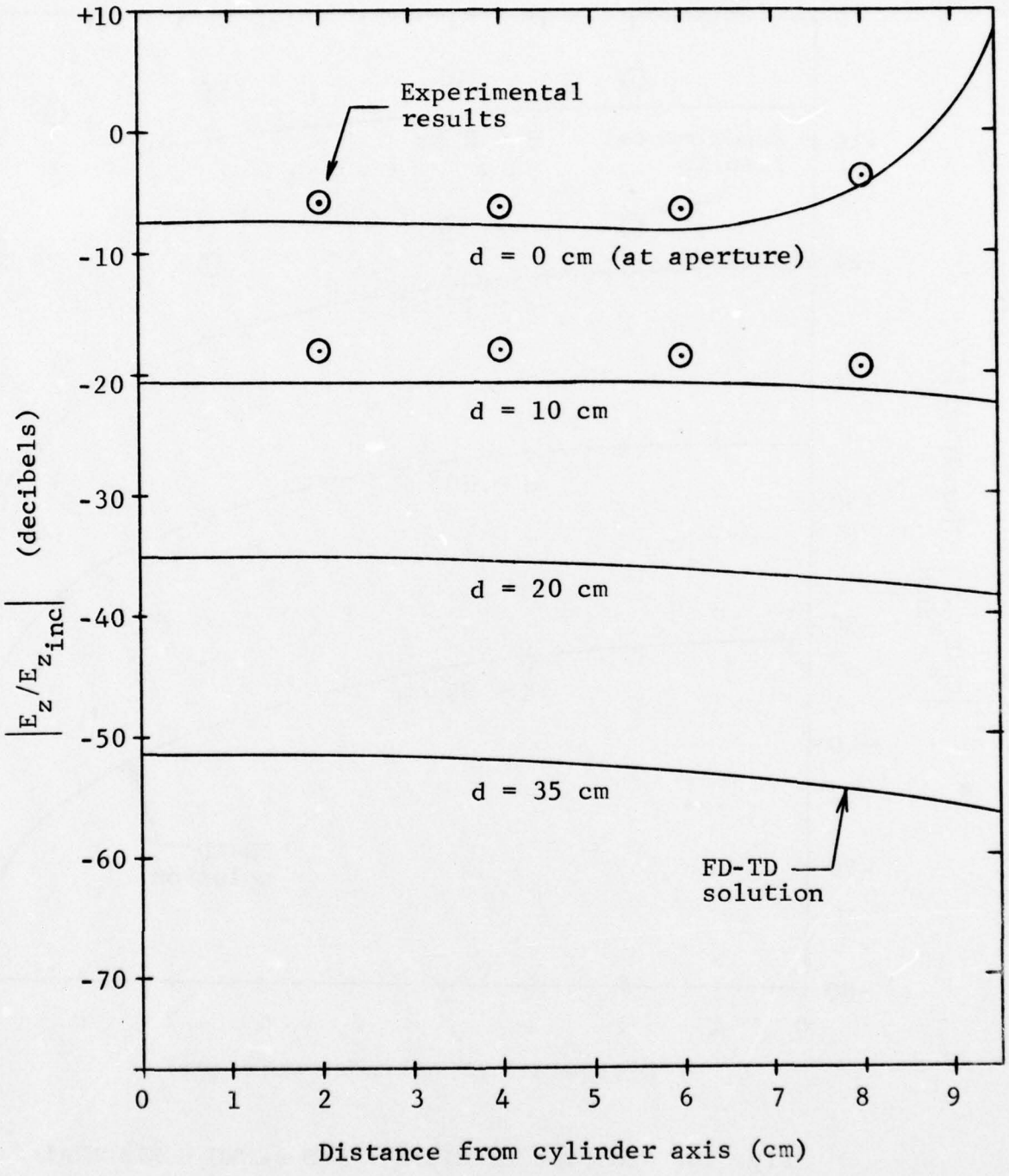

Fig. 15 COMPUTED ELECTRIC FIELD ALONG VERTICAL RADIAL LINES (PARALLEL TO $E_{z_{inc}}$) OF THE CYLINDER

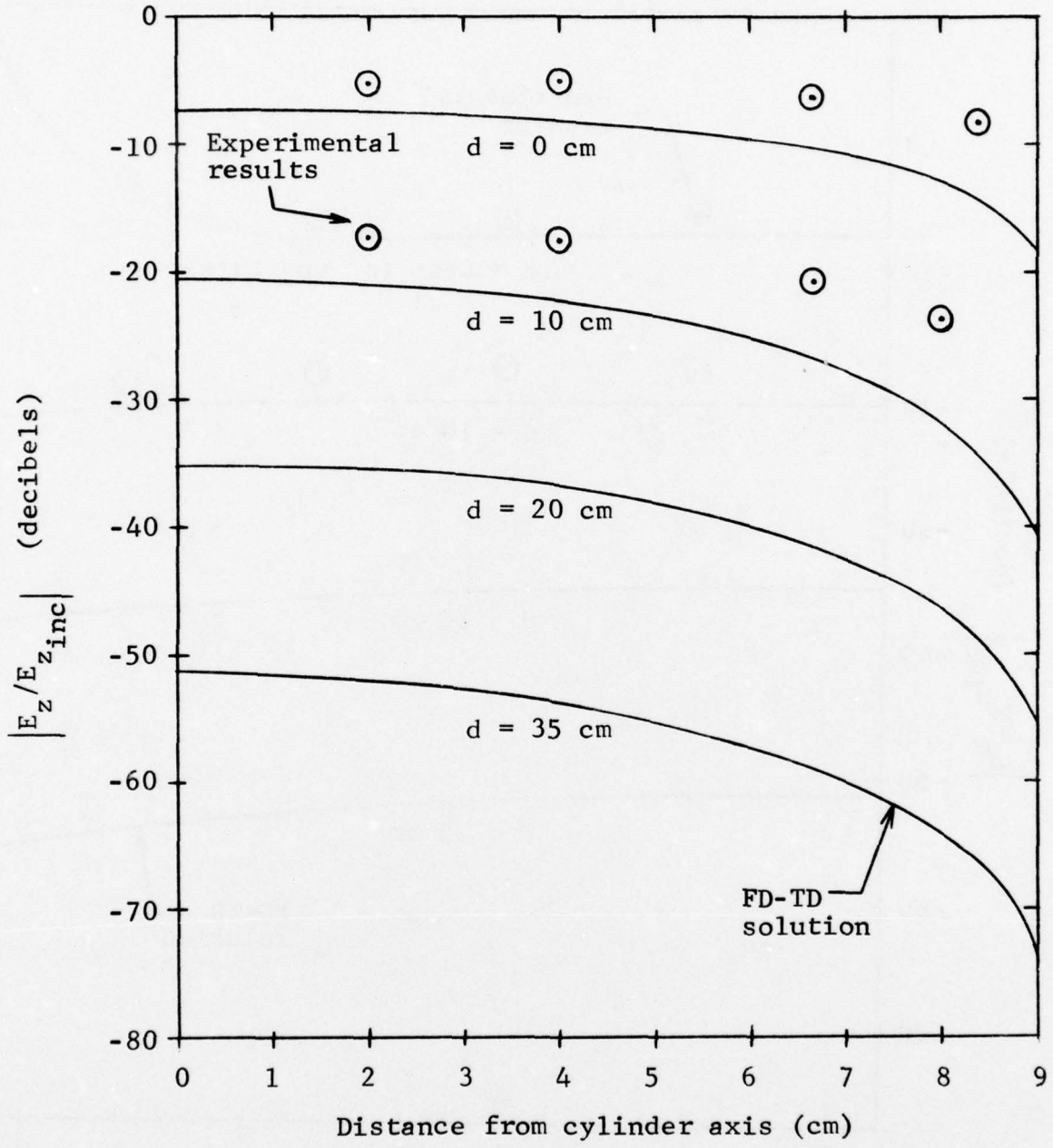

Fig. 16 COMPUTED ELECTRIC FIELD ALONG HORIZONTAL RADIAL LINES (PARALLEL TO $H_{x_{inc}}$) OF THE CYLINDER

4.3.4 Computed Field Maps

Using results of the FD-TD program (800 time steps, σ_{int} = 0.01 mho/m), Figures 17 and 18 graph contour maps of the computed field components at the cylinder's vertical and horizontal symmetry planes, respectively. All component magnitudes are normalized to either $|E_{z_{inc}}|$ or $|H_{x_{inc}}| = |E_{z_{inc}}|/377$, and are given as decibel numbers. Contours are plotted at exact 6 dB intervals by using a linear interpolation method to determine each contour's position between adjacent field envelope points. Although the lattice cell diameter, δ, equals 0.5 cm, this interpolation method allows the generation of smooth curves in most cases without a 0.5 cm-period stair-case effect.

It should be noted that only three field components are non-zero at each symmetry plane: E_z, H_x, and E_y at the vertical plane; and E_z, H_x, and H_y at the horizontal plane. This fact was derived in Section 3.4.5 of this report.

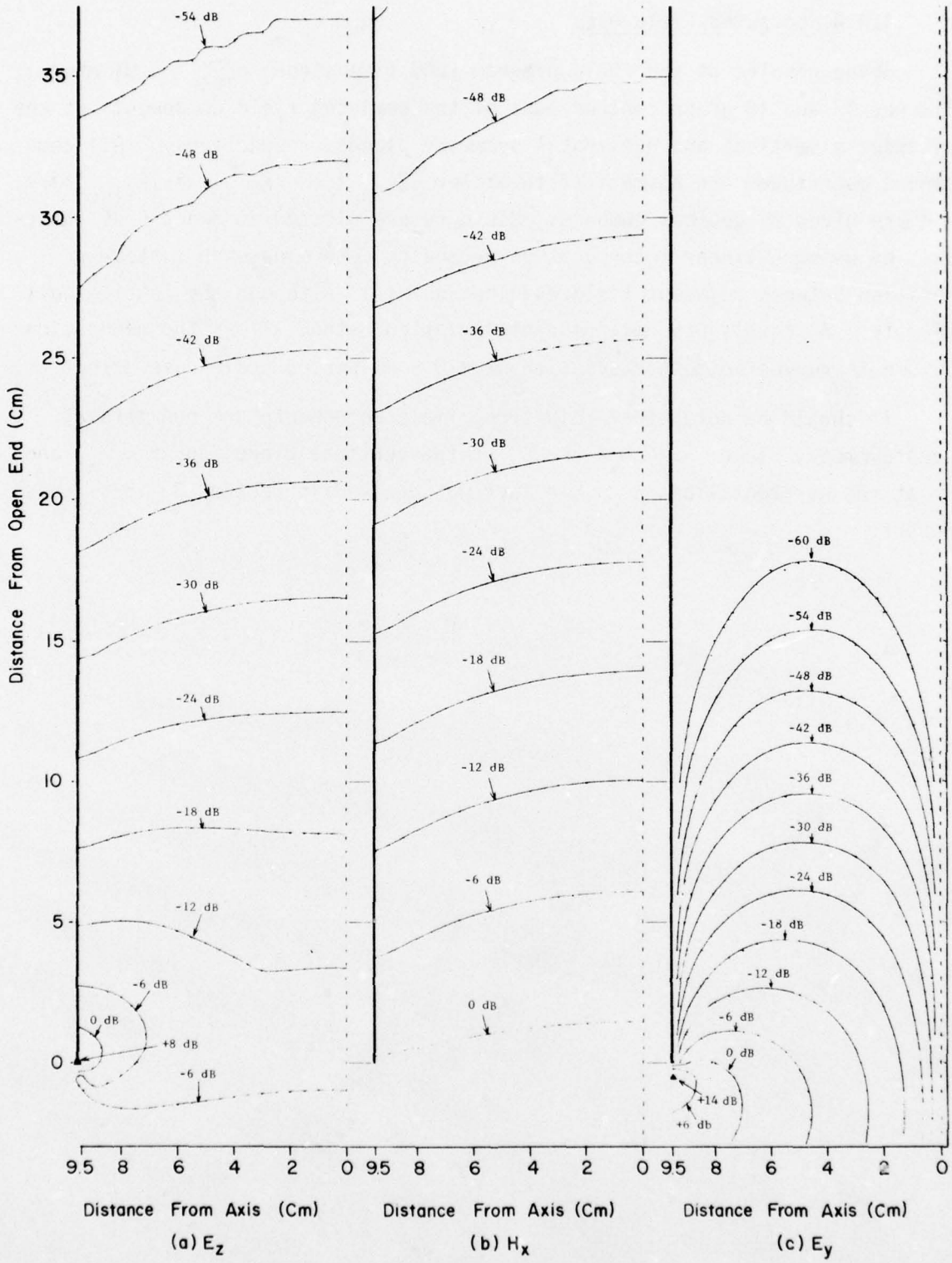

Fig. 17 FD-TD FIELD CONTOURS IN CYLINDER VERTICAL SYMMETRY PLANE

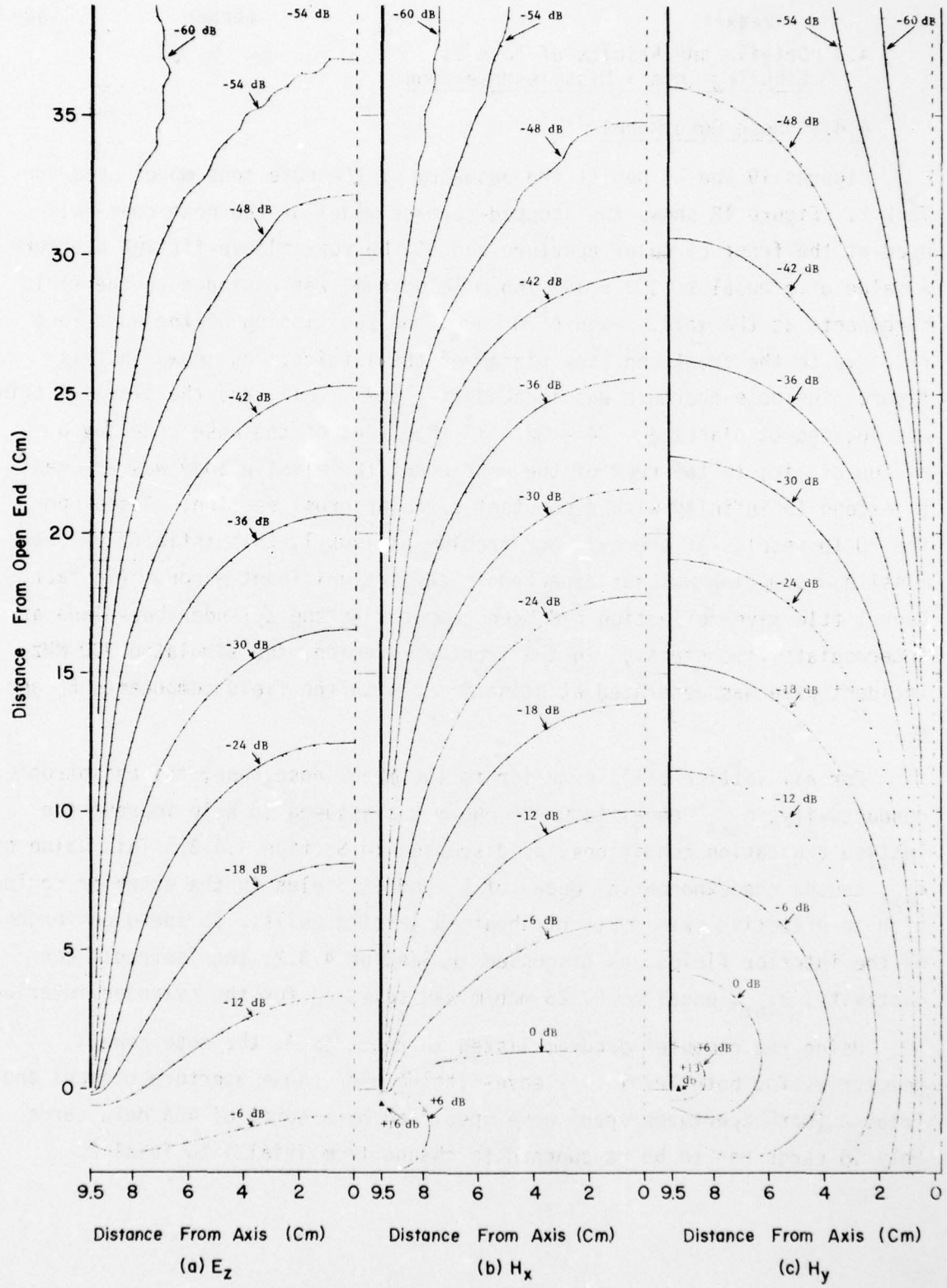

Fig. 18 FD-TD FIELD CONTOURS IN CYLINDER HORIZONTAL SYMMETRY PLANE

4.4 Details and Results of Task 2: Coupling Into a Missile Nose Cone

4.4.1 Nose Cone Model

Figures 19 and 20 depict the geometry of the nose cone model used for Task 2. Figure 19 shows the stepped-surface model of the nose cone wall used at the front circular aperture and at the rear sleeve-fitting aperture. A value of σ equal to 3.7×10^7 mho/m (aluminum) was assigned to the field components at the wall. Figure 20 shows the positioning of the nose cone relative to the front and back planes of the lattice. As shown in this figure, the nose aperture was located at plane j = 11, and the sleeve fitting was located at planes j = 74 - 82. To the front of the nose cone lay a region of air; to the rear of the nose cone, the missile body was assumed to extend to infinity with a constant circular cross section. Based upon the FD-TD results of the cylinder problem of Task 1, this infinitely-long-missile assumption was not expected to cause significant error. (In fact, very little wave reflection had been computed at the cylinder backplane at intermediate time steps.) In the front air region, the simulated 300 MHz incident wave was generated at plane j = 3 with the field components E_z and H_x.

For all lattice cells exterior to the model nose cone, the anisotropic conductivity, σ_{ext}, equal to 0.025 mho/m was assumed to help improve the lattice truncation conditions, as discussed in Section 3.4.3. This value of σ_{ext} caused the exponential decay of E_x and E_y fields in the exterior region with an effective skin depth of about 65 lattice cells. To speed convergence of the interior fields, as discussed in Section 4.3.2, the isotropic conductivity, σ_{int}, equal to 0.025 mho/m was selected for the cylinder interior.

Using the computer program listed in Appendix A, the nose cone geometries for both Trial 1 (sleeve-fitting open, nose aperture closed) and Trial 2 (both apertures open) were specified by a total of 464 data cards. Only 16 cards had to be re-punched to change from Trial 1 to Trial 2.

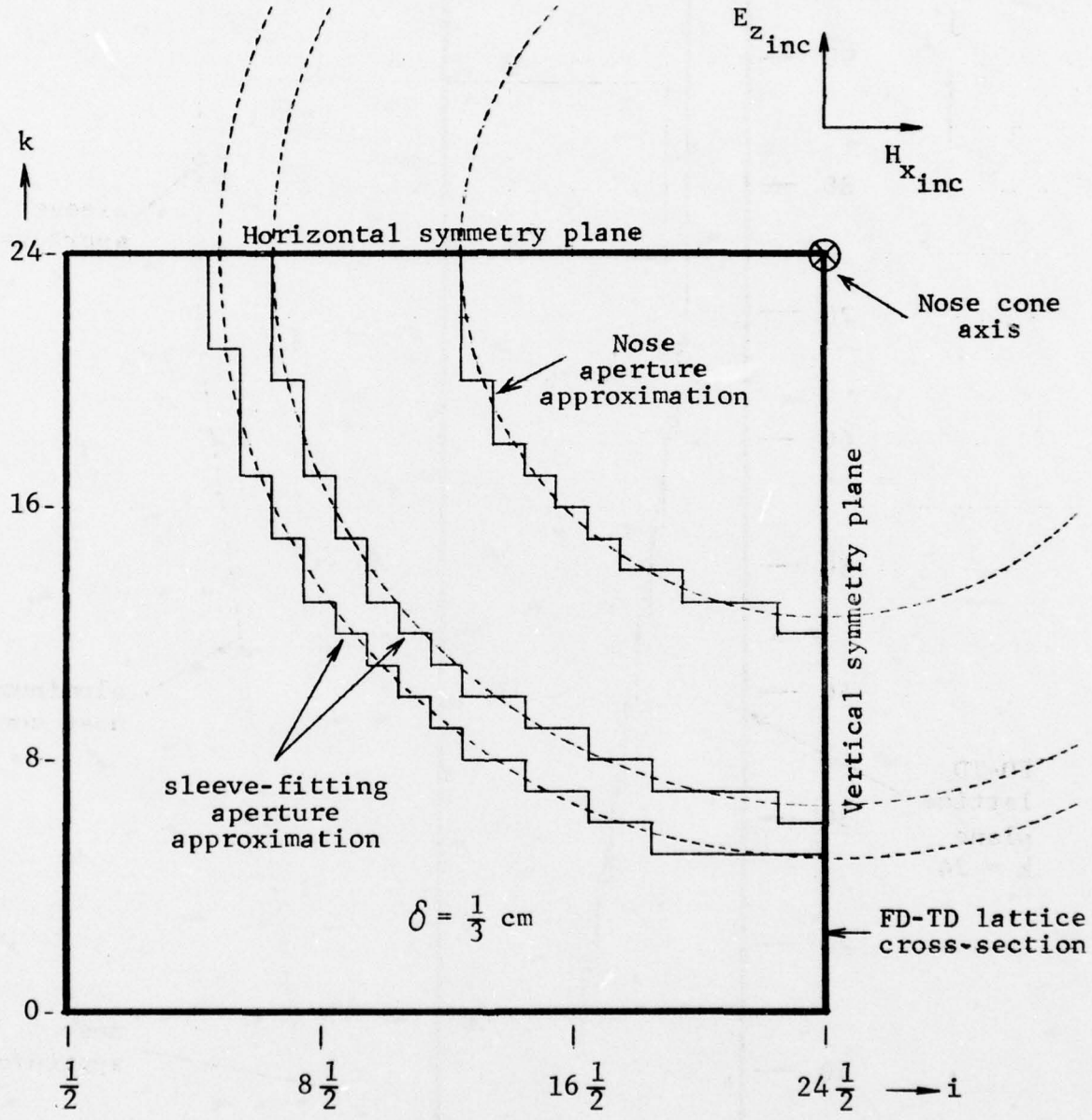

Fig. 19 KEY CROSS-SECTIONS OF NOSE-CONE MODEL FOR TASK 2

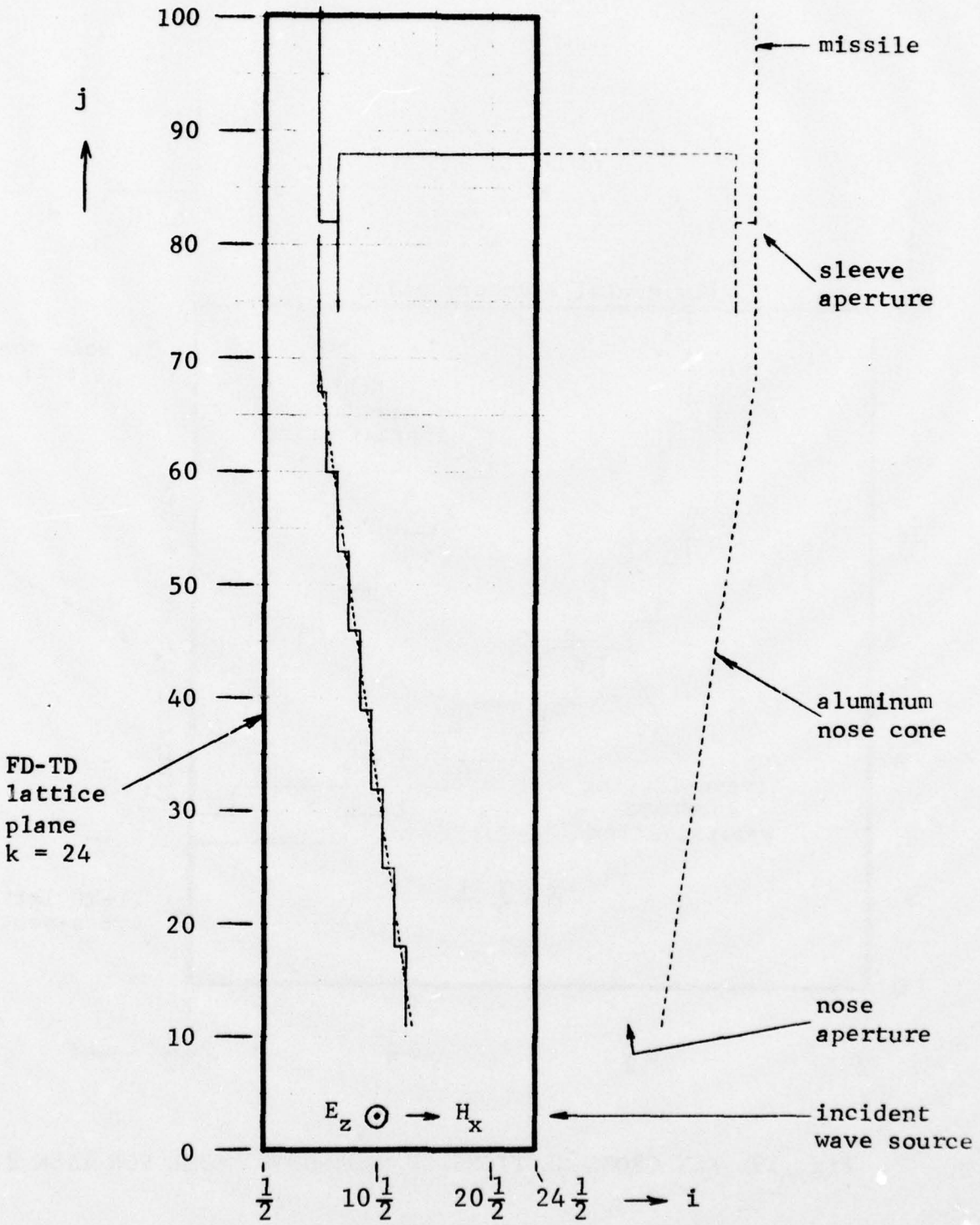

Fig. 20 VIEW OF NOSE CONE MODEL FOR TASK 2 AT HORIZONTAL SYMMETRY PLANE

4.4.2 Computed Field Maps

Trial 1 -- Only Sleeve-Fitting Open

Using results of the FD-TD program (900 time steps, σ_{int} = 0.025 mho/m), Figures 21 and 22 graph contour maps of the computed field components at the nose cone vertical and horizontal symmetry planes, respectively, for Trial 1. Contours are plotted at exact 10 dB intervals using linear interpolation. The intersections of the darker grid lines (spaced by 5 minor divisions, a total of δ = 1/3 cm) denotes the location of the field vector components in the lattice symmetry planes. Because of the staggered positions of the field components around a lattice unit cell, these darker grid lines may vary in position relative to the fixed nose cone walls by $\pm\delta/2$ = $\pm$1/6 cm, or 2.5 minor divisions.

It should be noted that the stepped-surface approximation of the smooth, tapered nose cone wall introduces cusp-like distortions in several of the field contours. However, these distortions are only manifested within about 1 cm of the point of each surface step. Very likely, the exact field contour here can be found simply by drawing a smooth curve connecting the adjacent undisturbed contour sections.

Trial 2 -- Both Apertures Open

Again, the FD-TD program was run for 900 time steps with σ_{int} = 0.025 mho/m. Figures 23 and 24 graph contour maps analogous to those of Figures 21 and 22. Comparing the corresponding maps for Trial 1 and Trial 2, it is seen that opening the nose aperture had very little effect upon the field contours near the sleeve fitting. Coupling between the two apertures occurred only at field levels lower than -40 dB. For this reason, it was decided not to run a Trial 3 (only nose aperture open) because the resulting field contours near the nose would almost certainly be the same as for Trial 2.

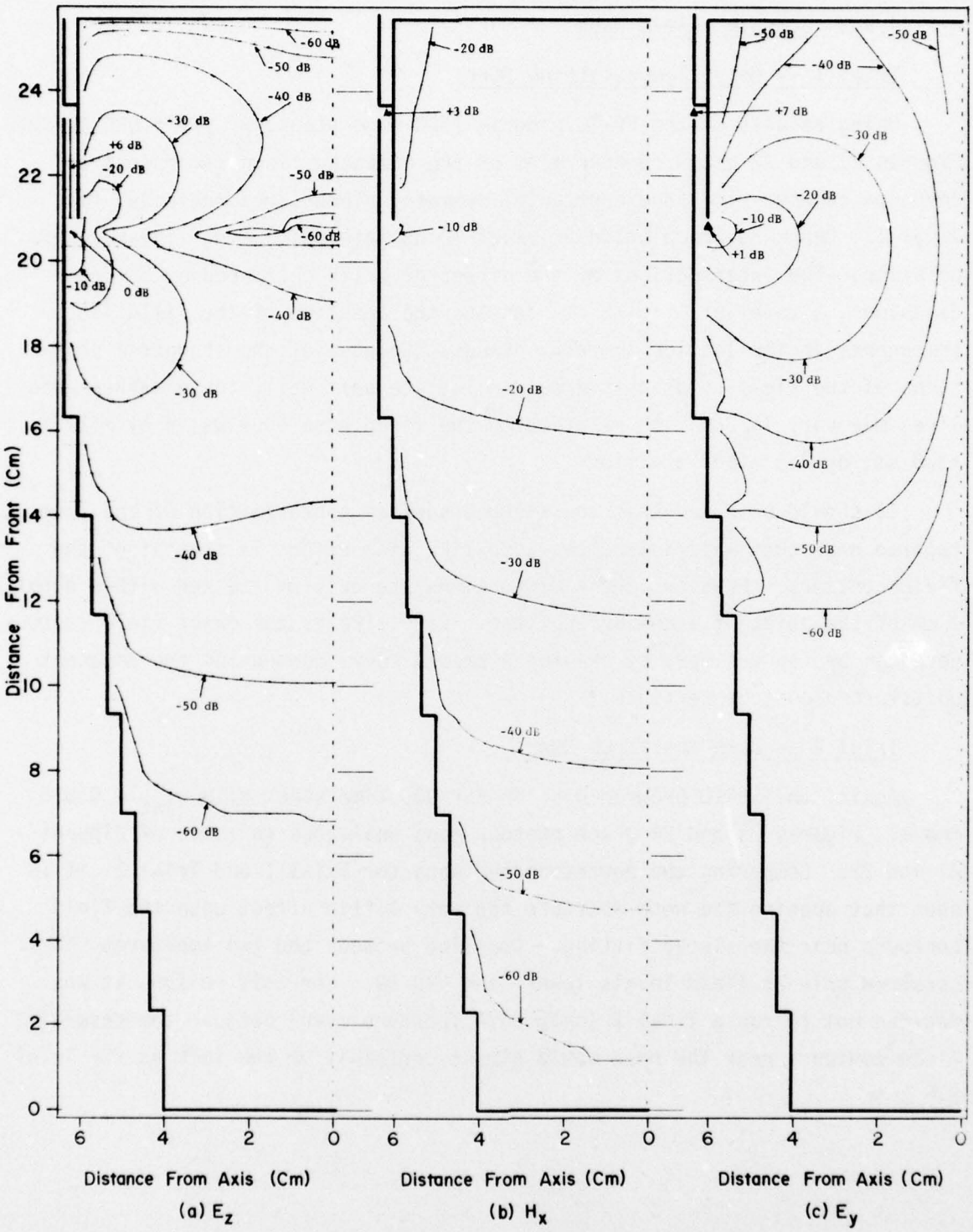

Fig. 21 FD-TD FIELD CONTOURS IN NOSE CONE VERTICAL SYMMETRY PLANE. TRIAL 1- ONLY SLEEVE-FITTING APERTURE OPEN

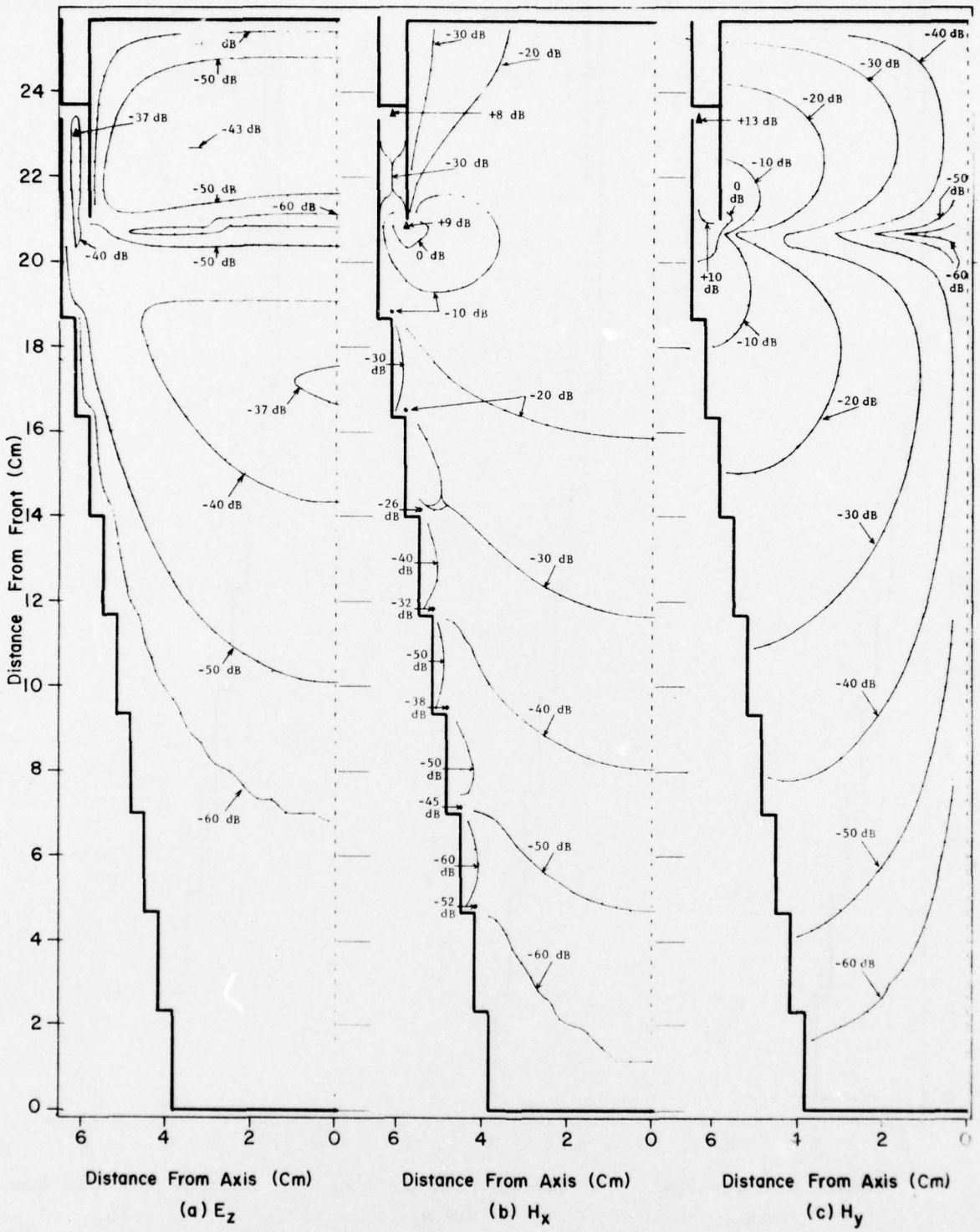

Fig. 22 FD-TD FIELD CONTOURS IN NOSE CONE HORIZONTAL SYMMETRY PLANE. TRIAL 1- ONLY SLEEVE-FITTING APERTURE OPEN

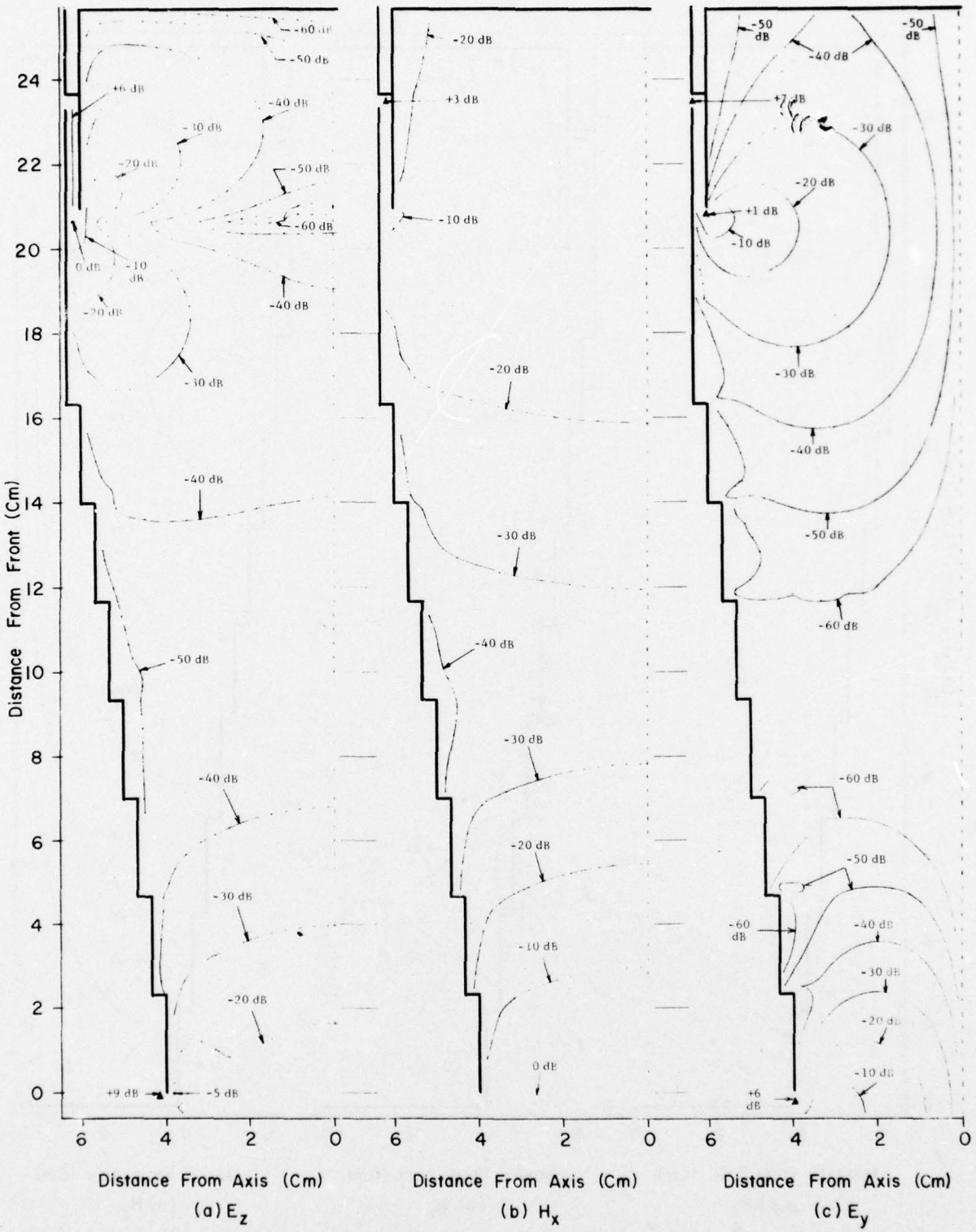

Fig. 23 FD-TD FIELD CONTOURS IN NOSE CONE VERTICAL SYMMETRY PLANE. TRIAL 2- BOTH SLEEVE AND NOSE APERTURES OPEN

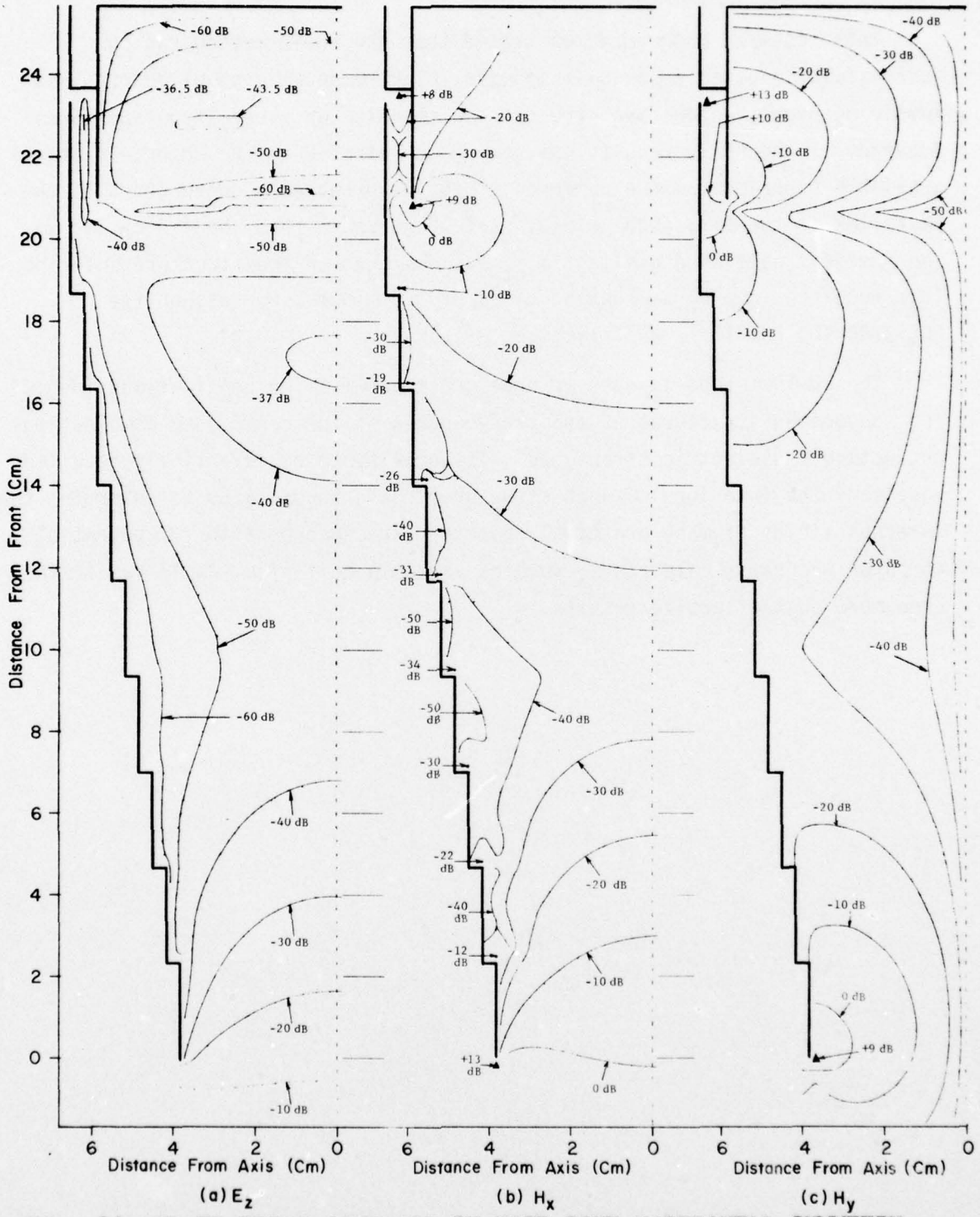

Fig. 24 FD-TD FIELD CONTOURS IN NOSE CONE HORIZONTAL SYMMETRY PLANE. TRIAL 2- BOTH SLEEVE AND NOSE APERTURES OPEN

5.0 DISCUSSION AND CONCLUSIONS

This research program demonstrated that the FD-TD method can be successfully applied to axial-incidence, electromagnetic coupling problems involving highly conducting structures with hole and sleeve-type apertures. Accuracy of the FD-TD results was very good relative to the uncertainties of available experimental and numerical-theory approaches. Convergence of the EM fields to the sinusoidal steady state occurred within about 2 cycles of the incident wave when a slight σ_{int} was assigned to the structure interior. This resulted in program running times of 3.5 minutes or less on the CDC STAR-100 for 10^5 - cell lattices.

The FD-TD method appears to have great promise for applications involving conducting structures at arbitrary angles of incidence, and combination conducting - dielectric structures. Its ability to achieve finely-detailed models of the interiors of such structures could be utilized to determine the internal fields of many practical objects. The incorporation of potential computer program accelerators, such as variable cell size, could result in even more cost-effective results.

REFERENCES

[1]Harrison, C. W., Jr., "Transient Electromagnetic Field Propagation Through Infinite Sheets, Into Spherical Shells, and Into Hollow Cylinder," IEEE Trans. Antennas Prop., Vol. AP-12, pp. 319-334, May 1964.

[2]Wilton, D. R. and R. Mittra, "A New Numerical Approach to the Calculation of Electromagnetic Scattering Properties of Two-Dimensional Bodies of Arbitrary Cross Section," IEEE Trans. Antennas Prop., Vol. AP-20, pp. 310-317, May 1972.

[3]Crow, T. T., Y. P. Liu, and C. D. Taylor, "Penetration of Electromagnetic Fields Through a Small Aperture Into a Cavity," Air Force Weapons Laboratory, Kirtland Air Force Base, New Mexico, Interaction Notes, No. 40, November 1968.

[4]Senior, T. B. and G. A. DesJardins, "Electromagnetic Field Penetration Into a Spherical Cavity," IEEE Trans. Electromagn. Compat., Vol. EMC-16, pp. 205-208, November 1974.

[5]Wu, T. K. and L. L. Tsai, "Numerical Analysis of Electromagnetic Fields in Biological Tissues," Proc. IEEE (Lett.), Vol. 62, pp. 1167-1168, August 1974.

[6]Livesay, D. E. and K. M. Chen, "Electromagnetic Fields Induced Inside Arbitrarily Shaped Biological Bodies," IEEE Trans. Microwave Theory Tech., Vol. MTT-22, pp. 1273-1280, December 1974.

[7]Senior, T. B., "Electromagnetic Field Penetration Into a Cylindrical Cavity," IEEE Trans. Electromagn. Compat., Vol. EMC-18, pp. 71-73, May 1976.

[8]Harrington, R. F., Field Computation by Moment Methods. New York: Macmillan, 1968.

[9]McDonald, B. H. and A. Wexler, "Finite-Element Solution of Unbounded Field Problems," IEEE Trans. Microwave Theory Tech., Vol. MTT-20, pp. 841-847, December 1972.

[10]Mittra, R., Editor, Computer Techniques for Electromagnetics. New York: Pergamon, 1973, Chapter 7.

[11]Baum, C. E., "Emerging Technology for Transient and Broadband Analysis and Synthesis of Antennas and Scatterers," Proc. IEEE, Vol. 64, pp. 1598-1616, November 1976.

REFERENCES (Continued)

[12]Cheng, D. K. and C. A. Chen, "On Transient Electromagnetic Excitation of a Rectangular Cavity Through an Aperture," Air Force Weapons Laboratory, Kirtland Air Force Base, New Mexico, Final Report No. AFWL-TR-75-91 on Contract No. F29601-74-C-0010, June 1976.

[13]Baum, C. E., "The Singularity Expansion Method," Ch. 3 in Transient Electromagnetic Fields, L. B. Felsen, Ed., New York: Springer-Verlag, 1975.

[14]Perala, R. A., "Integral Equation Solution for Induced Surface Currents on Bodies of Revolution," IEEE Trans. Electromagn. Compat., Vol. EMC-16, pp. 172-177, August 1974.

[15]Taylor, C. D. and C. W. Harrison, Jr., "On the Excitation of a Coaxial Line by an Incident Field Propagating Through a Small Aperture in the Sheath," IEEE Trans. Electromagn. Compat., Vol. EMC-15, pp. 127-131, August 1973.

[16]Burton, R. W. and R. W. King, "Induced Currents and Charges on Thin Cylinders in a Time-Varying Electromagnetic Field," IEEE Trans. Electromagn. Compat., Vol. EMC-17, pp. 149-155, August 1975.

[17]Yee, K. S., "Numerical Solution of Initial Boundary Value Problems Involving Maxwell's Equations in Isotropic Media," IEEE Trans. Antennas Prop., Vol. AP-14, pp. 302-307, May 1966.

[18]Taflove, A., Computation of the Electromagnetic Fields and Induced Temperatures Within a Model of the Microwave-Irradiated Human Eye. Ph.D. Dissertation, Northwestern University, Evanston, Ill., 1975.

[19]Taflove, A. and M. E. Brodwin, "Numerical Solution of Stead-State Electromagnetic Scattering Problems Using the Time-Dependent Maxwell's Equations," IEEE Trans. Microwave Theory Tech., Vol. MTT-23, pp. 623-630, August 1975.

[20]Taflove, A. and M. E. Brodwin, "Computation of the Electromagnetic Fields and Induced Temperatures Within a Model of the Microwave-Irradiated Human Eye," IEEE Trans. Microwave Theory Tech., Vol. MTT-23, pp. 888-896, November 1975.

[21]Tong, T. C., "Scattering by a Dielectric Rectangular Cylinder," Proc. 1973 IEEE G-AP Symp., Boulder, Colorado, pp. 79-82, August 1973.

REFERENCES (Continued)

[22]Jones, D. S., The Theory of Electromagnetism. New York: Macmillan, pp. 450-452, 1964.

[23]Stratton, J. A., Electromagnetic Theory. New York: McGraw Hill, pp. 563-573, 1941.

[24]Schuman, H. K. and D. E. Warren, "Coupling Through Rotationally Symmetric Apertures in Cavities of Revolution," Document No. RADC-TR-77-214, Griffiss Air Force Base, New York.

[25]Private communication with D. Warren, Engineer, Compatibility Branch, Rome Air Development Center, RADC/RBCT, Griffiss Air Force Base, New York.

[26]American National Standards Institute (ANSI) X3.9 - 1966.

[27]STAR Fortran Language Version 2 Reference Manual. Control Data Corporation, Sunnyvale, California, 1977.

APPENDIX A
FD-TD COMPUTER PROGRAMS

A.1 INTRODUCTION

This appendix documents the computer programs written during the present research effort. Included are listings of the programs for the cylinder problem and the nose cone problem and a description of the data card format employed. All computer programs were written using STAR Fortran Version 2.1 for processing by the Control Data STAR-100 computer system under its 1.2 operating system. This Fortran version contains certain extensions to standard Fortran[26] that permit usage of the vector processing capabilities of the STAR-100. The reader is referred to the STAR Fortran Manual for detailed discussion of these features.[27]

A.2 PROGRAM LISTING FOR TASK 1: COUPLING INTO AN OPEN-ENDED CYLINDER

The following 9 pages list the computer program for the 24 x 163 x 24 cell -- 800 time step run of the cylinder problem (Task 1). In the listed problem parameters, FREQ = 3.0 E + 8 denotes the operating frequency, f = 300 MHz; DX = 0.005 denotes the lattice cell diameter, δ = 0.005 m; MPR denotes the total number of media within the model, equal to 3 (lossless air, aluminum, slightly lossy air); DATA EPS and DATA SIG give the assumed relative dielectric constant and conductivity (mhos/m) of each medium; and MINDT and MAXDT give the number of the first and last time step of the algorithm.

```
      PROGRAM FDTD (INPUT,OUTPUT,TAPE60=INPUT)
C
C     RUN A- STEADY 300 MHZ TEM IRRADIATION OF A 19.0 CM DIAME-
C            TER, 68.5 CM LONG, OPEN-ENDED CONDUCTING CYLINDER
C     INCIDENT WAVE HAS THE COMPONENTS EZ AND HX, AND IS DIRECTE
C            ALONG THE CYLINDER AXIS INTO ITS OPEN END
C     24 X 163 X 24 CELL CUBIC LATTICE IS USED
C     UNIT CELL DIAMETER = DX = 0.5 CM = WAVELENGTH/200
C     EVEN SYMMETRY ABOUT LATTICE PLANES X = 24.5*DX AND Z = 24
C            *DX IS ASSUMED
C     SOFT TEM WAVE SOURCE CONDITION AT PLANE Y = 3.0*DX IS USED
C     SOFT LATTICE TRUNCATIONS ARE USED
C     PROGRAM IS OPTIMIZED FOR THE CDC STAR-100
C
      REAL MUR, MUZ
      DIMENSION A(973504),Z(5936),A1(600),A2(600),AAA(600),
     1  AA(25), N(25),DD(24),DE(24),CA(9),CB(9),EPS(3),SIG(3)
      COMMON A
      DESCRIPTOR D1,D2,D3,D4,D5,NF),BV,BW,BX,BY,A1X,A2X,A1Y,A2Y,
     1  A1Z,A2Z
      BIT BV,BBB(600),BW,BBW(600),BX,BBX(600),BY,BBY(24)
      ASSIGN A1X,A1(27:573)
      ASSIGN A2X,A2(27:573)
      ASSIGN A1Y,A1(26:574)
      ASSIGN A2Y,A2(26:574)
      ASSIGN A1Z,A1(1:599)
      ASSIGN A2Z,A2(1:599)
      ASSIGN BW,BBW(1:600)
      ASSIGN BX,BBX(1:600)
      ASSIGN BY,BBY(1:24)
      ASSIGN D4,DD(1:24)
      ASSIGN D5,DE(1:24)
      T1 = SECOND(CP)
      PRINT 150, T1
  150 FORMAT (F20.5)
C
C           .....I. PROBLEM PARAMETERS.....
      FREQ = 3.0E+8
      DX = 0.005
      MPR = 3
      DATA EPS /   1.0,      1.0,      1.0    /
      DATA SIG /   0.0,    3.7E+7,    0.01   /
      MINDT = 1
      MAXDT = 800
C
C           .....II. BASIC AND DERIVED CONSTANTS.....
      PI = 3.14159265
      MUZ = 4.0 * PI * 1.0E-7
      EPSZ = 8.854E-12
      DT = DX / 6.0E+8
      MHALF = 0.5 / FREQ / DT
```

```
      R = DT / 2.0 / EPSZ
      RA = DT**2 / DX**2 / MUZ / EPSZ
      RB = DT / DX / MUZ
      RD = 2.0 * PI * FREQ * DT
      DO 1 I=1,25
    1 N(I) = I
C
      A1(1:600) = 0.
      A2(1:600) = 0.
      CA(1:9) = 0.
      CB(1:9) = 0.
      BW = Q8VMKO(1,25:BW)
      BX = Q8VMKZ(24,25:BX)
      DO 2 I=1,MPR
      EAF = R * SIG(I) / EPS(I)
      CA(I) = (1.0-EAF) / (1.0+EAF)
    2 CB(I) = RA / EPS(I) / (1.0+EAF)
C
C           .....III. LOAD VECTOR DISC.....
C           .....ZERO INITIAL FIELDS.....
      Z(1:5936) = 0.
      A(1:5936) = 0.
      A(967569:5936) = 0.
C
C           .....TYPE OF MEDIUM.....
C           .....PLANES 2 - 13:  152 - 163 (ANISO. LOSSY AIR)....
      READ 4, (Z(I),I=1,600)
    4 FORMAT (75F1.0)
      READ 4, (Z(I),I=2601,3200)
      READ 4, (Z(I),I=1301,1900)
      DO 5 I=2,13
      IDEL = (I-1) * 5936
    5 A(IDEL+1:5936) = Z(1:5936)
      DO 6 I=152,163
      IDEL = (I-1) * 5936
    6 A(IDEL+1:5936) = Z(1:5936)
C
C           .....PLANES 14 - 150 (UNIFORM CIRCULAR CYLINDER).....
      READ 4, (Z(I),I=1,600)
      READ 4, (Z(I),I=2601,3200)
      READ 4, (Z(I),I=1301,1900)
      DO 7 I=14,150
      IDEL = (I-1) * 5936
    7 A(IDEL+1:5936) = Z(1:5936)
C
C           .....PLANE 151 (CYLINDER BACKPLANE).....
```

```
      PRINT 150, T2
C
C           .....IV. TIME-STEPPING LOOP.....
      DO 200 J=MINDT,MAXDT
      TERM = SIN(FLOAT(J)*RD)  * R3
      MCAL = 3 + IFIX(FLOAT(J)/6.0)
      MCALL = 54
      IF(MCAL.LT.54)MCALL=MCAL
C
C           .....TRANSVERSE PLANE =1.....
C           .....EX, EZ TRUNCATIONS.....
      A(626:625) = A(1:625)
      A(1:625) = A(6562:625)
      A(3226:625) = A(2601:625)
      A(2601:625) = A(9162:625)
C
C           .....EY ITERATION.....
      ASSIGN D1,.DYN.574
      ASSIGN D2,.DYN.574
      ASSIGN D3,.DYN.574
      A(1926) = 0.5 * (A(2551)+A(2552))
      A(1927:22) = 0.333 * (A(2551:22)+A(2552:22)+A(2553:22))
      A(1949) = 0.333333 * (A(2573) + 2.0*A(2574))
      A(2551:24) = A(1951:24)
      D1 = CA(3) * A(1951:574)
      D2 = A(3926:574) - A(3901:574) + A(5276:574) - A(5277:574)
      D3 = CB(3) * D2
      A(1951:574) = D1 + D3
      A(1926:600) = Q8VCTRL(0.0,BX:A(1926:600))
      FREE
C
C           .....TRANSVERSE PLANES 2 - 163.....
      DO 82 JY=1,MCALL
      JDEL = (JY-1) * 17808
C
C           .....EX ITERATION.....
      ASSIGN D1,.DYN.573
      ASSIGN D2,.DYN.573
      ASSIGN D3,.DYN.573
      ASSIGN NFD,.DYN.573
      ASSIGN BV,BBB(1:573)
C
      DO 30 MA=1,3
      M = JDEL + 5936*(MA-1)
C
C           .....SOFT LATTICE TRUNCATION.....
      A(6563+M) = 0.5 * (A(7188+M)+A(7189+M))
      A(6564+M:21) = 0.333 * (A(7188+M:21)+A(7189+M:21)+A(7190+M
     1     :21))
      A(6585+M) = 0.5 * (A(7209+M)+A(7210+M))
      A(7188+M:23) = A(6588+M:23)
C
```

```
C           .....MAIN EX LOOPS.....
      NFD = A(5963+M;573)
      DO 22 JJ=1,MPR
      BV = NFD.EQ.JJ
      A1X = Q8VCTRL(CA(JJ),BV;A1X)
   22 A2X = Q8VCTRL(CB(JJ),BV;A2X)
      D1 = A1X * A(6588+M;573)
      D2 = A(11213+M;573)-A(5277+M;573)+A(10513+M;573)-A(10538+M
     |      ;573)
      D3 = A2X * D2
   30 A(6588+M;573) = D1 + D3
      FREE
C
C           .....EY ITERATION.....
      ASSIGN D1,.DYN.574
      ASSIGN D2,.DYN.574
      ASSIGN D3,.DYN.574
      ASSIGN NFD,.DYN.574
      ASSIGN BV,888(1;574)
C
      DO 40 MA=1,3
      M = JDEL + 5936*(MA-1)
C
C           .....SOFT LATTICE TRUNCATION.....
      A(7862+M) = 0.5 * (A(8487+M)+A(8488+M))
      A(7863+M;22) = 0.333 * (A(8487+M;22)+A(8488+M;22)+A(8489+M
     |                ;22))
      A(7885+M) = 0.333 * (A(8509+M) + 2.0*A(8510+M))
      A(8487+M;24) = A(7887+M;24)
C
C           .....MAIN EY LOOPS.....
      NFD = A(7262+M;574)
      DO 32 JJ=1,MPR
      BV = NFD.EQ.JJ
      A1Y = Q8VCTRL(CA(JJ),BV;A1Y)
   32 A2Y = Q8VCTRL(CB(JJ),BV;A2Y)
      D1 = A1Y * A(7887+M;574)
      D2 = A(9862+M;574)-A(9837+M;574)+A(11212+M;574)-A(11213+M;
     |      574)
      D3 = A2Y * D2
      A(7887+M;574) = D1 + D3
C
C           .....EY ENVELOPE COMPUTATION.....
      D4 = Q8VCMPRS(A(7861+M;600),3X;D4)
      D5 = VABS(D4;D5)
      BY = D5.GT.A(8512+M;24)
   40 A(8512+M;24) = Q8VCTRL(D5,BY;A(8512+M;24))
      FREE
C
C           .....EZ ITERATION.....
      ASSIGN D1,.DYN.599
```

```
      ASSIGN D2,.DYN.599
      ASSIGN D3,.DYN.599
      ASSIGN NFD,.DYN.599
      ASSIGN BV,BBB(1:599)
C
      DO 50 MA=1,3
      M = JDEL + 5936*(MA-1)
C
C           .....MAIN EZ LOOPS.....
      NFD = A(8537+M:599)
      DO 42 JJ=1,MPR
      BV = NFD.EQ.JJ
      A1Z = Q8VCTRL(CA(JJ),BV:A1Z)
   42 A2Z = Q8VCTRL(CB(JJ),BV:A2Z)
      D1 = A1Z * A(9162+M:599)
      D2 = A(10513+M:599)-A(10512+M:599)+A(3901+M:599)-A(9837+M:
     1      599)
      D3 = A2Z * D2
      A(9162+M:599) = D1 + D3
C
C           .....EZ SOFT TEM WAVE SOURCE CONDITION.....
      IF(JY.GE.2.OR.MA.LE.2)GO TO 47
      A(21034:599) = TERM + A(21034:599)
C
C           .....EZ ENVELOPE COMPUTATION.....
   47 D4 = VABS(A(9737+M:24):D4)
      BY = D4.GT.A(9787+M:24)
      A(9787+M:24) = Q8VCTRL(D4,BY:A(9787+M:24))
      D4 = Q8VCMPRS(A(9161+M:600),3X:D4)
      D5 = VABS(D4:D5)
      BY = D5.GT.A(9812+M:24)
   50 A(9812+M:24) = Q8VCTRL(D5,BY:A(9812+M:24))
C
C           .....HX ITERATION.....
      DO 60 MA=1,3
      M = JDEL + 5936*(MA-1)
C
C           .....MAIN HX LOOPS.....
      D1 =          A(3901+M:599)
      D2 = A(1951+M:599)-A(1926+M:599)+A(3226+M:599)-A(9162+M:
     1      599)
      A(3901+M:599) = D1 + D2
C
C           .....HX ENVELOPE COMPUTATION.....
      D4 = VABS(A(4476+M:24):D4)
      BY = D4.GT.A(4526+M:24)
      A(4526+M:24) = Q8VCTRL(D4,BY:A(4526+M:24))
      D4 = Q8VCMPRS(A(3900+M:600),3X:D4)
      D5 = VABS(D4:D5)
      BY = D5.GT.A(4551+M:24)
   60 A(4551+M:24) = Q8VCTRL(D5,BY:A(4551+M:24))
      FREE
C
```

```
C           .....HY ITERATION.....
      ASSIGN D1,.DYN.598
      ASSIGN D2,.DYN.598
C
      DO 70 MA=1,3
      M = JDEL + 5936*(MA-1)
C
C           .....SOFT LATTICE TRUNCATION.....
      AA(1) = 0.5 * (A(11137+M)+A(11138+M))
      AA(2:22) = 0.333 * (A(11137+M:22)+A(11138+M:22)+A(11139+M:
     1            22))
      AA(24) = 0.333 * (A(11159+M) + 2.0*A(11160+M))
      AAA(1:600) = Q8VXPND(AA(1:24),BW:AAA(1:600))
      A(11137+M:24) = Q8VCMPRS(A(10513+M:600),BW:A(11137+M:24))
C
C           .....MAIN HY LOOPS.....
      D1 =        A(10513+M:598)
      D2 = A(9163+M:598)-A(9162+M:598)+A(6563+M:598)-A(6588+M:
     1     598)
      A(10513+M:598) = D1 + D2
C
      A(10512+M:600) = Q8VCTRL(AAA(1:600),BW:A(10512+M:600))
      A(10512+M:600) = Q8VCTRL(0.0,BX:A(10512+M:600))
C
C           .....HY ENVELOPE COMPUTATION.....
      D4 = VABS(A(11087+M:24):D4)
      BY = D4.GT.A(11162+M:24)
   70 A(11162+M:24) = Q8VCTRL(D4,BY:A(11162+M:24))
      FREE
C
C           .....HZ ITERATION.....
      ASSIGN D1,.DYN.573
      ASSIGN D2,.DYN.573
C
      DO 80 MA=1,3
      M = JDEL + 5936*(MA-1)
C
C           .....SOFT LATTICE TRUNCATION.....
      AA(2) = 0.5 * (A(5877+M)+A(5878+M))
      AA(3:21) = 0.333 * (A(5877+M:21)+A(5878+M:21)+A(5879+M:21))
      AA(24) = 0.5 * (A(5898+M) + A(5899+M))
      AAA(1:600) = Q8VXPND(AA(1:24),BW:AAA(1:600))
      A(5876+M:24) = Q8VCMPRS(A(5252+M:600),BW:A(5876+M:24))
C
C           .....MAIN HZ LOOPS.....
      D1 =        A(5277+M:573)
      D2 = A(6588+M:573)-A(652+M:573)+A(1951+M:573)-A(1952+M:573)
      A(5277+M:573) = D1 + D2
C
      A(5251+M:600) = Q8VCTRL(AAA(1:600),BW:A(5251+M:600))
   80 A(5251+M:600) = Q8VCTRL(0.0,BX:A(5251+M:600))
```

```
      FREE
   82 CONTINUE
      IF(MCALL.LE.53)GO TO 94
C
C           .....TRANSVERSE PLANE =164.....
      M = 162 * 5936
C
C           .....EX, EZ TRUNCATIONS.....
      A(6562+M:625) = A(5937+M:625)
      A(5937+M:625) = A(7237+M:625)
      A(7237+M:625) = A(626+M:625)
      A(9162+M:625) = A(8537+M:625)
      A(8537+M:625) = A(9837+M:625)
      A(9837+M:625) = A(3226+M:625)
C
C           .....HX ITERATION.....
      ASSIGN D1,.DYN.599
      ASSIGN D2,.DYN.599
      D1 =          A(3901+M:599)
      D2 = A(1951+M:599)-A(1926+M:599)+A(3226+M:599)-A(9162+M:
     1      599)
      A(3901+M:599) = D1 + D2
      D4 = VABS(A(4476+M:24):D4)
      BY = D4.GT.A(4526+M:24)
      A(4526+M:24) = Q8VCTRL(D4,BY:A(4526+M:24))
      D4 = Q8VCMPRS(A(3900+M:600),BX:D4)
      D5 = VABS(D4:D5)
      BY = D5.GT.A(4551+M:24)
      A(4551+M:24) = Q8VCTRL(D5,BY:A(4551+M:24))
     .FREE
C
C           .....HZ ITERATION.....
      ASSIGN D1,.DYN.573
      ASSIGN D2,.DYN.573
      AA(2) = 0.5 * (A(5877+M)+A(5878+M))
      AA(3:21) = 0.333 * (A(5877+M:21)+A(5878+M:21)+A(5879+M:21))
      AA(24) = 0.5 * (A(5898+M) + A(5899+M))
      AAA(1:600) = Q8VXPND(AA(1:24),BW:AAA(1:600))
      A(5876+M:24) = Q8VCMPRS(A(5252+M:600),BW:A(5876+M:24))
      D1 =        A(5277+M:573)
      D2 = A(6588+M:573)-A(652+M:573)+A(1951+M:573)-A(1952+M:573)
      A(5277+M:573) = D1 + D2
      A(5251+M:600) = Q8VCTRL(AAA(1:500),BW:A(5251+M:600))
      A(5251+M:600) = Q8VCTRL(0.0,BX:A(5251+M:600))
      FREE
   94 T3 = SECOND(CP)
      PRINT 150, T3
C
C           .....FIELD ENVELOPE ROUTINE.....
      DO 100 L=MHALF,MAXDT,MHALF
      IF(J.EQ.L)GO TO 101
  100 CONTINUE
```

```
      IF(J.EQ.MAXDT)GO TO 101
      GO TO 199
C
C           .....AT HORIZONTAL SYMMETRY PLANE.....
  101 PRINT 102, J
  102 FORMAT(1H1,52X,27HEZ ENVELOPE FOR TIME STEP =,I5,
     1        //,62X,15HPLANE Z = 24*DX,//,2X,1HJ,/)
      CALL ENV(3850,1.0E+4/RB)
      PRINT 103, (N(LI),LI=1,24)
  103 FORMAT(//,8X,24I5,2X,1HI)
C
      PRINT 104, J
  104 FORMAT(1H1,52X,27HHX ENVELOPE FOR TIME STEP =,I5,
     1        //,62X,15HPLANE Z = 24*DX,//,2X,1HJ,/)
      CALL ENV(4525,3.77E+6)
      PRINT 103, (N(LI),LI=1,24)
C
      PRINT 105, J
  105 FORMAT(1H1,52X,27HHY ENVELOPE FOR TIME STEP =,I5,
     1        //,62X,15HPLANE Z = 24*DX,//,2X,1HJ,/)
      CALL ENV(5225,3.77E+6)
      PRINT 103, (N(LI),LI=1,24)
C
C           .....AT VERTICAL SYMMETRY PLANE.....
      PRINT 106, J
  106 FORMAT(1H1,52X,27HEZ ENVELOPE FOR TIME STEP =,I5,
     1        //,62X,17HPLANE X = 24.5*DX,//,2X,1HJ,/)
      CALL ENV(3875,1.0E+4/RB)
      PRINT 107, (N(LI),LI=1,24)
  107 FORMAT(//,8X,24I5,2X,1HK)
C
      PRINT 108, J
  108 FORMAT(1H1,52X,27HHX ENVELOPE FOR TIME STEP =,I5,
     1        //,62X,17HPLANE X = 24.5*DX,//,2X,1HJ,/)
      CALL ENV(4550,3.77E+6)
      PRINT 107, (N(LI),LI=1,24)
C
      PRINT 109, J
  109 FORMAT(1H1,52X,27HEY ENVELOPE FOR TIME STEP =,I5,
     1        //,62X,17HPLANE X = 24.5*DX,//,2X,1HJ,/)
      CALL ENV(2575,1.0E+4/RB)
      PRINT 107, (N(LI),LI=1,24)
C
  199 CONTINUE
  200 CONTINUE
      T4 = SECOND(CP)
      PRINT 150, T4
      STOP
      END
```

```
      SUBROUTINE ENV(LOC,SCALE)
      DIMENSION IPR(25),A(973504)
      COMMON A
      DO 2 LA=1,162
      LB = 163 - LA
      LC = LB + 1
      LD = LB*5936 + LOC
      IPR(1:24) = SCALE * A(LD+1:24)
      A(LD+1:24) = 0.
    2 PRINT 3, LC, (IPR(LF),LF=1,24)
    3 FORMAT(1X,I3,5X,2415)
      RETURN
      END
```

A.3 PROGRAM LISTING FOR TASK 2: COUPLING INTO THE NOSE CONE OF A MISSILE

Most of the Fortran statements of the nose cone program are identical to those of the cylinder program of the preceding appendix section. The necessary changes involve only the reduction of the length of the main data storage vector, A, and new data-read cards. Therefore, in this section we list only the modifications of the cylinder program.

```
      PROGRAM FDTD (INPUT,OUTPUT,TAPE60=INPUT)
C
C     RUN B- STEADY 300 MHZ TEM IRRADIATION OF A 12.8 CM
C              DIAMETER, ALUMINUM NOSE CONE
C     TRIAL 2- BOTH SLEEVE FITTING AND NOSE APERTURES ARE OPEN
C     INCIDENT WAVE HAS THE COMPONENTS EZ AND HX, AND IS DIRECTE
C              ALONG THE NOSE CONE AXIS
C     24 X 100 X 24 CELL CUBIC LATTICE IS USED
C     UNIT CELL DIAMETER = Dx = 0.33 CM = WAVELENGTH/300
                        .
                        .
                        .
      DIMENSION A(599536),Z(5936),A1(600),A2(600),AAA(600),
     1  AA(25), N(25),DD(24),DE(24),CA(9),CB(9),EPS(3),SIG(3)
                        .
                        .
                        .
C           .....I. PROBLEM PARAMETERS.....
      FREQ = 3.0E+8
      Dx = 0.01/3.0
      MPR = 3
      DATA EPS /   1.0,     1.0,      1.0    /
      DATA SIG /   0.0,     3.7E+7,   0.025  /
      MINDT = 1
      MAXDT = 900
                        .
                        .
                        .
C           .....III. LOAD VECTOR A.....
C           .....ZERO INITIAL FIELDS.....
      Z(1:5936) = 0.
      A(1:5936) = 0.
      A(593601:5936) = 0.
C
C           .....TYPE OF MEDIUM.....
      READ 4, (Z(I),I=1,600)
    4 FORMAT (75F1.0)
      READ 4, (Z(I),I=2601,3200)
      READ 4, (Z(I),I=1301,1900)
      DO 5 I=2,10
      IDEL = (I-1) * 5936
    5 A(IDEL+1:5936) = Z(1:5936)
C
      DO 6 IA=11,67,7
      READ 4, (Z(I),I=1,600)
      READ 4, (Z(I),I=2601,3200)
```

```
      READ 4, (Z(I),I=1301,1900)
      IDEL = (IA-1) * 5936
      A(IDEL+1:5936) = Z(1:5936)
      READ 4, (Z(I),I=1,600)
      READ 4, (Z(I),I=2601,3200)
      DO 6 IB=1,6
      IDEL = (IA+IB-1) * 5936
    6 A(IDEL+1:5936) = Z(1:5936)
      DO 7 I=89,100
      IDEL = (I-1) * 5936
    7 A(IDEL+1:5936) = Z(1:5936)
C
      READ 4, (Z(I),I=1,600)
      READ 4, (Z(I),I=2601,3200)
      READ 4, (Z(I),I=1301,1900)
      DO 8 I=74,80
      IDEL = (I-1) * 5936
    8 A(IDEL+1:5936) = Z(1:5936)
      DO 9 I=83,87
      IDEL = (I-1) * 5936
    9 A(IDEL+1:5936) = Z(1:5936)
C
      READ 4, (Z(I),I=1301,1900)
      I = 81
      IDEL = (I-1) * 5936
      A(IDEL+1:5936) = Z(1:5936)
C
      READ 4, (Z(I),I=1,600)
      READ 4, (Z(I),I=2601,3200)
      READ 4, (Z(I),I=1301,1900)
      I = 82
      IDEL = (I-1) * 5936
      A(IDEL+1:5936) = Z(1:5936)
C
      READ 4, (Z(I),I=1,600)
      READ 4, (Z(I),I=2601,3200)
      READ 4, (Z(I),I=1301,1900)
      I = 88
      IDEL = (I-1) * 5936
      A(IDEL+1:5936) = Z(1:5936)
C
      T2 = SECOND(CP)
      PRINT 150, T2
C
C          .....IV. TIME-STEPPING LOOP.....
      DO 200 J=MINDT,MAXDT
      TERM = SIN(FLOAT(J)*RD)   * RR
      MCALL = 3 + IFIX(FLOAT(J)/6.0)
      IF(MCALL.GT.33) MCALL=33
```

```
   82 CONTINUE
      IF(MCALL.LE.32)GO TO 94
C
C           .....TRANSVERSE PLANE =101.....
      M = 99 * 5936
          .
          .
          .
          .
          .
      END
          .
          .
          .
          .
          .

      SUBROUTINE ENV(LOC,SCALE)
      DIMENSION IPR(25),A(599536)
      COMMON A
      DO 2 LA=1,99
      LB = 100 - LA
      LC = LB + 1
      LD = LB*5936 + LOC
      IPR(1:24) = SCALE * A(LD+1:24)
      A(LD+1:24) = 0.
    2 PRINT 3, LC, (IPR(LF),LF=1,24)
    3 FORMAT(1X,I3,5X,24I5)
      RETURN
      END
```

A.4 DATA CARD FORMAT

The data cards specify the type of medium at each location of an electric field component. Up to 9 distinct media can be specified within a lattice.

Using the Fortran statement 4 FORMAT (75F1.0) a medium-type integer 1, 2,..., 9 can be assigned to the 600 locations of an electric field component in one plane j = constant with only 8 data cards. The 600 locations are ordered as shown in Figure A-1. With the 75F1.0 format, we have

Data Card	Assigns Type Integer to Consecutive Locations
1	1 - 75
2	76 - 150
3	151 - 225
4	226 - 300
5	301 - 375
6	376 - 450
7	451 - 525
8	526 - 600

In all data cards, column 25, column 50, and columns 75 - 80 are left blank.

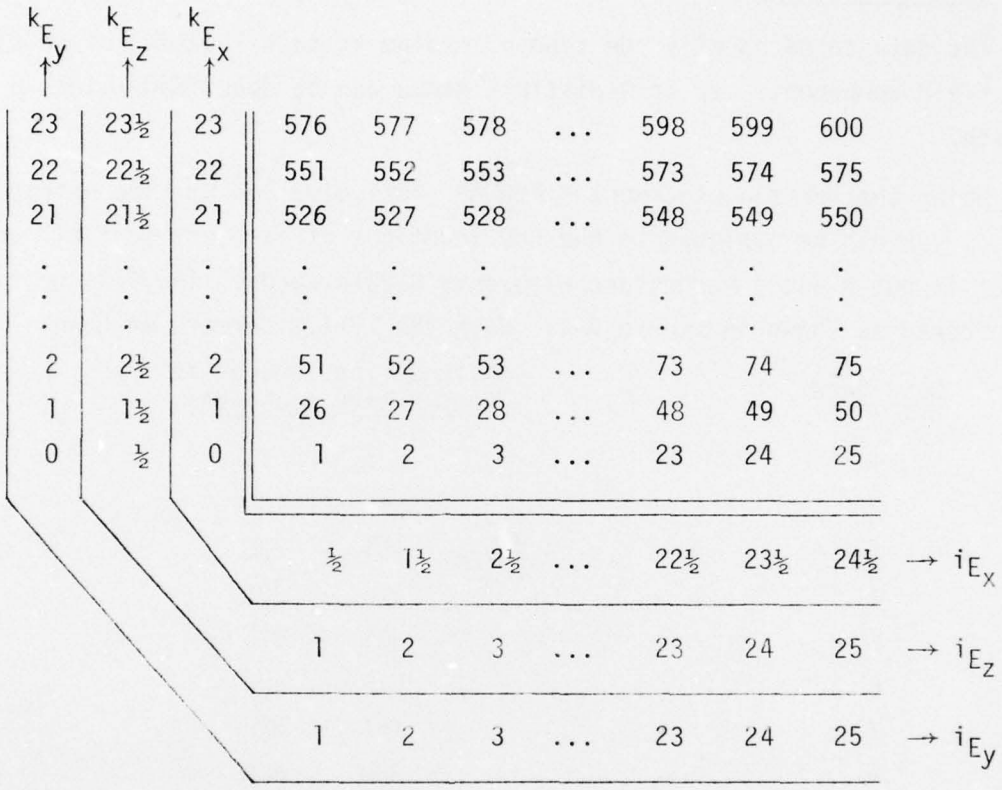

FIGURE A-1 ORDERING OF THE ELECTRIC FIELD COMPONENT LOCATIONS IN THE LATTICE PLANE j = CONSTANT

AD-A056 726 IIT RESEARCH INST CHICAGO ILL F/G 20/14
TIME DOMAIN SOLUTIONS FOR ELECTROMAGNETIC COUPLING.(U)
JUN 78 A TAFLOVE F30602-77-C-0163
UNCLASSIFIED RADC-TR-78-142 NL

2 OF 2
AD
A056728

END
DATE
FILMED
9-78
DDC

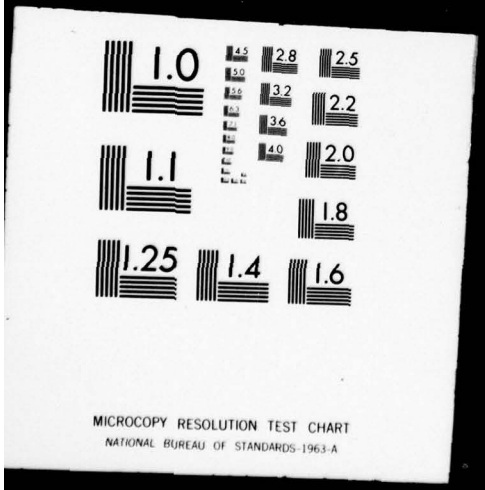

The media-typ
one plane j = cons
with plane j = J-½

	j Coordinate Field Compone
Card Group 1	1
	1
	1½
Card Group 2	2
	2
	2½
	.
	.
	.
Card Group J-1	J-1
	J-1
	J-½

Fewer than (J-1) c
pendent of j for a
statements READ 4
of this appendix.

ıta for each field component are read into the program
: at a time, beginning with plane j = 1 and ending
ı the following order:

Field Component	Number of Data Cards
E_x	8
E_z	8
E_y	8
E_x	8
E_z	8
E_y	8
.	
.	
.	
E_x	8
E_z	8
E_y	8

groups can be used if the system geometry is inde-
ıber of lattice planes. For example, see Fortran
DO 5, DO 6, and DO 7 of the cylinder program (Run A)

MISSION
of
Rome Air Development Center

RADC plans and conducts research, exploratory and advanced development programs in command, control, and communications (C^3) activities, and in the C^3 areas of information sciences and intelligence. The principal technical mission areas are communications, electromagnetic guidance and control, surveillance of ground and aerospace objects, intelligence data collection and handling, information system technology, ionospheric propagation, solid state sciences, microwave physics and electronic reliability, maintainability and compatibility.